

การวิเคราะห์เชิงเอนไซม์และคอมพิวเตอร์ของการผลิตไซโคลเด็กซ์ทรินชนิดวงใหญ่ด้วย

แอมิโลมอลเตสจาก *Corynebacterium glutamicum*



นางสาวสิริกุล งามวิเศษ

จุฬาลงกรณ์มหาวิทยาลัย

CHULALONGKORN UNIVERSITY

บทคัดย่อและแฟ้มข้อมูลฉบับเต็มของวิทยานิพนธ์ตั้งแต่ปีการศึกษา 2554 ที่ให้บริการในคลังปัญญาจุฬาฯ (CUIR)

เป็นแฟ้มข้อมูลของนิสิตเจ้าของวิทยานิพนธ์ ที่ส่งผ่านทางบัณฑิตวิทยาลัย

The abstract and full text of theses from the academic year 2011 in Chulalongkorn University Intellectual Repository (CUIR) are the thesis authors' files submitted through the University Graduate School.

วิทยานิพนธ์นี้เป็นส่วนหนึ่งของการศึกษาตามหลักสูตรปริญญาวิทยาศาสตรมหาบัณฑิต

สาขาวิชาชีวเคมีและชีววิทยาโมเลกุล ภาควิชาชีวเคมี

คณะวิทยาศาสตร์ จุฬาลงกรณ์มหาวิทยาลัย

ปีการศึกษา 2559

ลิขสิทธิ์ของจุฬาลงกรณ์มหาวิทยาลัย

ENZYMATIC AND COMPUTATIONAL ANALYSIS OF
LARGE-RING CYCLODEXTRIN PRODUCTION BY
Corynebacterium glutamicum AMYLOMALTASE

Miss Sirikul Ngawiset



A Thesis Submitted in Partial Fulfillment of the Requirements
for the Degree of Master of Science Program in Biochemistry and Molecular Biology
Department of Biochemistry
Faculty of Science
Chulalongkorn University
Academic Year 2016
Copyright of Chulalongkorn University

สิริกุล จ้าววิเศษ : การวิเคราะห์เชิงเอนไซม์และคอมพิวเตอร์ของการผลิตไซโคลเด็กซ์ทรินชนิดวงใหญ่ด้วยแอมิโลมอลเตสจาก *Corynebacterium glutamicum* (ENZYMATIC AND COMPUTATIONAL ANALYSIS OF LARGE-RING CYCLODEXTRIN PRODUCTION BY *Corynebacterium glutamicum* AMYLOMALTASE) อ.ที่ปรึกษาวิทยานิพนธ์หลัก: ศศ. ดร. เกื้อการุณย์ ครุสง, อ.ที่ปรึกษาวิทยานิพนธ์ร่วม: ศ. ดร. เปี่ยมสุข พงษ์สวัสดิ์, อ. ดร. รัชฎา รุ่งโรจน์มงคล, 144 หน้า.

แอมิโลมอลเตสเป็นเอนไซม์ในกลุ่มกลูแคนทรานส์เฟอเรสที่รู้จักกันว่าสามารถผลิตไซโคลเด็กซ์ทรินชนิดวงใหญ่ได้ผ่านปฏิกิริยาการเกิดโครงสร้างแบบวง (cyclization) ในการวิจัยนี้ต้องการระบุกรดอะมิโนที่มีความสำคัญต่อการผลิตไซโคลเด็กซ์ทรินชนิดวงใหญ่ของแอมิโลมอลเตสจาก *Corynebacterium glutamicum* (CgAM) จึงทำการกลายกรดอะมิโนในบริเวณโดเมนย่อย CA1 และ CA2 โดยทำให้เกิดการกลายเอนเฉพาะตำแหน่ง (site-directed mutagenesis) P228Y, E231Y, A413F และ G417F บนรีคอมบิแนนท์พลาสมิด CgAM ค่าความเป็นกรดเบสและอุณหภูมิที่เหมาะสมในการทำปฏิกิริยาของเอนไซม์ดั้งเดิมและเอนไซม์กลายอยู่ในช่วง pH 6.0 – 7.5 และอุณหภูมิ 25 - 35°C การกลายพันธุ์ไม่ส่งผลกระทบต่อความคงทนต่ออุณหภูมิและค่าความเป็นกรดเบส นอกจากนี้ มอลโทไตรโอส (G3) ยังเป็นสับสเตรทที่ดีที่สุดสำหรับเอนไซม์ดั้งเดิมและเอนไซม์กลายทุกตัวในการเกิดปฏิกิริยาโยกย้ายหมู่ไกลโคซิล (disproportionation) A413F มีค่าความจำเพาะต่อการเกิดแอกทีวิตี starch transglycosylation, starch degradation, disproportionation และ cyclization น้อยกว่าเอนไซม์ดั้งเดิม P228Y, E231Y และ G417F แสดงค่าความจำเพาะต่อการเกิดแอกทีวิตี starch transglycosylation และ starch degradation ใกล้เคียงกับเอนไซม์ดั้งเดิม P228Y มีความสามารถในการเกิดปฏิกิริยาการโยกย้ายหมู่ไกลโคซิลต่ำ เมื่อเปรียบเทียบกับ WT ในขณะที่ E231Y มีค่าแอกทีวิตีในการโยกย้ายหมู่ไกลโคซิลสูง ซึ่งแสดงให้เห็นว่า P228 และ E231 มีความสำคัญต่อปฏิกิริยาการโยกย้ายหมู่ไกลโคซิล จากการผลิตไซโคลเด็กซ์ทรินชนิดวงใหญ่เป็นเวลา 12 ชั่วโมง พบว่า เอนไซม์ดั้งเดิมจะให้ผลิตภัณฑ์หลักไซโคลเด็กซ์ทรินชนิดวงใหญ่ที่มีขนาด 27 โมเลกุลกลูโคส ในขณะที่ผลิตภัณฑ์หลักที่ได้จาก P228Y, E231Y, A413F และ G417F มีขนาด CD36, CD25, CD38 และ CD32 ตามลำดับ จากการทำ Molecular dynamic (MD) simulation แสดงให้เห็นถึงตำแหน่งกรดอะมิโน Y418, M474, L510, F534, Y23, R458, Q423, T666, Q475, L236, Q421, E231, Q420, N419 และ Y235 ที่น่าจะมีปฏิสัมพันธ์กับไซโคลเด็กซ์ทรินชนิดวงใหญ่

ภาควิชา ชีวเคมี

ลายมือชื่อนิสิต

สาขาวิชา ชีวเคมีและชีววิทยาโมเลกุล

ลายมือชื่อ อ.ที่ปรึกษาหลัก

ปีการศึกษา 2559

ลายมือชื่อ อ.ที่ปรึกษาร่วม

ลายมือชื่อ อ.ที่ปรึกษาร่วม

5772180123 : MAJOR BIOCHEMISTRY AND MOLECULAR BIOLOGY

KEYWORDS: AMYLOMALTASE / LARGE-RING CYCLODEXTRIN /
CORYNEBACTERIUM GLUTAMICUM / MD SIMULATION

SIRIKUL NGAWISET: ENZYMATIC AND COMPUTATIONAL ANALYSIS OF
LARGE-RING CYCLODEXTRIN PRODUCTION BY *Corynebacterium
glutamicum* AMYLOMALTASE. ADVISOR: ASST. PROF. KUAKARUN
KRUSONG, Ph.D., CO-ADVISOR: PROF. PIAMSOOK PONGSAWASDI, Ph.D.,
THANYADA RUNGROTMONGKOL, Ph.D., 144 pp.

Amylomaltase is a well-known glucanotransferase enzyme that can produce large-ring cyclodextrins (LR-CDs) via cyclization reaction. To determine important amino acid residues involved in LR-CDs production of amylomaltase from *Corynebacterium glutamicum* (CgAM), mutations at CA I and CA II subdomains were introduced by site-directed mutagenesis. P228Y, E231Y, A413F and G417F CgAM mutants were constructed from CgAM recombinant plasmid. The optimum pH and temperature of WT and mutants were around pH 6.0 - 7.5 and 25 - 35°C. The mutations did not affect the pH and temperature stability. In addition, WT and all mutated enzymes have Maltotriose (G3) as the best substrate for disproportionation activity. A413F possessed much lower specific activities of transglycosylation, starch degradation, disproportionation and cyclization activities than the WT enzyme. P228Y, E231Y and G417F exhibited similar specific activities of starch transglycosylation and starch degradation to the wild-type CgAM. P228Y had much lower disproportionation activity than the wild-type enzyme, while E231Y displayed higher disproportionation activity. This suggested that P228 and E231 of CgAM may play an important role in disproportionation. At 12 h, wild-type CgAM gave the principle CD of 27, whilst the principal product of P228Y, E231Y, A413F and G417F were CD36, CD25, CD38, and CD32, respectively. Molecular dynamic (MD) simulation showed that Y418, M474, L510, F534, Y23, R458, Q423, T666, Q475, L236, Q421, E231, Q420, N419 and Y235 might interact with LR-CDs.

Department:	Biochemistry	Student's Signature
Field of Study:	Biochemistry and Molecular Biology	Advisor's Signature
		Co-Advisor's Signature
Academic Year:	2016	Co-Advisor's Signature

ACKNOWLEDGEMENTS

First of all, I would like to say deeply gratitude to my advisor, Assistant Professor Kuakarun Krusong, for her advices, guidance and all supports to me in every single detail about this thesis. In addition, this is also including my co-advisor, Professor Piamsook Pongsawasdi and Dr. Thanyada Rungrotmongkol, who give a valuable comment and support me.

Second, sincerely thanks and appreciation are to Assistance Professor Kanoktip Packdibamrung, Assistance Professor Manchumas Prousoontorn and Associate Professor Jarunee Kaulpiboon for their valuable suggestion and comment and dedication of their valuable time for thesis examination.

Third, thank you to member in 705 room for their help and support. This thank also to Starch and Cyclodextrin Research Unit and Structural and Computational Biology Research Group.

Forth, thanks to Chulalongkorn University Graduate Scholarship to commemorate the 72nd Anniversary of His Majesty King Bhumibala Aduladeja for financial support. Moreover, the Overseas Research Experience Scholarship for Graduate student from the Graduate School and Department of Biochemistry, the Faculty of Science, Chulalongkorn University, Thailand, supported me for a short-term research visit at Graduate school of Agriculture, Meiji University, Japan.

This research was funded by the 90th Anniversary Chulalongkorn University Scholarship (Ratchadaphiseksomphot Endowment Fund) and partially supported by the TRF Grant IRG 5780008 and Structural and Computational Biology Research Group, Special Task Force for Activating Research (STAR), Faculty of Science, Chulalongkorn University. The Asahi Glass Foundation was also supported this research.

Finally, I would like to say thanks to my family for support and cheer me up all the time when I have got a problem or I was tired. This is valuable for me to go through all tasks and finish my master degree.

CONTENTS

	Page
THAI ABSTRACT	iv
ENGLISH ABSTRACT.....	v
ACKNOWLEDGEMENTS	vi
CONTENTS.....	vii
LIST OF FIGURES	xiii
LIST OF TABLES	xvi
ABBREVIATIONS	xvii
CHAPTER I.....	1
INTRODUCTION	1
1.1 Starch converting enzymes of α -amylase family	1
1.2 Amylomaltase.....	5
1.3 Reaction of amylomaltase	5
1.4 Applications of amylomaltase	7
1.5 Large ring cyclodextrins (LR-CDs)	8
11	
1.6 Large ring cyclodextrins application.....	12
1.7 <i>Corynebacterium glutamicum</i>	13
1.8 Amylomaltase from <i>Corynebacterium glutamicum</i>	13
1.9 Structure of <i>Corynebacterium glutamicum</i> amylomaltase.....	16
1.10 Improvement the properties of CgAM	22
1.11 Objectives.....	23
CHAPTER II.....	24
MATERIALS AND METHODS.....	24
2.1 Equipment	24
2.2 Chemicals	26
2.3 Enzymes, Restriction enzymes and Bacterial strains	28
2.4 Site-directed mutagenesis of P228Y, A413F and G417F mutants.....	29
2.4.1 Primer design.....	29

	Page
2.4.2 Amplification of mutated <i>CgAM</i> genes (P228Y, A413F and G417F) by PCR.	30
2.4.3 Restriction enzyme digestion	32
2.4.4 Plasmid transformation.....	32
2.4.5 Extraction of recombinant plasmid	32
2.4.6 Agarose gel electrophoresis.....	33
2.4.7 DNA sequencing	33
2.4.8 Preparation of competent cells	36
2.5 Optimization of mutated <i>CgAM</i> gene expression.....	36
2.6 Purification of mutated <i>CgAMs</i>	37
2.6.1 Purification of E231Y via DEAE FF™ and Phenyl FF™ column chromatography	37
2.6.1.1 DEAE FF™ column chromatography	37
2.6.1.2 Phenyl FF™ column chromatography.....	37
2.6.2 Purification of P228Y, A413F and G417F by HisTrap FF column	38
2.7 Protein determination	38
2.7.1 Determination of protein concentration.....	38
2.7.2 Sodium dodecyl sulfate polyacrylamide gel electrophoresis (SDS-PAGE)	39
2.7.3 Coomassie blue staining.....	39
2.8 Characterization of mutated amyloamylase	39
2.8.1 Enzyme assay	39
2.8.1.1 Starch transglycosylation activity.....	39
2.8.1.2 Starch degradation activity	40
2.8.1.3 Disproportionation activity.....	40
2.8.1.4 Cyclization activity.....	41
2.8.1.5 Coupling activity	41
2.8.1.6 Hydrolytic activity	42
2.8.2. Effect of temperature on <i>CgAM</i> activity.....	42

	Page
2.8.3 Effect of temperature on <i>CgAM</i> stability	43
2.8.4 Effect of pH on <i>CgAM</i> activity	43
2.8.5 Effect of pH on <i>CgAM</i> stability	43
2.8.6 Substrate specificity of <i>CgAM</i>	43
2.8.7 Circular dichroism spectra.....	44
2.8.8 Synthesis and analysis of large-ring cyclodextrins (LR-CDs)	44
2.8.9. Determination of kinetic parameters of <i>CgAM</i>	45
2.8.9.1 Kinetic parameters of starch transglycosylation activity..	45
2.8.9.2 Kinetic parameters of disproportionation activity	45
2.8.9.3 Kinetic parameters of cyclization activity	46
2.9 Computational analysis of <i>CgAM</i> and LR-CDs in complex.....	46
2.9.1 Preparation of <i>CgAM</i> and oligosaccharides structure.....	46
2.9.2 Prediction 3-dimensional structure by docking.....	46
2.9.3 Initial models and system preparation for molecular dynamic simulation	47
2.9.4 Interaction analysis via molecular dynamic simulation (MD simulation)	47
2.9.5 The root-mean square displacement (RMSD) and hydrogen bond (H-bond)	48
2.9.6 Binding Free Energy.....	48
2.9.7 Decomposition Free Energy	49
CHAPTER III	51
RESULTS	51
3.1 Cloning of mutated <i>CgAM</i> genes.....	51
3.2 Optimization of <i>CgAM</i> gene expression.....	53
3.3 Large scale production of <i>CgAMs</i> and preparation of <i>CgAM</i> crude extract	59
3.4 Purification of mutated <i>CgAMs</i>	59
3.4.1 Purification of E231Y by DEAE and phenyl column chromatography	59

	Page
3.4.1.1 DEAE FF™ column chromatography	59
3.4.1.2 Phenyl FF™ column chromatography.....	59
3.4.2 Purification of P228Y, A413F and G417F by His trap column chromatography	61
3.5 Characterization of WT and mutated <i>Cg</i> AMs.....	66
3.5.1 Enzyme assay	66
3.5.1.1 Starch Transglycosylation activity	66
3.5.1.2 Starch degradation activity	66
3.5.1.3 Disproportionation activity.....	66
3.5.1.4 Cyclization activity	66
3.5.1.5 Coupling activity	67
3.5.1.6 Hydrolytic activity	67
3.5.2 Effect of temperature on starch transglycosylation activity	69
3.5.3 Effect of temperature on starch transglycosylation stability	70
3.5.4 Effect of pH on starch transglycosylation activity	71
3.5.5 Effect of pH on starch transglycosylation stability	72
3.5.6 Substrate specificity of <i>Cg</i> AM	73
3.5.7 Enzyme conformation	75
3.5.8 Synthesis of large-ring cyclodextrins	76
3.5.9 Determination of kinetic parameters	80
3.5.9.1 starch transglycosylation activity	80
3.5.9.2 disproportionation activity.....	80
3.5.9.3 cyclization activity.....	80
3.6 Computational analysis	82
3.6.1 Preparation amyloamylase and oligosaccharides structure	82
3.6.2 Prediction 3-dimensional structure by molecular docking.....	84
3.6.3 Interaction analysis using molecular dynamic (MD) simulation	86
3.6.3.1 Starting models and system preparation.....	86
3.6.3.2 Molecular dynamics (MD) simulations.....	87

	Page
3.6.3.3 Stability of global structures	87
3.6.3.4 Flexibility of protein structure	90
3.6.3.5 Hydrogen bond interactions.....	93
3.6.3.6 Key residues of ligand binding.....	96
CHAPTER IV	100
DISCUSSIONS.....	100
4.1 Site-directed mutagenesis of amyloamylase gene (P228Y, E231Y, A413F and G417F).....	100
4.2 Condition for mutated amyloamylase gene expression.....	103
4.3 Purification of mutated amyloamylase.....	103
4.3.1 E231Y.....	103
4.3.2 P228Y, A413F and G417F.....	104
4.4 Characterization of WT and mutated <i>CgAM</i> enzymes	104
4.4.1 Enzyme assay	104
4.4.2 Effect of temperature and pH on starch transglycosylation activity	105
4.4.3 Effect of temperature and pH on starch transglycosylation stability	106
4.4.4 Substrate specificity of amyloamylase.....	106
4.4.5 Enzyme conformation	107
4.5 Synthesis of large-ring cyclodextrins	107
4.6 Determination of kinetic parameters	108
4.6.1 Starch transglycosylation activity.....	108
4.6.2 Disproportionation activity.....	109
4.6.3 Cyclization activity.....	109
4.7 Computational analysis	111
CHAPTER V	114
CONCLUSIONS	114
REFERENCES	116

	Page
Appendix 1	132
Preparation for Sodium Dodecyl Sulfate-Polyacrylamide Gel Electrophoresis (SDS-PAGE)	132
Appendix 2	135
Preparation of Iodine solution	135
Appendix 3	136
Preparation of DNS reagent	136
Appendix 4	137
Preparation of bicinchoninic acid reagents	137
Appendix 5	138
Restriction map of pET-17b (Novagen)	138
Appendix 6	139
Restriction map of pET-19b (Novagen)	139
Appendix 7	140
Standard curve for protein determination by Bradford assay	140
Appendix 8	141
Standard curve for starch determination by starch degradation assay	141
Appendix 9	142
Standard curve for glucose determination by glucose oxidase assay	142
Appendix 10	143
Amino acid reference chart	143
VITA	144

LIST OF FIGURES

Figure		Page
1.1	Different enzyme involved in the degradation of starch	4
1.2	Schematic representation of amyloamylase catalyzed reactions	6
1.3	Structures of α -, β -, and γ -cyclodextrin	9
1.4	Solid state structures of CD14 and CD26	10
1.5	^{13}C -NMR chemical shifts and predicted conformation of cyclodextrin	11
1.6	Amyloamylase amino acids sequence alignment of <i>SP Streptococcus pneumoniae</i> (AAA26923.1), <i>TF Thermus filiformis</i> (AKR04336.1), <i>TA Thermus aquaticus</i> (EED09753.1), <i>TT Thermus thermophiles</i> (BAA33728.1), <i>CG Corynebacterium glutamicum</i> (AKR04335.1) and <i>EC Escherichia coli</i> (CDZ22191.1)	14
1.7	HPAEC analysis of LR-CDs synthesized by amyloamylase from <i>C. glutamicum</i>	15
1.8	Top view and side view of a triosephosphateisomerase (TIM) barrel	18
1.9	Structural comparison of <i>CgAM</i> with <i>EcMalQ</i> , <i>TtAM</i> , and <i>AtDPE1</i>	19
1.10	Overall structure of <i>CgAM</i>	20
1.11	Amino acid sequence alignment of amyloamylases from <i>C. glutamicum</i> (<i>CgAM</i>), <i>E. coli</i> (<i>EcMalQ</i>), <i>Aquifex aeolicus</i> (<i>AaAM</i>), <i>T. thermophilus</i> (<i>TtAM</i>), and disproportionating enzyme 1 from <i>A. thaliana</i> (<i>AtDPE1</i>)	21
3.1	Agarose gel electrophoresis of PCR product of mutated <i>CgAM</i> genes	51

3.2	Multiple sequence alignment of WT, P228Y, E231Y, A413F and G417F sequences using Clustal W tool	52
3.3	SDS-PAGE analysis of expression level of P228Y CgAM in BL21 (DE3) using 1 mM IPTG for induction	55
3.4	SDS-PAGE analysis of expression level of A413F CgAM in BL21 (DE3) using 1 mM IPTG for induction at various temperature	56
3.5	SDS-PAGE analysis of expression level of G417F CgAM in BL21 (DE3) using 1 mM IPTG for induction at various temperature	57
3.6	SDS-PAGE analysis of expression level of G417F CgAM in BL21 (DE3) with 1% glucose using 1mM IPTG for induction at various temperature	58
3.7	SDS-PAGE analysis of WT CgAM and E231Y CgAM	60
3.8	Purification profile of mutated CgAMs by HisTrap column chromatography	62
3.9	SDS-PAGE analysis of purified mutated CgAMs by HisTrap column	63
3.10	Effect of temperature on starch transglycosylation activity	69
3.11	Effect of temperature on CgAM stability assayed by starch transglycosylation	70
3.12	Effect of pH on starch transglycosylation activity	71
3.13	Effect of pH on CgAM stability assayed by starch transglycosylation	72
3.14	Substrate specificity WT and mutated CgAMs assayed by disproportionation activity	73
3.15	Circular dichroism spectra of CgAMs	75

3.16	LR-CDs product patterns, analyzed by HPAEC-PAD, <i>CgAMs</i> of 0.05 U starch degradation activity were incubated with pea starch at various incubation times	78
3.17	<i>CgAM</i> crystal structure and oligosaccharides (G1 - G11) both linear and cyclic conformation	83
3.18	Docking complex between <i>CgAM</i> and G11 via SwissDock web server	85
3.19	<i>CgAM</i> in complex with ligand for MD simulation	86
3.20	RMSD plots for the complex atoms of <i>CgAM</i> in complex with CD25 and CD28	88
3.21	Binding site of <i>CgAM</i> in complex with CD28	89
3.22	Root-mean square fluctuations (RMSFs) for all amino acids in <i>CgAM</i> from MD simulation	91
3.23	B-factor analysis for <i>CgAM</i> in complex with CD25 and CD28	92
3.24	Hydrogen bond occupation between the twenty-five glucose units and twenty-eight glucose units	94
3.25	Per-residue decomposition free energy obtained from MM/PBSA calculation for <i>CgAM</i> in complex with CD25 and CD28	99
4.1	Amylomaltase amino acids sequence alignment of other organisms and <i>Corynebacterium glutamicum</i>	102

LIST OF TABLES

Table	Page
1.1 Characteristics of the activities of each type of 4 α GTase	4
1.2 Physicochemical properties of cyclodextrin	12
1.3 The four conserved regions and the corresponding β -sheets found in the amino acid sequence of α -amylase family enzymes	18
2.1 Primers for site-directed mutagenesis	29
2.2 PCR steps for amplification of P228Y and G417F <i>CgAM</i> genes	31
2.3 PCR steps for amplification of A413F <i>CgAM</i> genes	31
2.4 Primers for DNA sequencing	35
2.5 PCR steps for amplification of gene for DNA sequencing	35
3.1 Expression condition of WT and <i>CgAM</i> mutated enzymes	54
3.2 Purification table of WT and mutated <i>CgAMs</i>	64
3.3 Summary of purification conditions for <i>CgAM</i> mutants	65
3.4 Specific activity of WT and mutated <i>CgAMs</i>	68
3.5 Biochemical characteristics of WT and 4 mutant <i>CgAMs</i>	74
3.6 Percentage of secondary structure composition of <i>CgAMs</i> estimated by K2D3 program	75
3.7 The principal product of LR-CDs for WT and all mutants	77
3.8 Kinetic parameters of WT and <i>CgAM</i> mutants	81
3.9 The results from MM/PBSA approach giving the energy components and average binding free energies for both complexes	98

ABBREVIATIONS

A	absorbance
APS	ammonium persulfate
atm	atmosphere
BSA	bovine serum albumin
°C	degree Celsius
C	carbon
CA	cycloamylose
CD	cyclodextrin
CgAM	<i>Corynebacterium glutamicum</i> amylomaltase
CGTase	cyclodextrin glycosyltransferase
cm	centimeter
D-enzyme	disproportionating enzyme
DEAE	diethylaminoethyl
DNS	3,5-dinitrosalicylic acid
DMSO	dimethyl sulfoxide
<i>E. coli</i>	<i>Escherichia coli</i>
g	gram
GDE	glycogen debranching enzyme

HCl	hydrochloric
HPAEC-PAD	High-Performance Anion-Exchange Chromatography with Pulsed Amperometric Detection
h	hour
I ₂	iodine
IMOs	isomalto-oligosaccharides
K	Kelvin
KI	potassium iodide
<i>k_{cat}</i>	turnover number
<i>K_m</i>	Michaelis constant
LR-CDs	large-ring cyclodextrins
l	litre
M	molar
mA	milliampere
mg	milligram
min	minute
ml	millilitre
mM	millimolar
NaOH	sodium hydroxide

NMR	nuclear magnetic resonance spectroscopy
PAGE	polyacrylamide gel electrophoresis
PCR	polymerase chain reaction
PGs	palatinose glucosides
rpm	round per minute
SDS	sodium dodecyl sulfate
TEMED	tetramethyl ethylenediamine
U	unit enzyme
WT	wild-type
4 α GTase	4- α -glucanotransferase
μ g	microgram
μ l	microlitre
μ M	micromolar

CHAPTER I

INTRODUCTION

1.1 Starch converting enzymes of α -amylase family

Starch converting enzymes are used in a number of industrial applications for starch hydrolysis. For example, starch converting enzyme was applied to the production of maltodextrin, modification of starches, or glucose and fructose syrups, laundry and porcelain detergent including as anti-staling agents in baking (Van Der Maarl et al., 2002). There are several starch converting enzymes that can degrade starch (Figure 1). Basically, starch converting enzymes are classified into 4 groups (Van Der Maarl et al., 2002).

1. Endoamylases

Endoamylases cleave α -1,4 glycosidic bond which presented in the inner part (endo-) of amylose or amylopectin chain. The well-known enzyme of this group is α -amylase (EC 3.2.1.1).

2. Exoamylases

Exoamylases cleave α -1,4 glycosidic bond like endoamylases but it can also cleave both α -1,4 and α -1,6 glycosidic bond. Exoamylases act on the external glucose residues of amylose or amylopectin. Examples for this group are β -amylase (EC 3.2.1.2), amyloglucosidase or glucoamylase (EC 3.2.1.3) and α -glucosidase (EC 3.2.1.20). β -amylase and glucoamylase was capable in converting the anomeric configuration of the liberated maltose from α to β . Moreover, glucoamylase preferred to hydrolyze the long chain oligosaccharide while α -glucoamylase was favored to hydrolyze the short oligosaccharide.

3. Debranching enzymes

Debranching enzymes can hydrolyze α -1,6 glycosidic bond. Isoamylase (EC 3.2.1.68) and pullulanase type I (EC 3.2.1.41) are enzymes in this group. The activity that was different in isoamylase and pullulanase was hydrolytic activity for degrading pullulan and polysaccharide with repeating unit of maltotriose. For isoamylase, it can hydrolyze the α -1,6-amylopectin but cannot degrade pullulan whereas pullulanase can hydrolyze both of α -1,6- glycosidic bond in pullulan and amylopectin (Van Der Maarl et al., 2002).

4. Transferases

Transferases are the fourth group of starch converting enzymes which can break α -1,4 glycosidic bond from donor molecule and transfer resulting glucan to acceptor molecule, forming a new glycosidic linkage. Transferase or 4- α -glucanotransferase (4 α GTase) is divided into 5 types (Table 1.1);

- Type I: cyclodextrin glycosyltransferase (CGTase) (EC 2.4.1.19). This group is well known for cyclodextrins synthesis. Glucose is the smallest acceptor and transfer unit.
- Type II: amylomaltase and disproportionating enzyme (D-enzyme) (EC 2.4.1.25). Amylomaltase was found in bacteria while D-enzyme was found in plant. The smallest donor and acceptor molecule for D-enzyme is maltotriose and glucose, respectively. The transfer glucan is maltose unit. For amylomaltase, it catalyzes glycosyl transfer. Amylomaltase can use maltose as a donor molecule but maltotriose is more favorable.
- Type III: glycogen debranching enzyme (GDE) (EC 3.2.1.33 and EC 2.4.1.25). This group is bifunctional between amylo-1,6-glucosidase and 4 α GTase activities.

- Type IV and V: other 4 α GTase. For type IV, it included the 4 α GTase that found in hyper-thermophilic bacterium such as *Thermotoga maritima* while type V was found independently in the hyper-thermophilic archaea such as *Thermococcus litoralis* and *Pyrococcus* sp. KOD1. Enzymes in both groups can catalyzed the disproportionation activity and give maltose as a product (Takaha and Smith, 1999, Van Der Maarl et al., 2002).



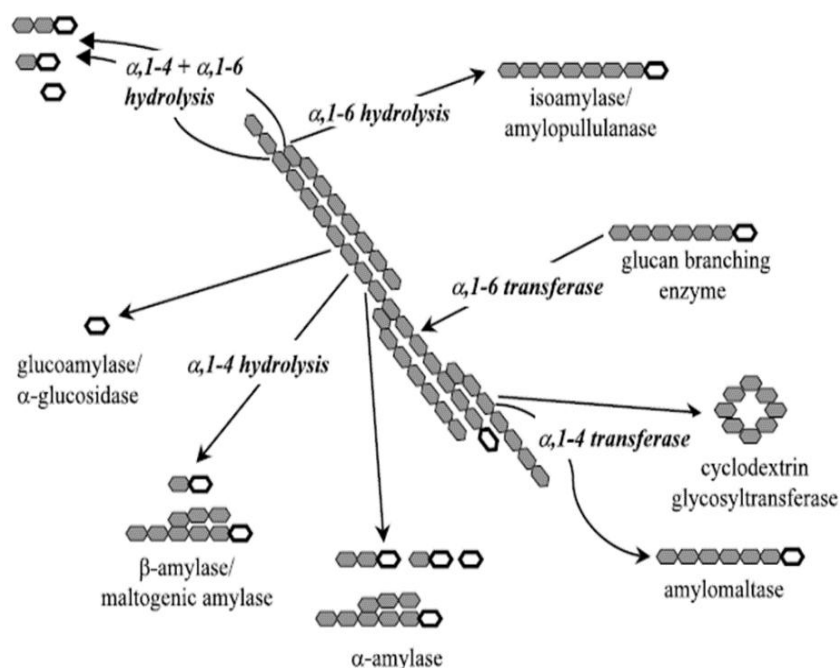


Figure 1.1 Different enzyme involved in the degradation of starch. The open ring structure symbolizes the reducing end of a polyglucose molecule (Van Der Maarl et al., 2002).

Table 1.1 Characteristics of the activities of each type of 4 α GTase (Takahashi and Smith, 1999).

4 α GTase	Strain	Smallest donor	Smallest acceptor	Smallest transferred unit	Disproportionated products	Cyclisation reaction	Smallest CA (DP)	References
Type I	<i>B. subtilis</i> 313	G4	nt	nt	G2,G3,Gn	+	8	Kato and Horikoshi (1986)
	<i>B. ohbensis</i>	G3	G	G	G,G2,G3,Gn	+	7	Kitahata (1995)
	<i>B. macerans</i>	G3	G	G	G,G2,G3,Gn	+	6	Kitahata (1995)
	<i>B. megaterium</i>	G2	G	G	G,G2,G3,Gn	+	6	Kitahata (1995)
Type II	Potato	G3	G	G2	G, G3,Gn	+	17	Takahashi et al. (1993, 1996)
	Barley	G3	G	G2	G, G3,Gn	nt		Yoshio et al. (1986)
	Sweet potato	nt	nt	G2	G, G3,Gn	nt		Suganuma et al. (1991)
	<i>C. butyricum</i>	G3	G	G	G,G2,G3,Gn	nt		Goda et al. (1997)
	<i>E. coli</i> ML308	G3	G	G	G,G2,G3,Gn	nt		Palmer et al. (1976)
	<i>E. coli</i> ATCC3806	G2	G	G	G,G2,G3,Gn	nt		Kitahata et al. (1989a)
	<i>E. coli</i> K12	G2	G	G	G,G2,G3,Gn	+	17	Unpublished
<i>T. aquaticus</i>	G2	G	G	G,G2,G3,Gn	+	22	Unpublished	
Type III	Yeast	G4	G3	G2	G2,G3,Gn	nt		Tabata and Ide (1988)
Type IV	<i>T. maritima</i>	G4	G2	G2	G2,G3,Gn	nt		Liebi et al. (1992)
Type V	<i>T. litoralis</i>	G2	G	G	G,G2,G3,Gn	+	nt	Jeon et al. (1997)
	<i>Pyrococcus</i> KOD1	G2	G	G	G,G2,G3,Gn	nt		Tachibana et al. (1987)
Others	<i>S. mitis</i>	G2	G	G	G,G2,G3,Gn	nt		Walker (1966)
	<i>S. bovis</i>	G3	G	G	G,G2,G3,Gn	nt		Walker (1965)
	<i>B. subtilis</i>	G4	G4	G2	G2,G3,Gn	nt		Pazur and Okada (1968)
	<i>S. mutans</i>	G2	G	G	G,G2,G3,Gn	nt		Medda and Smith (1984)

nt = not tested. G, G1, G2, Gn = glucose, maltose, maltotriose, etc. Organism names are given in the text.

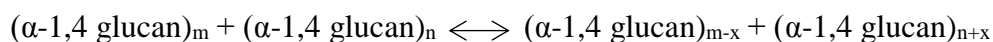
1.2 Amylomaltase

Amylomaltase (EC 2.4.1.25), which is classified in type II 4 α GTase, was first found in *Escherichia coli* as a maltose-inducible enzyme which is essential for maltose metabolism (Takahashi and Smith, 1999). Since then, amylomaltase enzymes were cloned from various organisms for characterization and determined the 3D structures including *E. coli* (Palmer et al., 1976, Pugsley and Dubreuil, 1988, Weiss et al., 2015), *Thermus aquaticus* (Terada et al., 1999, Przytylski et al., 2000a, Przytylski et al., 2000b), *Thermus brokianus* (Bang et al., 2006, Jung et al., 2011), *Thermus thermophilus* (Watanasatitarpaporn et al., 2014), *Thermus filiformis* (Kaewpathomsri et al., 2015) and *Corynebacterium glutamicum* (Srisimararat et al., 2010).

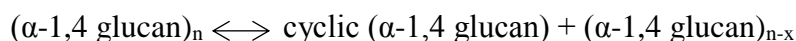
1.3 Reaction of amylomaltase

Amylomaltase transfer a glycosyl unit to acceptor using maltose or maltotriose as a smallest donor molecule. As belonging 4 α GTase, amylomaltase can catalyze both inter and intra molecular glucan transfer reactions which are shown in the following equation (Takahashi and Smith, 1999);

- An inter molecular transglycosylation: hydrolysis and disproportionation reaction



- An intra-molecular transglycosylation: cyclization and coupling reaction



Main 4 reactions of amylomaltase are summarized in Figure 1.2 (Van Der Veen et al., 2000).

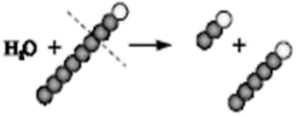
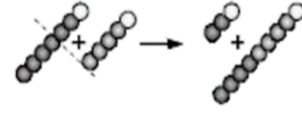
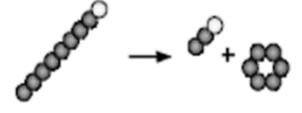
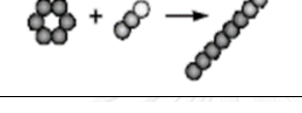
Reaction	Schematic	Action
Hydrolysis		starch \rightarrow oligosaccharides
Disproportionation		$(\alpha\text{-1,4 glucan})_m + (\alpha\text{-1,4 glucan})_n$ \downarrow $(\alpha\text{-1,4 glucan})_{m-x} + (\alpha\text{-1,4 glucan})_{n+x}$
Cyclization		starch \rightarrow oligosaccharide + cyclodextrin
Coupling		oligosaccharide + cyclodextrin \rightarrow starch

Figure 1.2 Schematic representation of amylomaltase catalyzed reactions. The circles represent glucose residues; the white circles indicate the reducing end sugars. (Van Der Veen et al., 2000)

1.4 Applications of amyloamylase

Amyloamylase can be used in many applications such as thermoreversible starch gel production (Takaha and Smith, 1999), isomalto-oligosaccharides production (Lee et al., 2002) and cycloamylose (CA) production (Van Der Maarl et al., 2002).

For thermoreversible starch gel production, starches were treated by amyloamylase in proper condition. After that, the modified starches show a thermo-reversible gelling behavior (Van Der Maarel et al., 2005). This production is interesting for commercial food industry because this product can be used to substitute gelatin, a product derived from the bone marrow of cows, for vegetarian foods (Kaper et al., 2004). This modified starch can be dissolves in water and formed a firm gel after heating and cooling and it can be dissolved again when it has a new heating step (Kaper et al., 2004, Kaper et al., 2005, Lee et al., 2006, Hansen et al., 2008). Modified cassava starch is an example for modified starch (Suriyakul Na Ayudhaya et al., 2016). Moreover, starch modified can be used to improve the properties of food product such as improvement creaminess of low-fat yoghurt (Alting et al., 2009) and combination with xanthan gum for fat substitution in reduced-fat mayonnaise (Mun et al., 2009).

A second application is isomalto-oligosaccharides (IMOs) production. IMOs are produced from starch using combination between maltogenic amylase from *Bacillus stearothermophilus* and α -glucanotransferase from *Thermotoga maritima*. Syrups from IMOs, which have a low viscosity and reduced sweetness including non digestible, can be applied as a substitute sugar for diabetics, to improve the intestinal microflora, or to prevent dental caries (Lee et al., 2002) e.g. palatinose glucosides

(PGs) synthesis using as sucrose or palatinose in food products for health benefits (Naumthong et al., 2015).

The third application is cycloamyloses (CAs) or large ring cyclodextrins (LR-CDs) production. Amylomaltase can produce cyclic α -1,4-glucans with a degree of polymerization ranging from 17 to a few hundred (Terada et al., 1999, Kaper et al., 2004). LR-CDs can be applied in many industries such as in pharmaceuticals clinical, cosmetic, environment, food science and biotechnology (Tomono et al., 2002), (Zheng et al., 2002).

1.5 Large ring cyclodextrins (LR-CDs)

Cyclodextrins (CDs) are common name for cyclic oligosaccharides comprised of a number of α -1,4-D-glucose units. CDs were first found in 1891 from *Bacillus amylobacter* digest of potato starch. The most common and well-known CDs are α -, β - and γ - CDs which consists of 6, 7 and 8 glucose molecules, respectively (Figure 1.3) (Larsen, 2002). For LR-CDs, it consists of glucose molecules at least 9 molecules. In the previous researches, solid state structures of CD9 (Fujiwara et al., 1990, Miyazawa et al., 1995), CD10, CD14 (Saenger et al., 1998) and CD26 (Gessler et al., 1999) have been reported (Figure 1.4). Moreover, other sizes of CDs, which still have no crystal structure, were predicted using ^{13}C NMR spectroscopy (Saenger et al., 1998) including CD48 model prediction (Figure 1.5) (Larsen, 2002).

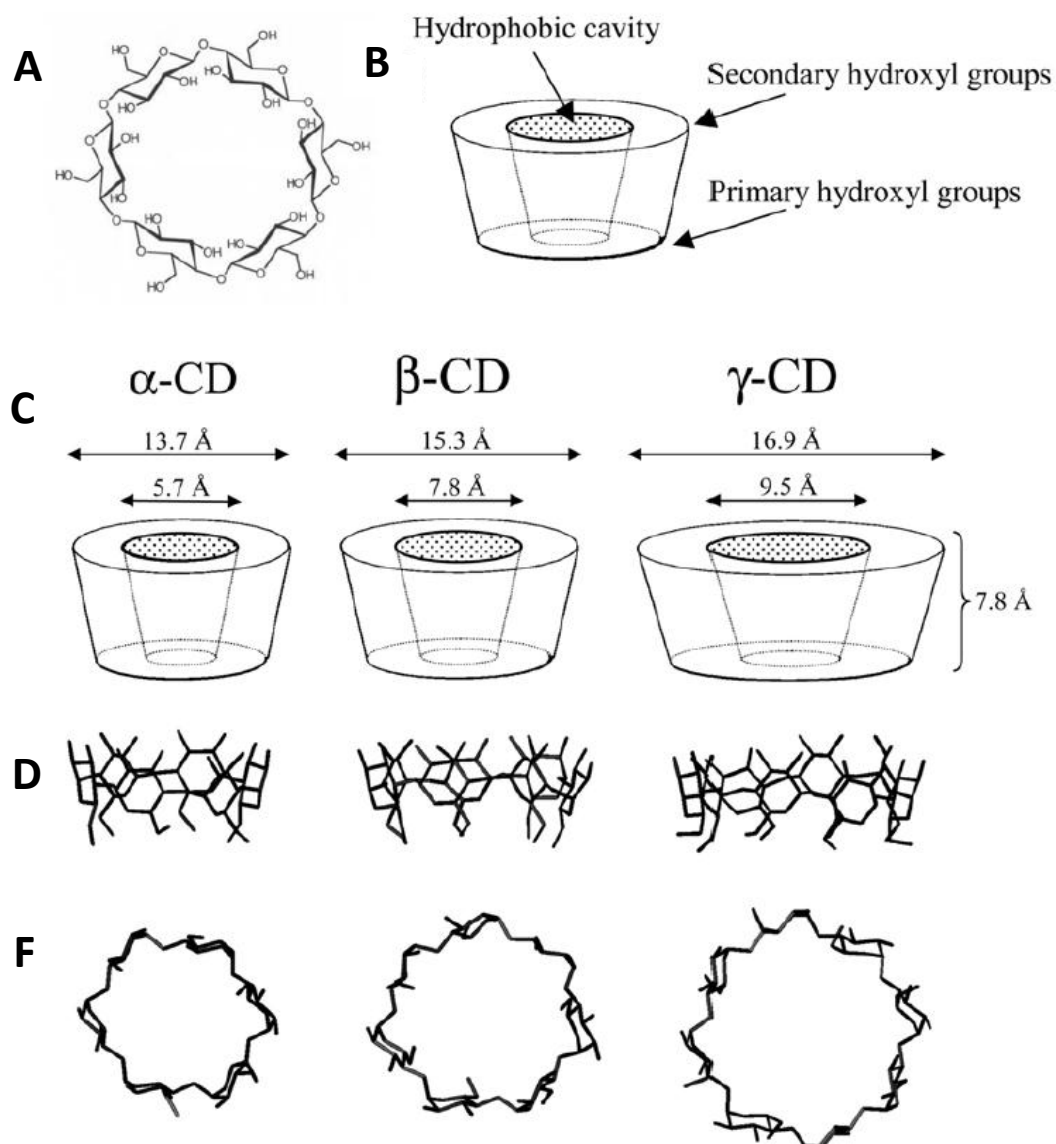


Figure 1.3 Structures of α -, β -, and γ -cyclodextrin (Larsen, 2002).

A: Schematic presentation of α -cyclodextrin.

B: Basic graphical illustration of a cyclodextrin. A hollow truncated cone is often used to illustrate cyclodextrins, where the C6 primary hydroxyl groups crown the narrow rim and the C2 and C3 secondary hydroxyl groups crown the wide rim.

C: Approximate molecular dimensions of α -, β -, and γ -cyclodextrin.

D: Side view of α -, β -, and γ -cyclodextrin stick models.

E: Stick models of α -, β -, and γ -cyclodextrin viewed from the wide rim.

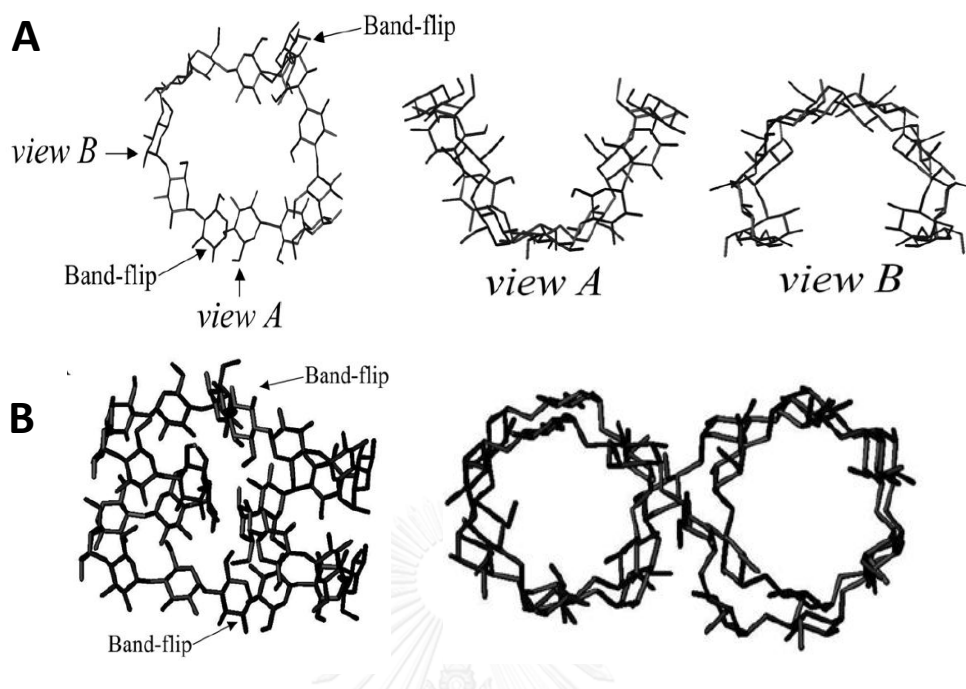
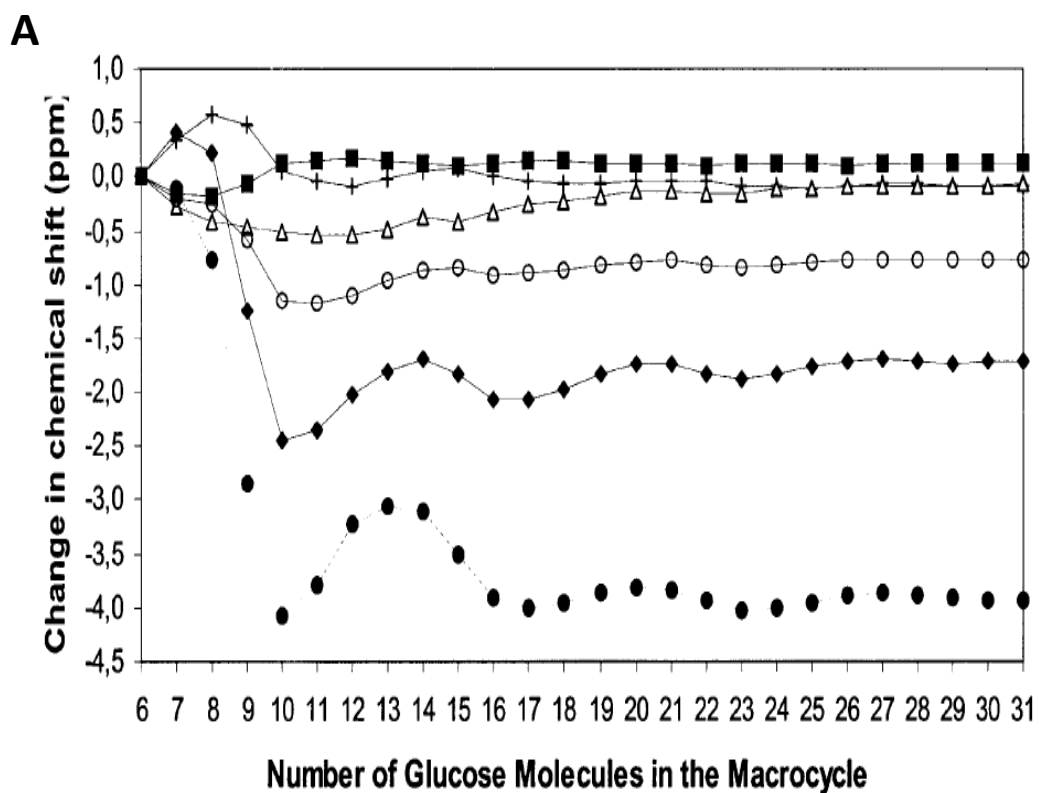


Figure 1.4 Solid state structures of CD14 and CD26.

A: Structure of CD14 indicating the position of the band-flips.

B: Structure of CD26 indicating the position of the band-flips and the V-amylose like segments (left) and CD26 viewed from the top (right). Modified from Larsen (2002).



B

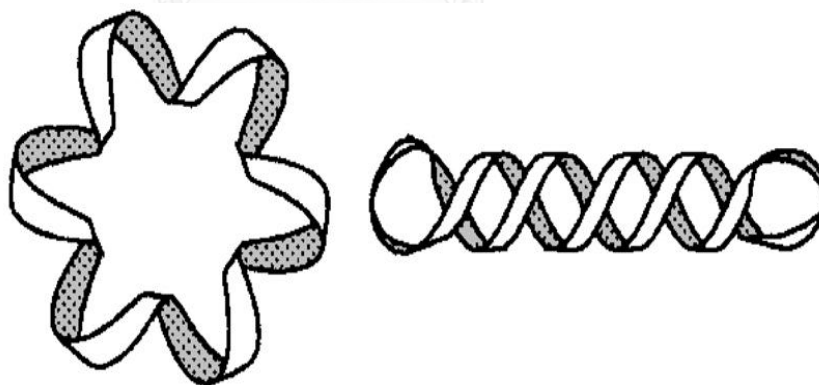


Figure 1.5 ^{13}C -NMR chemical shifts and predicted conformation of cyclodextrin. Modified from Larsen (2002).

A: Changes in ^{13}C -NMR chemical shifts of cyclodextrins relative to α -cyclodextrin. \blacklozenge : $^{13}\text{C}1$; $+$: $^{13}\text{C}2$; \diamond : $^{13}\text{C}3$; \bullet : $^{13}\text{C}4$; \circ : $^{13}\text{C}5$; \blacksquare : $^{13}\text{C}6$.

B: Schematic representations of two possible conformations of CD48. Circularized single helical form (left) and anti-parallel double helical form with fold backs at each end (right).

1.6 Large ring cyclodextrins application

LR-CDs have a high solubility in water. Its conformation was assumed like a single helical V-amylose and toroidal shape which forms hydrophobic cavity and hydrophilic outer surface (Gessler et al., 1999). This is why LR-CDs can form inclusion complexes with both organic and inorganic molecules and help to improve the properties of guest molecules such as solubility and stability (Table 1.2) (Kitamura et al., 1999, Takaha and Smith, 1999, Tomono et al., 2002, Ueda, 2002). For example, LR-CDs in complex with vitamin E acetate enhanced the solubility of the Vitamin E (Kuttiyawong et al., 2015). Therefore, LR-CDs are useful for several industries. For example, LR-CDs can be used as an artificial chaperone for protein refolding. This is for promoting proper protein folding (Machida et al., 2000). Moreover, LR-CDs can be used as a nanogel in a gene delivery system (Toita et al., 2010, Fujii et al., 2014).

Table 1.2 Physicochemical properties of cyclodextrin (Ueda, 2002).

	Number of glucopyranose units	Aqueous ^a solubility (g/100 mL)	Surface ^a tension (mN/m)	Specific rotation $[\alpha]_D^{25}$	Half-life of ^b ring opening (h)
α -CD	6	14.5	72	+147.8	33
β -CD	7	1.85	73	+161.1	29
γ -CD	8	23.2	73	+175.9	15
δ -CD	9	8.19	73	+187.5	4.2
CD ₁₀	10	2.82	72	+204.9	3.2
CD ₁₁	11	>150	72	+200.8	3.4
CD ₁₂	12	>150	72	+197.3	3.7
CD ₁₃	13	>150	72	+198.1	3.7
CD ₁₄	14	2.30	73	+199.7	3.6
CD ₁₅	15	>120	73	+203.9	2.9
CD ₁₆	16	>120	73	+204.2	2.5
CD ₁₇	17	>120	72	+201.0	2.5
CD ₁₈	18	>100	73	+204.0	3.0
CD ₁₉	19	>100	73	+201.0	3.4
CD ₂₀	20	>100	73	+199.7	3.4
CD ₂₁	21	>100	73	+205.3	3.2

^a Observed at 25 °C.

^b In 1 mol/L HCl at 50 °C.

1.7 *Corynebacterium glutamicum*

Corynebacterium glutamicum is a rod-shaped gram positive soil bacteria which is non-pathogen. *C. glutamicum* was first found in Japan in the 1957 (Kinoshita et al., 2004, Udaka, 1959, Kumagai, 2000, Vertès et al., 2005). *C. glutamicum* can produce several compounds such as amino acids, vitamins, and nucleotides including enzymes (Vertès et al., 2005). Several characteristics of *C. glutamicum* are useful in biotechnology so *C. glutamicum* is an important organism for the industrial in this field. Moreover, *C. glutamicum* can be used for bioremediation, such as for arsenic. Arsenic is a toxic metalloid that had an effect to global environment if it was contaminated to soil, water and air. *C. glutamicum* has resistant gene for arsenic so some researches aim to mutate *C. glutamicum* that was able to remove arsenic from contaminated water (Mateos et al., 2006).

1.8 Amylomaltase from *Corynebacterium glutamicum*

Amylomaltase from *Corynebacterium glutamicum* (CgAM) was firstly reported in 2010. A novel amyloamylase from *C. glutamicum* ATCC 13032 was cloned and expressed in *E. coli* BL21 (DE3). The open reading frame of amyloamylase gene was 2,121 bp which encoded 706 amino acids (Srisimararat et al., 2010). Comparing amino acid sequence with the thermostability amyloamylase from *Thermus sp.*, the identity is quite low around 20 – 25% while comparing with mesophilic amyloamylase from *E. coli* (*EcMalQ*) has 30% amino acid identity (Figure 1.6) (Srisimararat et al., 2010, Joo et al., 2016). Molecular weight of CgAM is 84 kDa. According to disproportionation activity, CgAM can transfers only a single glucose molecule from donor to acceptor molecule. CgAM can produce LR-CDs product via cyclization reaction using pea starch as a substrate. The LR-CDs mixture is in range

of CD19 – CD50. The smallest size of LR-CDs product from CgAM is CD19 while principal product is around CD24 - CD25 for 24 h incubation (Figure 1.7) (Srisimarat et al., 2010).

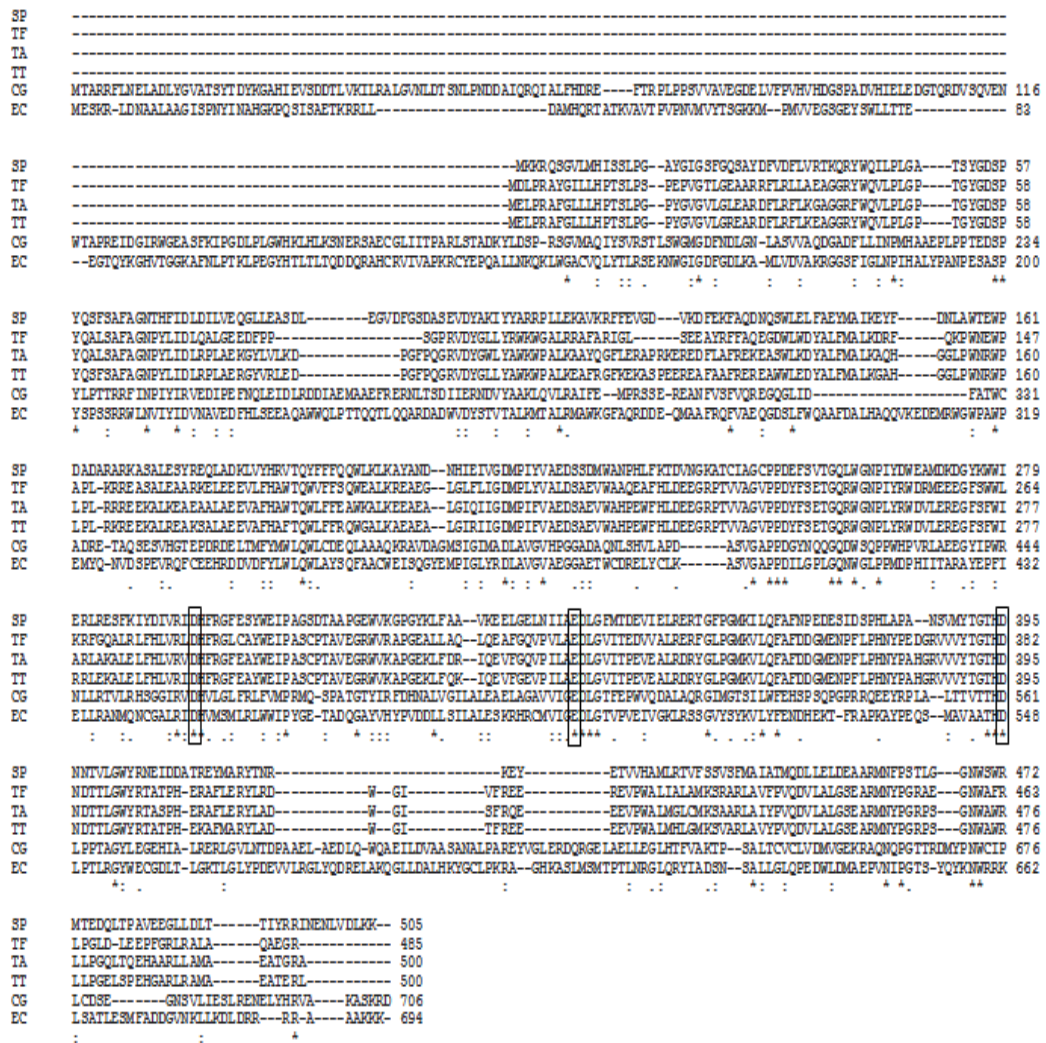


Figure 1.6 Amylo maltase amino acids sequence alignment of SP *Streptococcus pneumoniae* (AAA26923.1), TF *Thermus filiformis* (AKR04336.1), TA *Thermus aquaticus* (EED09753.1), TT *Thermus thermophilus* (BAA33728.1), CG *Corynebacterium glutamicum* (AKR04335.1) and EC *Escherichia coli* (CDZ22191.1). Catalytic residues were shown in black boxes. Positions of mutated residues were shown in red boxes. Asterisk, colon and dot across the aligned sequences were represented identical, conserved substitutions and semi-conserved substitutions, respectively (Srisimarat et al., 2010).

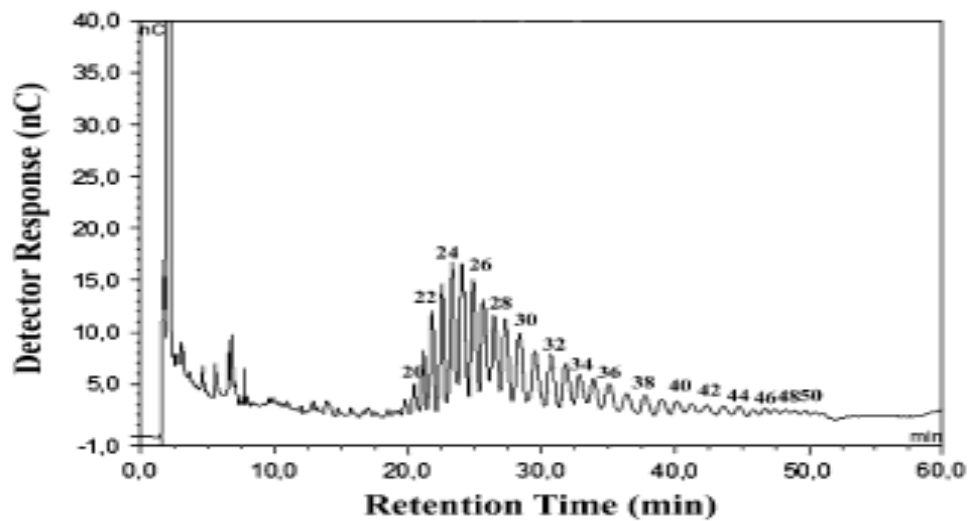


Figure 1.7 HPAEC analysis of LR-CDs synthesized by amyloamylase from *C. glutamicum* using 0.15 U/ml of enzyme incubated with 0.2% (w/v) of pea starch for 24 h (Srisimarath et al., 2010).



1.9 Structure of *Corynebacterium glutamicum* amyломaltase

In general, amyломaltase has one core domain structure which consists of $(\beta, \alpha)_8$ barrel (or called TIM barrel) fold (Figure 1.8), three catalytic residues (two Aspartic acid residues and one Glutamic acid residue) and conserved flexible loop which covered near active site (Table 1.3) (Van Der Maarl et al., 2002). Surprisingly, amyломaltase from mesophilic bacteria like *E. coli* and *C. glutamicum* has a unique subdomain which is not found in other enzyme in α -amylase superfamily (Figure 1.9) (Schmidt et al., 1998, Przylas et al., 2000b, Weiss et al., 2015, Joo et al., 2016). From CgAM crystal structure (Joo et al., 2016), it consisted of N-terminal domain (N-domain) and C-terminal domain (C-domain) (Figure 1.10). N-domain (Met1 – Arg165) is divided into two subdomains: subdomain I (N1-subdomain; Met1 – Pro72) and subdomain II (N2-subdomain; Leu73 – Arg165) (Figure 1.10 A). The N1-subdomain comprises of three α -helices, form as a bundle - like shape, and one double stranded antiparallel β -sheet which is attached to the C-domain. So, the N1-subdomain has a directed interaction with C-domain. For N2-subdomain, it consists of two four-stranded β -sheets that form a β -sandwich (Figure 1.10 B). According to independent fold of N2-subdomain, it is loosely attached to C-domain. For now, the functional of N-domain, which is a unique structural feature in CgAM, still is mysterious. For C-domain (Leu166 – Asp706), there are four subdomains: one core subdomain and three auxiliary subdomains (Figure 1.10 A, B). The center of the C-domain, which forms a TIM barrel structure, is called core subdomain or CC subdomain. In CC subdomain, there are catalytic site and the formation of the substrate-binding site occurs in this subdomain. In the active site, catalytic triad residues, which were Asp460, Glu508 and Asp561, are located on (Figure 1.10 C, D,

E). This site is involved in enzyme catalysis (Joo et al., 2016). Apart from catalytic site, CgAM also has a second glucan binding site. One of residues that involved in secondary binding site is Tyr172 (Srisimarat et al., 2012). The three auxiliary subdomains form a triangle that covers the top of the CC-subdomain (Figure 1.10 B). For three auxiliary subdomains, Auxiliary subdomain I (CA1-subdomain; Met221 – Trp358) is composed of three 3_{10} -helices and three α -helices, and is located at the edge of $(\beta/\alpha)_8^1$ and $(\beta/\alpha)_8^2$. Auxiliary subdomain II (CA2-subdomain; Val391 – Gly439 and His461 – Phe485) comprises two 3_{10} -helices and a three-stranded twisted β -sheet, and is attached to $(\beta/\alpha)_8^3$ and $(\beta/\alpha)_8^4$ of the CC-subdomain. For the first part of CA2-subdomain (Val391 – Gly439), it is claimed as a flexible lid (like 400s loop for *E. coli* (Weiss et al., 2015)) (Figure 1.11). His392 and Tyr418 are recognized that it located on the edge of the substrate binding site. Trp425 is also essential for catalytic activity from its hydrophobicity (Rachadech et al., 2015). Moreover, there are highly conserved amino acids (Figure 1.10 F). This lid has a conformation change upon substrate binding. In addition, The CA2-subdomain also has an interaction with N-domain via the N1-subdomain. The last subdomain is called auxiliary subdomain III or CA3-subdomain; Thr558 – Gly625 and Leu650 – Asn693. It consists of two 3_{10} -helices and four α -helices, which covers the edge of $(\beta/\alpha)_8^7$ and $(\beta/\alpha)_8^8$, and also contacts the CA1-subdomain. Although the CA2-subdomain is the main contributor, the auxiliary subdomains are also involved in the formation of the substrate-binding pocket (Joo et al., 2016).

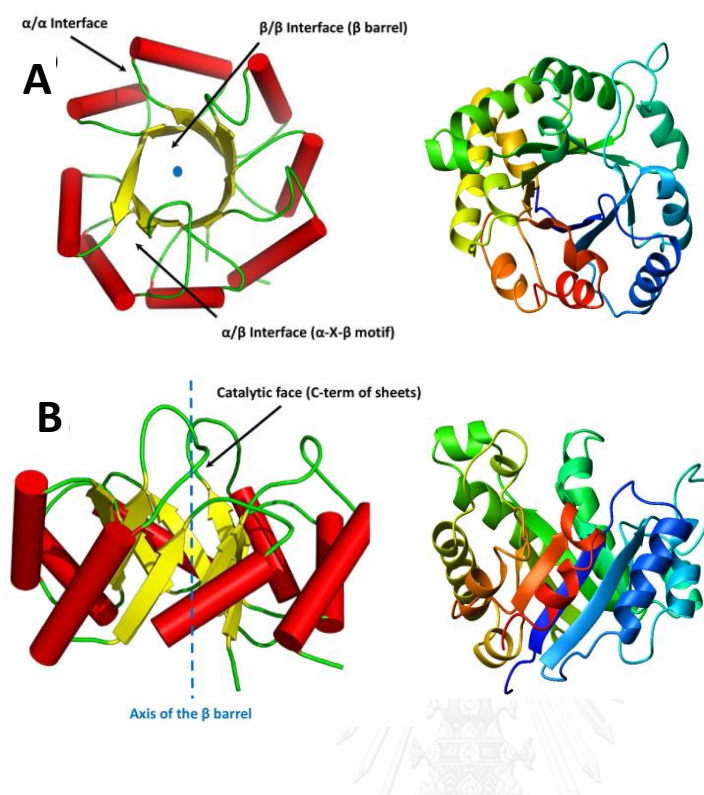


Figure 1.8 (A) Top view and (B) side view of a triosephosphate isomerase (TIM) barrel (PDB accession code 8TIM), colored from blue (N-terminus) to red (C-terminus).

Table 1.3 The four conserved regions and the corresponding β -sheets found in the amino acid sequence of α -amylase family enzymes (Van Der Maarl et al., 2002).

	I β 2	II β 4	III β 5	IV β 7
Amylomaltase	EALGIRIIGDMPIFVAED	LFHLVRIIDHFRG	VPVLAEDLGVI	VVYTGTHDNDT
Amylosucrase	HEAGISAVVDFIFNHTSN	GVDILRMDAVAF	VFFKSEAIIVHP	VNYVRSDDIG
CGTase	HAKNIKVIIDFAPNHTSP	GIDGIRMDAVKH	VFTFGEWFLGV	VTFIDNHMER
CMDase	HDNGIKVIFDAVFNHCGY	DIDGWRLDVANE	AIIVGEVWVHDA	FNLIGSHDTER
BE	HQAGIGVILDWVPGHFCK	HVDGFRVDAVAN	ILMIAEDSTDW	FILPFSHDEVV
Isoamylase	HNAGIKVYMDVVYNHTAE	GVDGFRFDLASV	LDLFAEPWAIG	INFIDVHDGMT
M. amylase	HQKAIRVMLDAVFNHSGY	DIDGWRLDVANE	AYILGEIWHDA	FNLLGSHDTPR
Pullulanase	HAHGVRVILDGVFNHTGR	GVDGWRLDVPNE	AYIVGEIWEAA	MNLLTSHDTPR
Sucrose Pase	LGECSHLMFDFVCNHMSA	GAEYVRLDAVGF	TVIITETNVPH	FNFLASHDGIG
BLamylase	HERGMYLMVDVVANHMGY	SIDGLRIDTVKH	VYCIGEVLDGD	GTFVENHDNPR

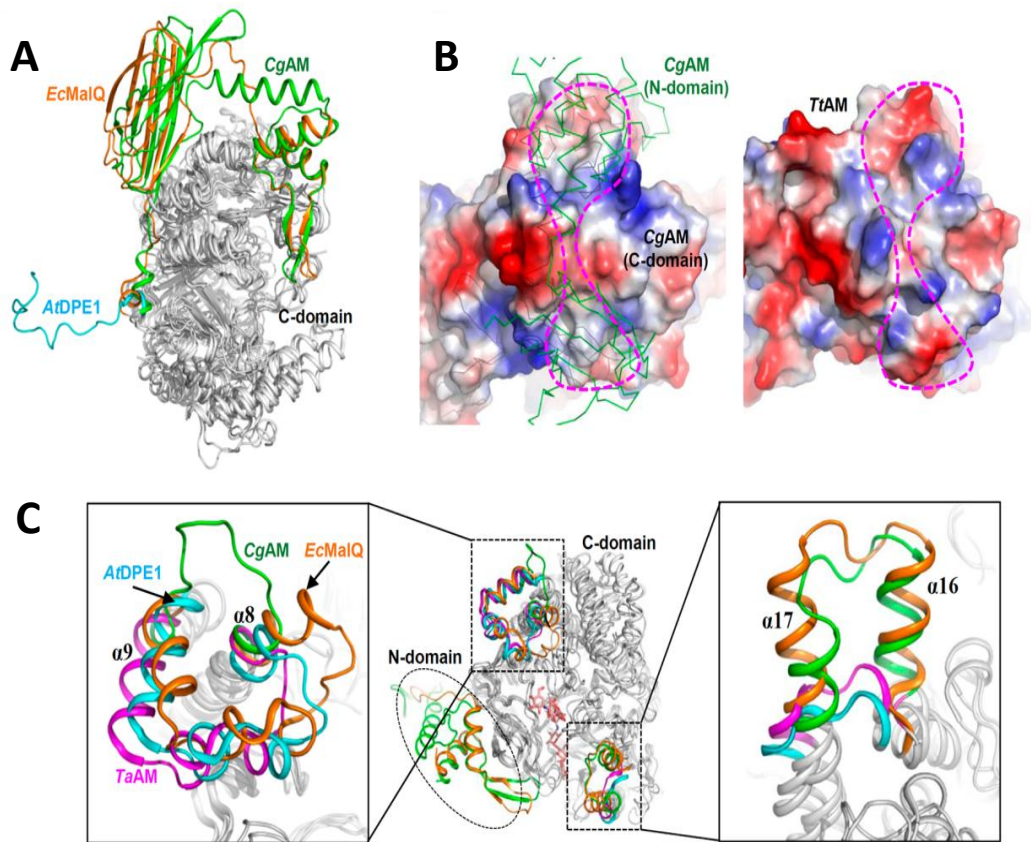


Figure 1.9 Structural comparison of *CgAM* with *EcMalQ*, *TtAM*, and *AtDPE1* (Joo et al., 2016).

(A) Comparison of N-domains of *CgAM*, *EcMalQ*, *TtAM*, and *AtDPE1* by superposed. C-domains of four proteins are shown with a gray color. N-domains of *CgAM* and *EcMalQ* are shown with colors of green and orange, respectively, and N-terminal arm region of *AtDPE1* is shown with a cyan color.

(B) Charge distribution on the surfaces of C-domains of *CgAM* and *TtAM*. The N-domain and the C-domain of *CgAM* are shown as a ribbon and an electrostatic potential surface mode, respectively (left), and *TtAM* is shown as an electrostatic potential surface mode (right). N-domain interacting region on the C-domain is indicated with a magenta-colored dotted line (left), and the corresponding region of *TtAM* is indicated as in *CgAM*.

(C) Structural differences on C-domain. Structures of *CgAM*, *EcMalQ*, *TtAM*, and *AtDPE1* are superposed. C domains of four proteins are shown with a gray color. N-domains of *CgAM* and *EcMalQ* are shown as in panel A. An AGA molecule bound in *EcMalQ* is shown as a stick model with a salmon color. The left side and the right-side figures are magnified figures of two structurally different regions shown in the middle figure. Structurally different regions of *CgAM*, *EcMalQ*, *TtAM*, and *AtDPE1* are shown in green, orange, magenta, and cyan colors, respectively. Key

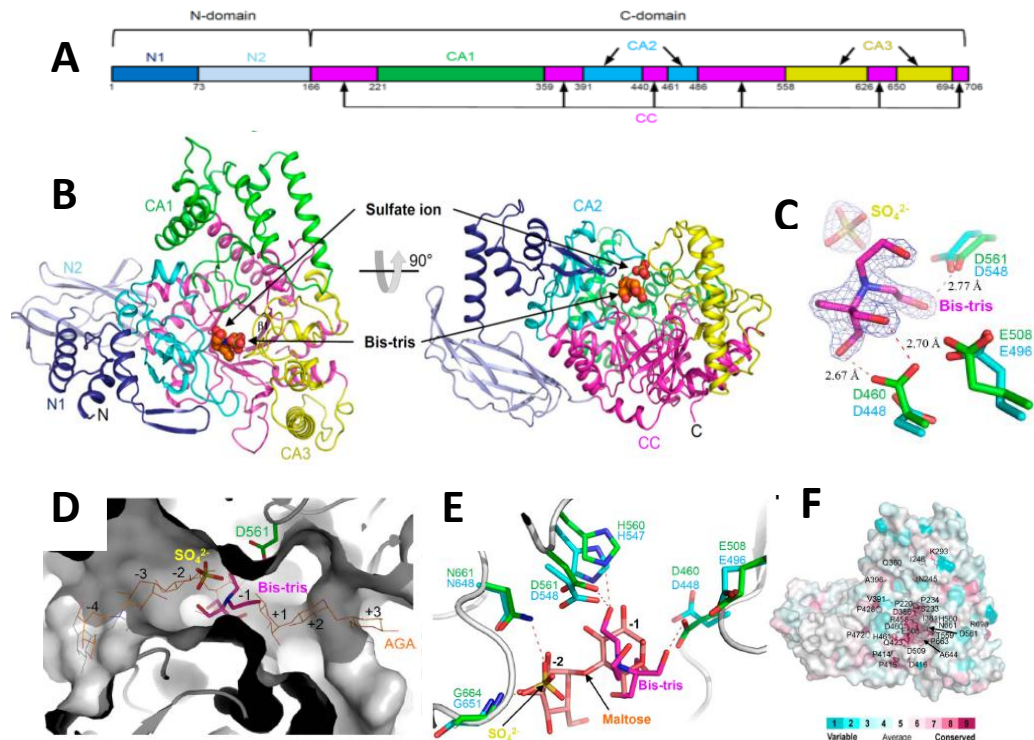


Figure 1.10 Overall structure of *CgAM* (Joo et al., 2016).

(A) Overall structure of *CgAM*. The structure of *CgAM* is presented as a cartoon diagram. The right-side figure is rotated 90° in horizontal direction. A bis-tris molecule and a sulfate ion bound in *CgAM* are shown as sphere models and labeled. The subdomains of *CgAM* are distinguished with color scheme as in panel B.

(B) Domain identification of *CgAM*. N1 and N2 are representatives of N1- and N2-subdomains of N-domain, CC is core subdomain of C-domain, and CA1, CA2, and CA3 are auxiliary subdomains I, II, and III of C-domain, respectively.

(C) Electron density map of a Bis-tris molecule and a sulfate ion bound at the active site pocket. A simulated annealing composite omit map of a bis-tris molecule and a sulfate ion bound at the active site pocket are shown with blue-colored mesh and contoured in 3 σ . The structures of *CgAM* and *EcMalQ* are superposed, and three catalytic residues are shown with green- and cyan-colored sticks, respectively. The polar contacts between the ligands and the residues are shown with red-colored dotted lines, and the distances are labeled.

(D) Substrate binding pocket of *CgAM*. The *CgAM* structure and the *EcMalQ* structure in complex with AGA are superposed. Subsites based on AGA are labeled (-4 to +3). The *CgAM* structure is shown as a surface model, and the AGA molecule bound in *EcMalQ* is shown as an orange-colored line. The bis-tris methane molecule and the sulfate ion bound in *CgAM* are shown as stick models and labeled. One catalytic residue, D561, is shown as a green-colored stick.

(E) Stabilization of the bis-tris methane molecule and the sulfate ion. The *CgAM* structure and the *EcMalQ* structure in complex with maltose are superposed. The bis-tris methane molecule is shown as a stick with a magenta color, and the sulfate ion is shown as a stick with a yellow color. The maltose molecule bound in *EcMalQ* is shown as a salmon-colored stick. Residues involved in the stabilization of the bis-tris methane molecule and the sulfate ion in *CgAM* are shown as green-colored sticks, and their corresponding residues in *EcMalQ* are shown as cyan colored sticks. Bis-tris methane molecule and the sulfate ion

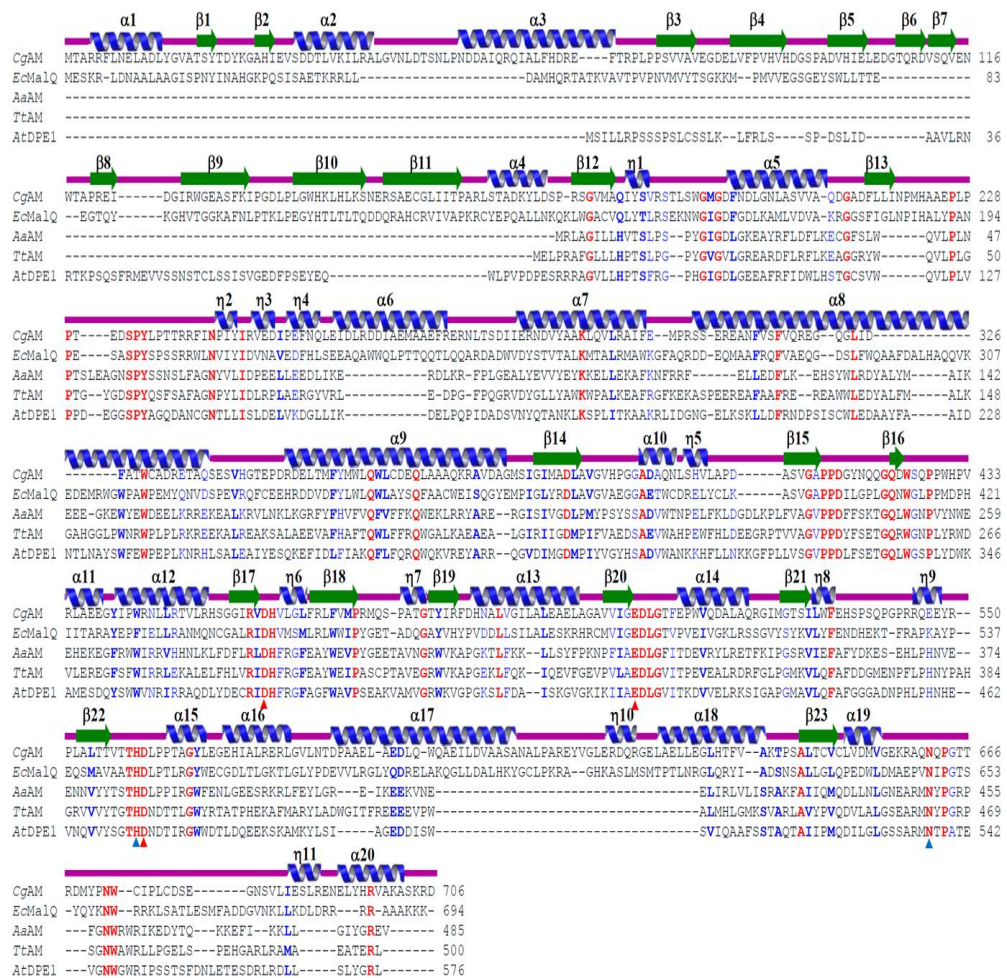


Figure 1.11 Amino acid sequence alignment of amyloamylases from *C. glutamicum* (CgAM), *E. coli* (EcMalQ), *Aquifex aeolicus* (AaAM), *T. thermophilus* (TtAM), and disproportionating enzyme 1 from *A. thaliana* (AtDPE1). (Joo et al., 2016). The secondary structure elements are marked on top of the alignment based on the CgAM structure: α -helices and β -strands by a helix and β -strands by an arrow. The η symbol refers to a 3_{10} -helix. Conserved residues are boxed in white on a red background; similar residues are boxed in red with a white background. Residues involved in enzyme catalysis and maltose binding are indicated with triangles colored with red and blue, respectively. This figure was produced using Clustal W.

1.10 Improvement the properties of CgAM

According to amyloamylase application, improvement the properties of CgAM such as thermostability and LR-CDs production is necessary for the industrial. Mutation for improvement CgAM properties is used in several researches. For thermostability, *C. glutamicum* is a mesophilic bacterium so CgAM is unendurable with heat. Mutation at A406 showed that thermostability of CgAM increased to 50°C especially A406V (Nimpiboon et al., 2016a). In addition, mutation N287 to aromatic ring also slightly increase the thermostability (Nimpiboon et al., 2016b). According to the characterization of LR-CDs production, CgAM could produce LR-CDs in range of CD19 – CD50. The smallest LR-CD product is CD19 while major product is CD25 (Srisimararat et al., 2010). Mutation in various positions gives a different pattern of LR-CDs profile including yield of LR-CDs product. Y172A gives CD28-29 as a dominant product while N287Y, is another mutant, alters major LR-CDs product to CD30 (Srisimararat et al., 2012, Nimpiboon et al., 2016b). In addition, A406V and A406L give a higher LR-CDs products yield than the wild-type CgAM (Nimpiboon et al., 2016a).

1.11 Objectives

Although there are several researches that have studied about *CgAM*, mechanism of LR-CDs production of *CgAM* was still mysterious. A study of *CgAM* mutation will lead us to understand and reveal the key residues which affected to LR-CDs production of *CgAM*. In this research, we focus on 4 mutants that located on CAI and CAII subdomain in *CgAM*. The aims of this research are

1. To characterize mutated amylomaltase
2. To analyze position of amino acid that effects on large-ring cyclodextrins production by computational method



CHAPTER II

MATERIALS AND METHODS

2.1 Equipment

Autoclave (Model H-88LL, Kokusan Ensinki Co., Ltd, Japan)

Autopipette (Pipetman, Gilson, France)

Balance PB303-L (Mettler Toledo, Switzerland)

Biophotometer (Eppendorf, Germany)

Centrifuge Sorvall Legend XTR (Thermo Scientific)

Centrifuge 5804 R (Eppendorf, Germany)

Centrifuge, refrigerator centrifuge (Beckman Coulter Avanti J30I, USA)

Electrophoresis units:

- Power supply (BIO-RAD, USA)
- Short plates (BIO-RAD, USA)
- Spacer plates (BIO-RAD, USA)

FPLC ÄKTA Amersham Pharmacia Biotech unit:

- Column: Amersham Biosciences DEAE FF™ and HiPrep Phenyl FF™
(High Sub) 16/10
- Detector: UPC-900
- Pump: P-920
- Fraction collector: Frac-900

FPLC ÄKTA start (GE Healthcare Life Sciences, England)

Freezer (- 20 °C) (Whirlpool, USA)

Gel Document (SYNGENE, England)

Hot plate: C-MAG HS7 (IKA, Germany)

HPAEC DX-600 (Dinox Corp., Sunnydale USA)

- Column: Carbobac PA-100™ 4 × 250 mm
- Pulsed amperometry detector (PAD): DIONEX ED40
- Autosampler: DIONEX AS40
- Column oven: DIONEX ICS-3000 SP

Incubator (Memmert, Germany)

Incubator box (Hercuvan, USA)

Incubator shaker Innova™ 44 (New Brunswick Scientific, USA)

Incubator shaker Innova™ 4000 (New Brunswick Scientific, USA)

Incubator shaker Innova™ 4080 (New Brunswick Scientific, USA)

Incubator shaker (Kühner, Switzerland)

Laminar flow Bio Clean Bench (SANYO, Japan)

Magnetic stirrer: Model Fisherbrand (Fisher Scientific, USA)

Membrane filter: polyethersulfone (PES), pore size 0.45 μm, Whatman™ (GE Healthcare, England)

pH meter (Mettler Toledo, Switzerland)

Sonicator (Bendelin, Germany)

SpectraMax M5 Microplate Reader (Molecular Devices, USA)

Spectrophotometer (Eppendorf, Germany)

Syringe (Nipro (Thailand) Corporation Limited)

Ultra-Low Temperature Freezer (- 80 °C) (New Brunswick Scientific, USA)

Vortex: Model K-550-GE (Scientific Industries Inc., USA)

2.2 Chemicals

2-Log DNA Ladder (New England Biolabs Inc., USA)

5-Bromo-4-chloro-3-indolyl phosphate (BCIP) (Fermentas, Canada)

β -Mercaptoethanol (Fluka, Switzerland)

Acrylamide (GE Healthcare, England)

Agar (Merck, Germany)

Agarose: SEKEM LE Agarose (FMC Bioproducts, USA)

Ammonium per sulfate (APS) (BIO-RAD, USA)

Ammonium sulphate (Sigma, USA)

Ampicillin (BIO BASIC INC., Canada)

Bovine serum albumin (BSA) (Sigma, USA)

ColorPlus prestained Protein Marker, P7709S, Lot: 0201203 (New England Biolabs Inc., USA)

Coomassie Brilliant Blue G (Fluka, Switzerland)

Coomassie Brilliant Blue R-250 (BIO BASIC INC., Canada)

Cycloamylose (Wako, Japan)

D-Glucose (Ajax Finechem, Australia)

Dimethyl sulfoxide (DMSO) (Merck, Germany)

Dipotassium hydrogen phosphate (Ajax Finechem, Australia)

Ethidium bromide (Sigma, USA)

Ethylene diamine tetraacetic acid (EDTA) (Ajax Finechem, Australia)

Glacial acetic acid (Carlo Earba Reagenti, Italy)

Glucose liquicolor (Glucose oxidase kit) (HUMAN, Germany)

Glycerol (Ajax Finechem, Australia)

Glycine (Fisher Chemical, USA)

Hydrochloric acid (Carlo Erba Reagenti, Italy)

Iodine (Baker chemical, USA)

Isopropyl β -D-1- thiogalactopyranoside (IPTG) (Thermo Fisher Scientific, USA)

Magnesium sulfate (Carlo Erba Reagenti, Italy)

Maltoheptaose (Hayashibara biomedical laboratories Inc., Japan)

Maltohexaose (Hayashibara biomedical laboratories Inc., Japan)

Maltopentaose (Hayashibara biomedical laboratories Inc., Japan)

Maltose (Conda, Spain)

Maltotetraose (Hayashibara biomedical laboratories Inc., Japan)

Maltotriose (Hayashibara biomedical laboratories Inc., Japan)

Methanol (Sigma, USA)

Nitrocellulose Membrane (BIO-RAD, USA)

Pea starch (Emsland-Stärke GmbH, Germany)

Plasmid extraction Kit (Flavogen Biotech corp., Taiwan)

Potassium dihydrogen phosphate (Ajax Finechem, Australia)

Potassium iodide (Mallinckrodt, USA)

Protein Marker, P7702S, Lot: 0441201 (New England Biolabs Inc., USA)

QIA quick Gel Extraction Kit (QIAGEN, Germany)

Sodium chloride (Ajax Finechem, Australia)

Sodium dodecyl sulfate (SDS) (Vivantis Technologies, Malaysia)

Sodium hydroxide (Carlo Erba Reagenti, Italy)

Sodium nitrate (Carlo Erba Reagenti, Italy)

Soluble starch (potato) (Scharlau microbiology, Spain)

Standard protein marker (Amersham Pharmacia Biotech Inc., USA)

Tetramethylethylenediamine (TEMED) (BIO-RAD, USA)

Tris-(hydroxyl methyl)-aminomethane (Carlo Erba Reagenti, Italy)

Tryptone (HIMEDIA, India)

Yeast extract (Affymetrix, USA)

2.3 Enzymes, Restriction enzymes and Bacterial strains

Escherichia coli BL21 (DE3) (Novagen, Germany)

Glucoamylase from *Aspergillus niger* (Fluka, Switzerland)

KOD-Plus-Neo DNA polymerase (TOYOBO, Japan)

Plasmid pET-17b (Novagen, Germany)

Plasmid pET-19b (Novagen, Germany)

Restriction enzymes (*DpnI*, *XhoI*, *NdeI*) (New England Biolabs Inc., USA and

Fermentus, Canada)

T4 DNA ligase (New England Biolabs Inc., USA)

METHOD

In this research, E231Y plasmid was from Asst. Prof. Kuakarun Krusong, Ph.D. E231Y CgAM gene was in pET17b expression vector.

2.4 Site-directed mutagenesis of P228Y, A413F and G417F mutants

2.4.1 Primer design

To construct P228Y, A413F and G417F CgAM recombinant plasmids, PCR mediated site-directed mutagenesis was performed. P228Y meant that proline (P) at the position 228 of CgAM was mutated to tyrosine (Y) Similarly, A413F and G417F meant that alanine (A) at position 413 and glycine (G) at 417 of CgAM were mutated to phenylalanine (F). Primers were designed based upon the assigned amino acids. The sequences of primers were shown in Table 2.1;

Table 2.1 Primers for site-directed mutagenesis

Mutant	Primer	Sequence	T _m (°C)	GC content
P228Y	Forward primer	5' CAGAGCCGCTGT <u>ATC</u> CCTAC 3'	57	58%
	Reverse primer	5' CTCAGTAGG <u>ATAC</u> CAGCGGC 3'	57	58%
A413F	Forward primer	5' GGATGCGTCAGTGGGCT <u>TTT</u> CCACCAG 3'	66	62%
	Reverse primer	5' CCATCTGGTGG <u>AAAG</u> CCCACTGACG 3'	65	60%
G417F	Forward primer	5' CCCACCCAGAT <u>TTT</u> TACAACC 3'	56	48%
	Reverse primer	5' GCTGGTTGT <u>AAA</u> ATCTGGTG 3'	54	43%

*** Mutation sites are underlined ***

2.4.2 Amplification of mutated *CgAM* genes (P228Y, A413F and G417F) by PCR.

PCR reaction consisted of 10xPCR buffer 5 μ l, 2mM dNTPs 5 μ l, 25mM MgSO₄ 3 μ l, 50 ng/ μ l plasmid DNA 1 μ l and KOD-Plus Neo DNA polymerase (1 U/ml) 1 μ l and adjusted the volume to 50 μ l by autoclaved distilled water. *CgAM*-pET19b recombinant plasmid was used as a template for site-directed mutagenesis of P228Y, A413F and G417F. The PCR steps for amplification of mutated *CgAM* genes were described in Table 2.2 and 2.3. Then, the PCR product was digested with *DpnI*. The digestion reaction contained 5 μ l of PCR product, 2 μ l of 10xTA buffer, 1 μ l of *DpnI* and adjusted the volume to 20 μ l by autoclaved distilled water. The reaction mixture was incubated at 37°C for 1 h. PCR products were checked by agarose gel electrophoresis.

Table 2.2 PCR steps for amplification of P228Y and G417F CgAM genes

PCR step	Temperature (°C)	Time (s)
Initial denaturation	94	2 min
Annealing (*40)	98	10 s
	52	30 s
	68	4 min
Final extension	68	7 min

*** 3-step PCR was recommended by KOD Plus Neo DNA polymerase

Table 2.3 PCR steps for amplification of A413F CgAM genes

PCR step	Temperature (°C)	Time (s)
Pre-denaturation	94	2 min
Denaturation and Extension (*45)	98	10 s
	68	4 min

*** 2-step PCR was recommended by KOD Plus Neo DNA polymerase

2.4.3 Restriction enzyme digestion

P228Y, A413F and G417F *CgAM* recombinant plasmids were digested with *NdeI* and *XhoI*. Reaction mixture contained 8 μl of 0.5 $\mu\text{g}/\mu\text{l}$ plasmid, 1 μl for each of restriction enzymes, 5 μl of CutSmart buffer (10x) and adjusted the volume to be 50 μl with distilled water. The reaction was incubated at 37°C for 1 h. pET19b was also digested with *NdeI* and *XhoI*.

2.4.4 Plasmid transformation

Recombinant plasmid obtained from section 2.4.2 was transformed into *E. coli* host cells via heat shock transformation technique. Two microlitres of plasmid of approximately 100 ng/ μl were added and gently mixed with the competent cells, and chilled on ice for 5 min. After that, the reaction was incubated at 42°C for 45 s and immediately chilled on ice for 5 min. LB medium of 900 μl was added to the reaction and incubated at 37°C with 250 rpm shaking for 45 min. Cells were spreaded on 100 $\mu\text{l}/\text{ml}$ ampicillin agar plate and incubated at 37°C overnight (16 to 18 h).

2.4.5 Extraction of recombinant plasmid

Cells carrying recombinant plasmid were grown in 10 ml of LB medium supplemented with 100 $\mu\text{g}/\text{ml}$ of ampicillin at 37°C overnight. Cells were harvested via centrifugation at 6,000xg for 10 min. Recombinant plasmid harboring mutated *CgAM* gene was extracted by plasmid extraction kit (Flavogen, Taiwan). The concentration of recombinant plasmid was estimated by measuring A_{260} (Green and Sambrook, 2001). Calculation of plasmid concentration was done by this following equation.

$$\text{Concentration } (\mu\text{g}/\text{ml}) = A_{260} \times \text{dilution factor} \times 50 \mu\text{g}/\text{ml}$$

The purity of plasmid was also measured by calculating the ratio of $A_{260/280}$ of DNA sample and agarose gel electrophoresis. DNA with the ratio of $A_{260/280}$ above 1.8 was considered as high purity.

2.4.6 Agarose gel electrophoresis

Agarose gel was prepared by adding 1% agarose powder into 100 ml of TBE buffer (89 mM Tris-HCl, 8.9 mM boric acid and 2.5 mM EDTA, pH 8.0). DNA sample was mixed with 6x gel loading dye (30% of glycerol and 0.25% of bromophenol blue) and loaded into the well of agarose gel. A constant voltage of 100 volts was applied for 30 min or until the dye front reached almost the gel's bottom. Gel was then soaked in 2.5 $\mu\text{g/ml}$ ethidium bromide solution for 5 min before destaining with distilled water for 30 min. DNA sample was visualized under a long wavelength UV light and photographed with Gel document apparatus (SYNGENE). The size of DNA sample was estimated by comparing to the standard DNA marker (New England Biolabs Inc.).

2.4.7 DNA sequencing

DNA sequencing was performed to confirm mutated positions on CgAM gene. In the first step, DNA template 100 ng/ μl was amplified by PCR technique. The reaction mixture consisted of DNA template 100 ng/ μl 2.3 μl , 5xBig dye sequencing buffer 4 μl , Primer (Table 2.4) (1 pmol/ μl) 3.2 μl , Ready reaction premix (DNA polymerase) 0.5 μl and autoclaved distilled water 10 μl . PCR was performed as described in Table 2.5. PCR product was transferred into 1.5 ml microtube and then precipitated with ethanol (EtOH). PCR product was mixed with 2 μl of 3 M sodium acetate (AcO-Na) (pH 5.2) and 50 μl of EtOH and incubated at

room temperature for 15 min. PCR product was centrifuged at 19,270xg, 20°C for 20 min and supernatant was removed by vacuum suction. Twenty-five microlitres of EtOH was added into this tube and centrifuged at 18,000xg for 10 min. Supernatant was removed via vacuum suction for 15 min or until DNA pellet was dried. DNA pellet was then mixed with 15 µl of HiDi before loading into 96-well plate. Finally, DNA sequencing was performed by Automated DNA Sequencer. GENETYX-WIN software was used to analyze DNA sequence.



Table 2.4 Primers for DNA sequencing

Primer	Sequence	T _m (°C)	GC content
T7 promoter	5' TAATACGACTCACTATAGGG 3'	47.7	40%
Seq_FW1	5' GCTCGTCTGTCTACTGCTGAT 3'	54.4	52%
Seq_RV1	5' CCACTGCGAGGGGAATCAAG 3'	55.9	60%
Seq_FW2	5' CCGCGATGAGCTGACCAT 3'	52.6	61%
Seq_RV2	5' GCCACTGCAACCACATGTAG 3'	53.8	55%
Seq_FW3	5' GGCTCAGCGTGGCATCATG 3'	55.4	63%
Seq_RV3	5' CGAACCATAGGATCGAGGTGC 3'	56.3	57%
T7 terminator	5' GCTAGTTATTGCTCAGCGG 3'	51.1	53%

Table 2.5 PCR steps for amplification of gene for DNA sequencing

PCR step	Temperature (°C)	Time (s)
Initial denaturation	96	60
Annealing (*40)	96	10
	50	5
	60	240
Hold	4	∞

2.4.8 Preparation of competent cells

A single colony of each *E. coli* bacterial strain (DH5 α , Top10 and BL21 (DE3)) was cultivated in 5 ml of LB medium at 37°C overnight. One percent (v/v) of overnight culture was inoculated into 100 ml of LB medium. Cells were cultured at 37°C, 250 rpm until the optical density was about 0.3. Cells were suddenly chilled on ice for 30 min. After that, cells were harvested via centrifugation at 4°C, 4000xg for 10 min. Supernatant was discarded and cells were resuspended with 30 ml of cold 0.1 M CaCl₂. This step was repeated twice. In the last step, cells were resuspended with 1 ml of cold 0.1 M CaCl₂ containing 1% glycerol. A hundred microlitre of competent cells was aliquoted into microtube and stored at -80°C.

2.5 Optimization of mutated *CgAM* gene expression

E. coli host cell carrying recombinant *CgAM* plasmid was grown overnight in 10 ml LB broth containing 100 μ l/ml ampicillin at 37°C with 250 rpm shaking. After that, 1.5% (v/v) of overnight culture was transferred to 125 ml of LB medium with 100 μ g/ml ampicillin and continued cultured at 37° with 250 rpm shaking until absorbance at 600 nm reached 0.4 – 0.6. Then, Isopropyl β -D-1-thiogalactopyranoside (IPTG) was added to the final concentration of 1 mM. Cells were collected by centrifugation at 4,000xg for every 0, 2, 4 and 6 h after IPTG induction. Harvested cells were resuspended with 50 mM phosphate buffer pH 7.4 and disrupted by sonication with 25% (pulse-on 1 s pulse-off 3 s) via centrifugation at 16,000xg for 45 min. The expression pattern of *CgAM* was analyzed by sodium dodecyl sulfate polyacrylamide gel electrophoresis (SDS-PAGE).

If low amount of mutated CgAM in soluble form was observed, the expression condition was adjusted by lowering temperature or adding a final concentration of 1% of glucose.

When the optimum expression condition was obtained, production of CgAM was scaled up using 2 L of LB medium containing 100 µg/ml ampicillin.

2.6 Purification of mutated CgAMs

2.6.1 Purification of E231Y via DEAE FF™ and Phenyl FF™ column chromatography

2.6.1.1 DEAE FF™ column chromatography

Column was first equilibrated with binding buffer (50 mM phosphate buffer and 0.01% β-mercaptoethanol) for at least 10 column volumes. Crude enzyme obtained from 2.5 was applied onto the column and the column was washed with the same buffer for at least 5 column volumes until A_{280} reached the baseline level. Bound proteins were eluted by a gradient of sodium chloride from 0 to 1 M for 100 ml. Fractions of 1 ml were collected throughout all elution steps. The protein fraction containing starch glycosylation activity were pooled and dialyzed against 50 mM phosphate buffer pH 7.4.

When knowing the concentration of sodium chloride required for elution of mutated enzyme, step-wise elution was performed instead of gradient elution.

2.6.1.2 Phenyl FF™ column chromatography

Partial purified E231Y CgAM was further purified by HiTrap Phenyl FF (high sub), a hydrophobic interaction chromatography (HIC). Initially, ammonium

sulfate ((NH₄)₂SO₄) was gradually added to partial purified enzyme until the final concentration of salt was about 1 M. Column was equilibrated at least 10 column volumes with binding buffer (50 mM phosphate buffer pH 7.4, 0.01% β-mercaptoethanol and 1M (NH₄)₂SO₄). Sample was loaded onto the column and the column was washed the same buffer for at least 5 column volumes until A₂₈₀ reached the baseline level. During the step of elution, a linear gradient elution of (NH₄)₂SO₄, decreasing from 1.0 to 0 M, was performed. Fractions of 1 ml were collected and those carrying high starch transglycosylation activity were pooled and dialyzed in 50 mM phosphate buffer pH 7.4.

2.6.2 Purification of P228Y, A413F and G417F by HisTrap FF column

P228Y, A413F and G417F CgAMs were expressed in pET19b so the his-tagged proteins were purified by HisTrap FF column.

Initially, HisTrap FF column was equilibrated with at least 10 column volumes of binding buffer (50 mM phosphate buffer pH 7.4 and 500 mM NaCl). Crude enzyme was then applied onto the column and the column was washed with binding buffer until the baseline level was reached. Bound proteins were eluted by a gradient of imidazole (0 - 1 M). Fractions of 1 ml were collected throughout all elution steps and the fraction containing starch glycosylation activity were pooled and dialyzed against 50 mM phosphate buffer pH 7.4

2.7 Protein determination

2.7.1 Determination of protein concentration

Concentration of protein was estimated by Bradford's assay (Bradford, 1976). Standard curve for determining protein concentration was generated using 1

mg/ml of bovine serum albumin as a standard protein (Appendix 8). One microlitre of Bradford's working reagent was mixed with 100 μ l of protein sample for 2 min. After that, the mixture was suddenly measured at A_{595} .

2.7.2 Sodium dodecyl sulfate polyacrylamide gel electrophoresis (SDS-PAGE)

A gel with 8% (w/v) separating gel and 5 % stacking gel containing 0.1% (w/v) SDS was prepared (Appendix 1). Sample buffer with SDS loading dye (5x) was mixed to the protein sample and boiled for 10 min before loading into the gel. In the process of electrophoresis, a constant current of 25 mA and running time of 45 min were set. When the running time was completed, the gel was stained by coomassie blue staining solution (1% Coomassie blue R-250, 45% methanol and 10% glacial acetic acid) in order to visualize the protein bands.

2.7.3 Coomassie blue staining

Coomassie blue staining was a common method used for investigating the protein band. The gel obtained from section 4.8 was stained with Coomassie blue staining solution and destained by destaining solution (10% methanol and 10% glacial acetic acid).

2.8 Characterization of mutated amylomaltase

2.8.1 Enzyme assay

2.8.1.1 Starch transglycosylation activity

Starch transglycosylation activity was an activity that transferred a glycosyl unit of starch donor to maltose acceptor. This activity aimed to determine

residual starch in reaction by the iodine method (Park et al., 2007, Srisimararat et al., 2012). The reaction mixture contained 100 μ l of enzyme, 250 μ l of 0.2% (w/v) soluble potato starch, 50 μ l of 1% (w/v) maltose and 600 μ l of 50 mM phosphate buffer pH 6.0. The reaction was performed at 30°C for 10 min, and was then stopped by boiling for 10 min. A hundred of reaction was withdrawn and mixed with 1 ml of iodine solution (0.02% I₂ in 0.2% KI). The absorbance at 600 nm was monitored. One unit of starch transglycosylation was defined as the amount of enzyme that could degrade one per cent of starch per min under the described condition (Srisimararat et al., 2012).

2.8.1.2 Starch degradation activity

Starch degrading activity was an activity that measured the amount of degraded starch in the reaction, assayed by the iodine method (Srisimararat et al., 2012). The reaction mixture consisted of 50 μ l of enzyme, 100 μ l of 0.75% (w/v) soluble potato starch and 100 μ l of 50 mM phosphate buffer pH 6.0. The reaction was incubated at 30°C for 10 min. Reaction was stopped by adding 1 N HCl. Then, 100 μ l aliquot was withdrawn and mixed with 900 μ l of iodine solution (0.005% I₂ in 0.05% KI), and the absorbance at 660 nm was measured. One unit of starch degradation was defined as the amount of enzyme that degrade 1 mg per ml of starch per min under described condition (Srisimararat et al., 2012, Fuwa, 1954).

2.8.1.3 Disproportionation activity

Disproportionation activity was used to measure the amount of glucose released from catalyzing a substrate maltotriose (G3). Disproportionation activity was detected by the glucose oxidase method (Knegt et al., 1995). The reaction mixture consisted of 20 μ l of enzyme and 30 μ l of 5% maltotriose (G3). The reaction was

performed at 30°C for 10 min and stopped by adding 1 N HCl 30 μ l. Glucose oxidase reagent 920 μ l was added into reaction mixture and incubated in the dark at 30°C for 10 min. Absorbance at 505 nm was suddenly measured. One unit of disproportionation activity was defined as the amount of enzyme that could produce 1 μ mol of glucose per ml per min under described condition (Srisimararat et al., 2012).

2.8.1.4 Cyclization activity

Cyclization activity was an activity that produced cyclodextrin (CD) and linear short oligosaccharide using pea starch as substrate. Cyclization activity was analyzed by High Performance Anion Exchange Chromatography with Pulsed Amperometric Detection (HPAEC-PAD) (Koizumi et al., 1999). The reaction mixture consisted of 50 μ l of enzyme, 150 μ l of 2% (w/v) pea starch, and 1,300 μ l of 50 mM phosphate buffer pH 6.0. The reaction was performed at 30°C for 90 min before inactivating by boiling for 10 min. The reaction mixture was then treated with 8 U of glucoamylase at 40°C for 16 h and inactivating by boiling for 10 min. LR-CDs profiles were analyzed by HPAEC-PAD. One unit of cyclization activity was defined as the amount of enzyme required for the production of 1 nC of total LR-CDs per min under described condition (Srisimararat et al., 2012).

2.8.1.5 Coupling activity

Coupling activity was a reverse reaction of cyclization activity. Coupling activity was determined by 3,5-dinitrosalicylic (DNS) assay (Chaplin and Kennedy, 1994). The reaction mixture contained 20 μ l of enzyme, 20 μ l of 3 mg/ml LR-CDs, 20 μ l of 1 mg/ml cellobiose and 40 μ l of 50 mM phosphate buffer pH 6.0. Incubation was carried out at 30°C for 10 min and stopped by boiling for 10 min. After that, the mixture was treated with 8 U of glucoamylase at 40°C for 30 min and

inactivated by boiling for 10 min. Subsequently, DNS reagent was added to the reaction mixture and incubated further for 15 min. Then, it was chilled on ice for 5 min. A hundred microlitre of aliquot was transferred and mixed with 400 μ l of distilled water. Absorbance at 540 nm was monitored. One unit coupling was defined as the amount of enzyme that produce 1 μ mol of glucose per ml per min under described condition (Srisimarat et al., 2012).

2.8.1.6 Hydrolytic activity

Hydrolytic activity was determined by the bicinchoninic acid (BCA) assay (Sinner and Puls, 1978). Reaction mixture, comprising 10 μ l of enzyme, 30 μ l of 0.5 mg/ml cycloamylose and 10 μ l of 50 mM phosphate buffer pH 6.0, was performed at 30°C for 10 min. Reaction was stopped by adding 1 N HCl 30 μ l. After that, 950 μ l of BCA reagent was added into reaction mixture and then incubated at 80°C for 25 min. The reaction mixture was chilled on ice for 5 min before measuring absorbance at 562 nm. One unit of hydrolytic activity was defined as the amount of enzyme that could produce 1 μ mol of reducing sugar per min under described condition (Srisimarat et al., 2012).

2.8.2. Effect of temperature on CgAM activity

The effect of temperature on CgAM activity was observed on starch transglycosylation activity. The reaction was performed in 50 mM phosphate buffer pH 6.0 at various temperatures (20 to 70 °C) for 10 min. The assay of starch transglycosylation was performed as described in section 2.8.1.1.

2.8.3 Effect of temperature on *CgAM* stability

For temperature stability, residual starch transglycosylation of *CgAM* was observed at different temperatures. Purified enzyme was pre-incubated at temperatures in range of 20°C to 70 °C for 1 h before determining starch transglycosylation activity as described in section 2.8.1.1.

2.8.4 Effect of pH on *CgAM* activity

To determine the optimum pH of *CgAM* on starch transglycosylation activity, the purified enzyme was pre-incubated with buffer of different pHs under optimum temperature obtained from section 5.3. The pH range was varied from pH 3.5 to pH 10.0. Different buffer systems were used as follows; acetate buffer for pH 3.5 – pH 6.0, phosphate buffer for pH 6.0 – pH 8.0 and Tris-HCl for pH 7.0 – pH 10.0. The activity was assayed by starch transglycosylation as described in section 2.8.1.1.

2.8.5 Effect of pH on *CgAM* stability

To observe pH stability on starch transglycosylation of *CgAM*, the purified enzyme was incubated with 20 mM buffer of different pHs as described in section 5.5 for 1 h before investigating the residual starch transglycosylation activity by the assay explained in section 2.8.1.1.

2.8.6 Substrate specificity of *CgAM*

The specificity of *CgAM* towards different malto-oligosaccharide substrates (maltose G2, maltotriose G3, maltotetraose G4, maltopentose G5, maltohexose G6 and maltoheptose G7) was carried out on disproportionation activity. *CgAM* of 0.05 U (disproportionation activity) was incubated with 50 mM of substrate

in 50 mM phosphate buffer pH 6.0 and the disproportionation activity was assayed as described in section 5.2.3. The result was illustrated as a percentage of relative activity.

2.8.7 Circular dichroism spectra

Spectropolarimeter (J-815CD spectrometer, Jasco, Japan) was used to generate CD spectra of CgAM under wavelength excitation in range of 190-240 nm at 25°C. Protein sample of 0.2 mg/ml was used in this experiment. The average CD spectrum was derived from three scans. The Mean Residue Weight (MRW) of CD spectrum, which was defined as an average of molecular weight of amino acids in which the protein contained, was calculated and submitted to K2D3 server program, aiming to predict the secondary structure of protein (<http://cbdm-01.zdv.uni-mainz.de/~andrade/k2d3//index.html>) (Louis-Jeune et al., 2011).

2.8.8 Synthesis and analysis of large-ring cyclodextrins (LR-CDs)

In this reaction, the purified enzyme of 0.05 U starch degradation activity was incubated with 100 µl of 0.2% (w/v) pea starch in 50 mM phosphate buffer pH 6.0 at 30°C, 150 rpm shaking for 6, 12 and 24 h. The reaction was stopped by boiling for 10 min. After that, the mixture was treated with 8 U of glucoamylase at 40°C for 16 h and inactivated by boiling for 10 min. The LR-CDs products were analyzed by HPAEC-PAD using Carbopac PA-100 column (Srisimararat et al., 2010) (4 x 250 mm, Dionex, USA). Sample of 110 µl was injected into the column and eluted with a step gradient of 200 mM sodium nitrate (NaNO₃) in 150 mM NaOH as follows

- 1) at 0 – 2 min, NaNO₃ increased from 4% to 8;
- 2) at 2-10 min, NaNO₃ increased from 8% to 18%;
- 3) at 10-20 min, NaNO₃ increased from 18% to 28%;
- 4) at 20-40 min,

NaNO₃ increased from 28% to 35%; 5) at 40-55 min, NaNO₃ increased from 35% to 45%, and 6) at 55-60 min, NaNO₃ increased from 45% to 63% (Koizumi et al., 1999, Srisimararat et al., 2010, Srisimararat et al., 2012). The size of the LR-CD products was determined by comparing to the size of standard LR-CDs (Wako, Japan).

2.8.9. Determination of kinetic parameters of CgAM

In the study of enzyme kinetics, all kinetic parameters of CgAM activities including K_m and V_{max} were calculated from Lineweaver-Burk plot. Besides, the k_{cat} (turnover number) and k_{cat}/K_m values (catalytic efficiency) were also determined.

2.8.9.1 Kinetic parameters of starch transglycosylation activity

Purified enzyme of 1 U starch transglycosylation activity was incubated with 0.05% soluble starch and various concentrations of glucose, ranging from 0 to 10 mM, in 50 mM phosphate buffer pH 6.0 at 30°C for 20 min. Reaction was then stopped by boiling for 10 min. Degraded starch was detected by iodine method as previously described in section 2.8.1.1.

2.8.9.2 Kinetic parameters of disproportionation activity

Purified enzyme carrying 4 U disproportionation activity was incubated in 50 mM phosphate buffer pH 6.0 with various concentrations of maltotriose (0 to 200 mM) at 30°C for 10 min. Reaction was stopped by adding 1 N HCl and the amount of glucose in reaction was determined via the glucose oxidase method (Knegtel et al., 1995) as described in section 2.8.1.3.

2.8.9.3 Kinetic parameters of cyclization activity

In the reaction, purified enzyme of 0.05 U starch degradation activity was incubated in 50 mM phosphate buffer pH 6.0 under varying concentrations of pea starch in 3% DMSO (Vongpichayapaiboon et al., 2016) from 0 to 5 mg/ml at 30°C for 60 min. Reaction was stopped by boiling. Glucoamylase 8 U was provided and incubation was continued at 40°C for 16 h. The reaction mixture was terminated by boiling. The activity of cyclization activity was determined as described in section 2.8.1.4. For this activity, kinetic parameters were calculated in term of total LR-CDs.

2.9 Computational analysis of CgAM and LR-CDs in complex

2.9.1 Preparation of CgAM and oligosaccharides structure

Crystal structure of CgAM (PDB: 5B68) was used as a model. All miscellaneous atoms in PDB file was deleted by Discovery studio 2.5^{Accerys inc.}

Oligosaccharide (G11) and cyclodextrins (CD25 and CD28) were built and minimized the structure by HyperChem (TM) Professional 7.51.

2.9.2 Prediction 3-dimensional structure by docking

SwissDock is a web server for prediction the molecular interactions that may occur between a target protein and a small molecule (Grosdidier et al., 2011b). Amylomaltase model and oligosaccharide structure was uploaded to SwissDock server. Due to the limited size of ligand in SwissDock, G11 is the largest molecule for ligand that could be docked via SwissDock. An α -1,4 D glucan was inserted into G11 ligand until the size was up to 25 and 28 monomers in cyclic conformation via Discovery studio 2.5^{Accerys inc.}. It was noted that amyloamaltase-G11 complex was used as a template.

2.9.3 Initial models and system preparation for molecular dynamic simulation

The structures of the complexation between *CgAM-CD25* and *CgAM-CD28* were obtained from section 6.2. AMBER14 package program was used to perform all system preparations and MD simulation processes (Case et al., 2005). The protonation states of the ionizable amino acids such as lysine (K), arginine (R), histidine (H), aspartic acid (D) and glutamic acid (E) were characterized by PROPKA 3.1 (Olsson et al., 2011). The missing hydrogen atoms were added using the Leap module in AMBER14.

The optimum structures of the *CgAM-CD25* and *CgAM-CD28* complex was performed by following these steps; (i) minimized hydrogen atoms with 1500 steps of steepest descents (SD) and followed by 1500 steps of conjugated gradient (CG) by using SANDER module implemented in AMBER14; (ii) subsequently solvated each system with the TIP3P water model (Jorgensen et al., 1983) in a cubic box within 10 Å around the protein surface; (iii) added sodium counterions to neutralize the total negative charge of the complex; (iv) optimized the counterions and water molecules with 1500 steps of SD and CG minimizations, respectively, while the protein and ligand were constrained with a force constant of 500 kcal/mol·Å; (v) kept the whole complex in free of any constraint and eventually minimized with 1500 steps each for SD and CG (Meeprasert et al., 2014).

2.9.4 Interaction analysis via molecular dynamic simulation (MD simulation)

Interaction analysis of *CgAM-CD25* and *CgAM-CD28* complexes were performed by MD simulations under a periodic boundary condition with the NPT ensemble. All covalent bonds involving hydrogen atoms in each system were constrained with the SHAKE algorithm (Ryckaert et al., 1977). The short-range cutoff

of 10 Å for nonbonded interactions was applied, while the particle mesh Ewald (PME) summation method (York et al., 1993) was used for calculating the long-range electrostatic interactions. The simulation time step was of 0.2 ps. The system was initially heated up to 298 K for 200 ps and was then simulated at this temperature at 1 atm till 100 ns. The trajectories were collected every 2 ps for analysis.

2.9.5 The root-mean square displacement (RMSD) and hydrogen bond (H-bond)

RMSD and H-bond were explored using the ptraj module of AMBER. The data was collected and plotted with Origin program. The result was reported in the RMSD plot.

2.9.6 Binding Free Energy

The binding free energy (ΔG_{bind}) was calculated by the MM/PBSA and MM/GBSA approaches using mm_pbsa module (Hou et al., 2011, Li et al., 2007, Meeprasert et al., 2014). In this study, both methods were applied to estimate the ΔG_{bind} between CgAM and ligand (CD25 and CD28) by computing $\Delta \Delta G_{\text{bind}}$ as the free energy difference between the complex (ΔG_{cpx}), protein (ΔG_{prot}), and ligand (ΔG_{lig}) as shown in following equation; $\Delta \Delta G_{\text{bind}} = \Delta G_{\text{cpx}} - (\Delta G_{\text{prot}} + \Delta G_{\text{lig}})$. Each term was obtained from the averaged free energy over 100 trajectories taken from the last 20-ns simulation. The enthalpy in the gas phase (ΔH) and the entropy term ($-T\Delta S$) was used to calculate the free energy of each complex as shown in following equation; $\Delta G = \Delta H - T\Delta S \approx \Delta E_{\text{MM}} + \Delta G_{\text{solv}} - T\Delta S$. The ΔH of the system was predicted from the summation of the gas phase (ΔE_{MM}) and solvation free (ΔG_{solv}) energies. The ΔE_{MM} term was the internal (ΔE_{int}), electrostatic (ΔE_{ele}), and van der

Waals (ΔE_{vdW}) energies, as shown in following equation; $\Delta EMM = \Delta E_{int} + \Delta E_{ele} + \Delta E_{vdW}$, while the ΔG_{solv} term was the sum of the electrostatic ($\Delta G_{ele,solv}$) and nonpolar components ($\Delta G_{nonpolar,solv}$) as outlined by following equation; $\Delta G_{solv} = \Delta G_{ele,solv} + \Delta G_{nonpolar,solv}$. The $\Delta G_{ele,solv}$ was monitored by the means of the Poisson–Boltzmann (PB) and the generalized Born (GB) models, while $\Delta G_{nonpolar,solv}$ was determined using solvent accessible surface area (SASA) (Gohlke and Case, 2004, Kollman et al., 2000) with a probe radius of 1.4 Å using following equation; $\Delta G_{nonpolar,solv} = \gamma SASA$. The dielectric constants of solute and surrounding solvent were set at 1 and 80, respectively. The value for surface tension constant γ of 0.0072 kcal/mol·Å² was used.

2.9.7 Decomposition Free Energy

The per-residue decomposition free energy ($G_{bind/residue}$) was used to estimate the contribution of each residue towards the ligand binding based on the MM/ GBSA approach. One half of the electrostatic interaction (ΔE_{ele}^i) between atoms i and j of the protein and ligand, respectively, was used to calculate the electrostatic contribution as followed;

$$E_{ele}^i = \frac{1}{2} \sum_{i \neq j} \frac{q_i q_j}{r_{ij}}$$

; q_i and q_j represent the atomic charges of atoms i and j , respectively, and r_{ij} is the distance between these two atoms.

For the per-residue intermolecular vdW interaction (E_{vdW}^i) to avoiding double counting, the internal energy (ΔE_{int}) was equal to zero and the electrostatic free energy component was calculated based on the GB method following equation;

$$\Delta G_{ele,solv} = -\frac{1}{2} \left(1 - \frac{e^{-\kappa f_{GB}}}{\epsilon_{\omega}} \right) \sum_{ij} \frac{q_i q_j}{f_{GB}}$$

; The dielectric constant of solvent (ϵ_{ω}) and the Debye–Hückel screening parameter (κ) were identified as 80 and 0, respectively. And f_{GB} was a smooth function interpolating between atomic radii and the distance between atoms i and j , in which the double sum runs over all pairs of atoms. The equation is following;

$$f_{GB} = \left[r_{ij}^2 + \alpha_i \alpha_j \exp\left(\frac{-r_{ij}^2}{4\alpha_i \alpha_j}\right) \right]^{1/2}$$

; The α_i and α_j are the effective Born radii of atoms i and j , respectively. The contribution of atom i on the electrostatic free energy could define by the following equation;

$$\Delta G_{ele,solv}^i = -\frac{1}{2} \sum_y \left(1 - \frac{e^{-\kappa f_{GB}}}{\epsilon_{\omega}} \right) \frac{q_i q_j}{f_{GB}(r_{ij})} + \frac{1}{2} \sum_{i \neq j} \frac{q_i q_j}{r_{ij}}$$

Moreover, the SASA of atom i in the complex and the separated parts in the nonpolar component was calculated by following equation;

$$\Delta G_{nonpolar,solv}^i = \gamma \times \left(SASA^{i,com} - \left(SASA^{i,prot} + SASA^{i,lig} \right) \right)$$

; The $SASA_{prot}^i$ and $SASA_{lig}^i$ are equal to zero depending on molecule that atom belonged to. So, the $\Delta G_{bind}^{residue}$ was summarized from E_{ele}^i , E_{vdW}^i , $\Delta G_{nonpolar,solv}^i$ and $\Delta G_{ele,solv}^i$.

Similarly, the binding free energy contributions of the residue, backbone, and side chain were calculated separately from the related atoms.

CHAPTER III

RESULTS

3.1 Cloning of mutated *CgAM* genes

All mutants were constructed by PCR mediated site-directed mutagenesis, except E231Y which was given by Asst. Prof. Kuakarun Krusong, Ph.D. PCR products were successfully amplified and then checked by agarose gel electrophoresis. For P228Y, A413F and G417F, all recombinant plasmids were constructed by site-directed mutagenesis using *CgAM*-pET19b as a template followed by the condition described in section 1. The size of P228Y, A413F and G417F *CgAM*-pET19b recombinant plasmid was 7,838 bp. The size of PCR products was confirmed by agarose gel electrophoresis (Figure 3.1). All mutated clones were subjected to DNA sequencing, aiming to verify mutated amino acid of *CgAM* (Figure 3.2).

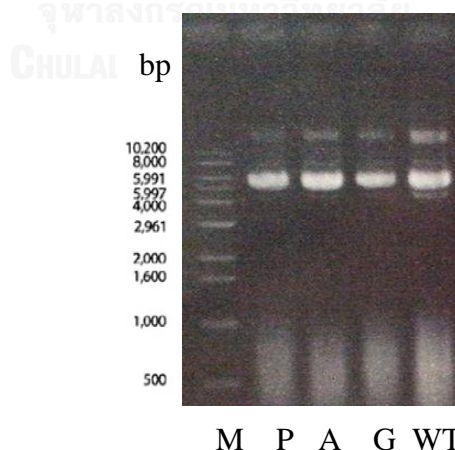


Figure 3.1 Agarose gel electrophoresis of the recombinant plasmids carrying mutated *CgAM* genes

Lane M = DNA Marker, P = P228Y, A = A413F and G = G417F, WT = Wild type

```

CLUSTAL O(1.2.1) multiple sequence alignment

G417F 1 MTARRFLNELADLYGVATSYTDYKGAHIEVSDDTLVKILRALGVNLDTSNLPNDDAIQRQ 60
A413F 1 MTARRFLNELADLYGVATSYTDYKGAHIEVSDDTLVKILRALGVNLDTSNLPNDDAIQRQ 60
P228Y 1 MTARRFLNELADLYGVATSYTDYKGAHIEVSDDTLVKILRALGVNLDTSNLPNDDAIQRQ 60
E231Y 1 MTARRFLNELADLYGVATSYTDYKGAHIEVSDDTLVKILRALGVNLDTSNLPNDDAIQRQ 60
CgAM 1 MTARRFLNELADLYGVATSYTDYKGAHIEVSDDTLVKILRALGVNLDTSNLPNDDAIQRQ 60
*****

G417F 61 IALFHDREFRTRPLPPSVVAVEGDELVFPVHVHDGSPADVHIELEDGTQRDVSQVENWTAP 120
A413F 61 IALFHDREFRTRPLPPSVVAVEGDELVFPVHVHDGSPADVHIELEDGTQRDVSQVENWTAP 120
P228Y 61 IALFHDREFRTRPLPPSVVAVEGDELVFPVHVHDGSPADVHIELEDGTQRDVSQVENWTAP 120
E231Y 61 IALFHDREFRTRPLPPSVVAVEGDELVFPVHVHDGSPADVHIELEDGTQRDVSQVENWTAP 120
CgAM 61 IALFHDREFRTRPLPPSVVAVEGDELVFPVHVHDGSPADVHIELEDGTQRDVSQVENWTAP 120
*****

G417F 121 REIDGIRWGEASFKIPGDLPLGWKHLHLSNERSAECGLIITPARLSTADKYLDSPRSGV 180
A413F 121 REIDGIRWGEASFKIPGDLPLGWKHLHLSNERSAECGLIITPARLSTADKYLDSPRSGV 180
P228Y 121 REIDGIRWGEASFKIPGDLPLGWKHLHLSNERSAECGLIITPARLSTADKYLDSPRSGV 180
E231Y 121 REIDGIRWGEASFKIPGDLPLGWKHLHLSNERSAECGLIITPARLSTADKYLDSPRSGV 180
CgAM 121 REIDGIRWGEASFKIPGDLPLGWKHLHLSNERSAECGLIITPARLSTADKYLDSPRSGV 180
*****

G417F 181 MAQIYSVRSTLSWGMGDFNDLGNLASVVAQDGADFLINPMHAAEPLPTE181DSPLYLTTR 240
A413F 161 MAQIYSVRSTLSWGMGDFNDLGNLASVVAQDGADFLINPMHAAEPLPTE181DSPLYLTTR 240
P228Y 161 MAQIYSVRSTLSWGMGDFNDLGNLASVVAQDGADFLINPMHAAEPLPTE181DSPLYLTTR 240
E231Y 161 MAQIYSVRSTLSWGMGDFNDLGNLASVVAQDGADFLINPMHAAEPLPTE181DSPLYLTTR 240
CgAM 161 MAQIYSVRSTLSWGMGDFNDLGNLASVVAQDGADFLINPMHAAEPLPTE181DSPLYLTTR 240
*****

G417F 241 RFINPIYIRVEDIPEFNQLEIDLRRDIAEMAAEFRENRNTSDIERNDVYAAKLQVLRAI 300
A413F 241 RFINPIYIRVEDIPEFNQLEIDLRRDIAEMAAEFRENRNTSDIERNDVYAAKLQVLRAI 300
P228Y 241 RFINPIYIRVEDIPEFNQLEIDLRRDIAEMAAEFRENRNTSDIERNDVYAAKLQVLRAI 300
E231Y 241 RFINPIYIRVEDIPEFNQLEIDLRRDIAEMAAEFRENRNTSDIERNDVYAAKLQVLRAI 300
CgAM 241 RFINPIYIRVEDIPEFNQLEIDLRRDIAEMAAEFRENRNTSDIERNDVYAAKLQVLRAI 300
*****

G417F 301 FEMPRSSEREANFVSVQREGQGLIDFATWCADRETAQSESVHGTEPDRDELTMFYMWLQ 360
A413F 301 FEMPRSSEREANFVSVQREGQGLIDFATWCADRETAQSESVHGTEPDRDELTMFYMWLQ 360
P228Y 301 FEMPRSSEREANFVSVQREGQGLIDFATWCADRETAQSESVHGTEPDRDELTMFYMWLQ 360
E231Y 301 FEMPRSSEREANFVSVQREGQGLIDFATWCADRETAQSESVHGTEPDRDELTMFYMWLQ 360
CgAM 301 FEMPRSSEREANFVSVQREGQGLIDFATWCADRETAQSESVHGTEPDRDELTMFYMWLQ 360
*****

G417F 361 WLCDEQLAAQKRAVDAGMSIGIMADLAVGVHGGADAQNL361SHVLAPDASVGPDP361Y361NQ 420
A413F 361 WLCDEQLAAQKRAVDAGMSIGIMADLAVGVHGGADAQNL361SHVLAPDASVGPDP361Y361NQ 420
P228Y 361 WLCDEQLAAQKRAVDAGMSIGIMADLAVGVHGGADAQNL361SHVLAPDASVGPDP361Y361NQ 420
E231Y 361 WLCDEQLAAQKRAVDAGMSIGIMADLAVGVHGGADAQNL361SHVLAPDASVGPDP361Y361NQ 420
CgAM 361 WLCDEQLAAQKRAVDAGMSIGIMADLAVGVHGGADAQNL361SHVLAPDASVGPDP361Y361NQ 420
*****

G417F 421 QGQDWSQPPWHVRLAEEGYIPWRNLLRTVLRHSGGIRVDHVLGLFRLFVMPRMQSPATG 480
A413F 421 QGQDWSQPPWHVRLAEEGYIPWRNLLRTVLRHSGGIRVDHVLGLFRLFVMPRMQSPATG 480
P228Y 421 QGQDWSQPPWHVRLAEEGYIPWRNLLRTVLRHSGGIRVDHVLGLFRLFVMPRMQSPATG 480
E231Y 421 QGQDWSQPPWHVRLAEEGYIPWRNLLRTVLRHSGGIRVDHVLGLFRLFVMPRMQSPATG 480
CgAM 421 QGQDWSQPPWHVRLAEEGYIPWRNLLRTVLRHSGGIRVDHVLGLFRLFVMPRMQSPATG 480
*****

G417F 481 TYIRFDHNALVGI481LAE481LAGAVVIGEDLGT481FEPWVQDALAQRGIMGTSILWFEHSPSQ 540
A413F 481 TYIRFDHNALVGI481LAE481LAGAVVIGEDLGT481FEPWVQDALAQRGIMGTSILWFEHSPSQ 540
P228Y 481 TYIRFDHNALVGI481LAE481LAGAVVIGEDLGT481FEPWVQDALAQRGIMGTSILWFEHSPSQ 540
E231Y 481 TYIRFDHNALVGI481LAE481LAGAVVIGEDLGT481FEPWVQDALAQRGIMGTSILWFEHSPSQ 540
CgAM 481 TYIRFDHNALVGI481LAE481LAGAVVIGEDLGT481FEPWVQDALAQRGIMGTSILWFEHSPSQ 540
*****

G417F 541 PGPRRQEEYRPLALTTVTT541HDL541PPTAGYLEGEHIALRERLGV541LNTP541PAE541LAEDLQ541WQAE 600
A413F 541 PGPRRQEEYRPLALTTVTT541HDL541PPTAGYLEGEHIALRERLGV541LNTP541PAE541LAEDLQ541WQAE 600
P228Y 541 PGPRRQEEYRPLALTTVTT541HDL541PPTAGYLEGEHIALRERLGV541LNTP541PAE541LAEDLQ541WQAE 600
E231Y 541 PGPRRQEEYRPLALTTVTT541HDL541PPTAGYLEGEHIALRERLGV541LNTP541PAE541LAEDLQ541WQAE 600
CgAM 541 PGPRRQEEYRPLALTTVTT541HDL541PPTAGYLEGEHIALRERLGV541LNTP541PAE541LAEDLQ541WQAE 600
*****

G417F 601 ILDVAASANALPAREYVGLERDQ601RGELAE601LLEGLHTFVAKT601PSALT601CVCLVDMVGEKRAQ 660
A413F 601 ILDVAASANALPAREYVGLERDQ601RGELAE601LLEGLHTFVAKT601PSALT601CVCLVDMVGEKRAQ 660
P228Y 601 ILDVAASANALPAREYVGLERDQ601RGELAE601LLEGLHTFVAKT601PSALT601CVCLVDMVGEKRAQ 660
E231Y 601 ILDVAASANALPAREYVGLERDQ601RGELAE601LLEGLHTFVAKT601PSALT601CVCLVDMVGEKRAQ 660
CgAM 601 ILDVAASANALPAREYVGLERDQ601RGELAE601LLEGLHTFVAKT601PSALT601CVCLVDMVGEKRAQ 660
*****

G417F 661 NQPCTTRDMPNWCIP661LCDS661EGNSV661LIES661LR661ENEL661YHRVAKASKRD 706
A413F 661 NQPCTTRDMPNWCIP661LCDS661EGNSV661LIES661LR661ENEL661YHRVAKASKRD 706
P228Y 661 NQPCTTRDMPNWCIP661LCDS661EGNSV661LIES661LR661ENEL661YHRVAKASKRD 706
E231Y 661 NQPCTTRDMPNWCIP661LCDS661EGNSV661LIES661LR661ENEL661YHRVAKASKRD 706
CgAM 661 NQPCTTRDMPNWCIP661LCDS661EGNSV661LIES661LR661ENEL661YHRVAKASKRD 706
*****

```

Figure 3.2 Multiple sequence alignment of WT, P228Y, E231Y, A413F and G417F sequences using Clustal W tool. The highlights indicated where the mutation located.

3.2 Optimization of CgAM gene expression

WT, E231Y, P228Y, A413F and G417F mutants were expressed in *E. coli* BL21 (DE3). To optimize the highest level of CgAM gene expression, the effect of temperature, concentration of inducer (IPTG) and expression time were investigated. Induction temperature was at 16, 30 and 37°C under various time for IPTG induction (0, 2, 4, 6 and 18 h). For A413F and G417F CgAM mutants, they were expressed insoluble form at 6 and 18 h IPTG induction time (Figure 3.4 (A), (B) and 3.5). To increase the expression level of A413F and G417F in soluble form, 1% (w/v) of glucose was added into LB medium, in order to tighten the protein expression control. It was found that the expressions of mutated CgAMs in soluble form were successfully enhanced as shown in Figure 3.4 (C) and 3.6. Figure 3.3 – 3.6 showed that the expression level of mutated CgAMs was successfully increased by addition of 1 mM IPTG. Generally, higher level of expression of soluble CgAM was obtained from cultivating at 16°C using 1 mM IPTG. For A413F and G417F CgAMs, 1% (w/v) of glucose was required prior to IPTG induction. The optimum expression conditions of all CgAMs were described in Table 3.1

Table 3.1 Expression condition of WT and CgAM mutated enzymes

CgAM	Vector	Expression	Remarks
WT	pET17b, pET19b	Induction at 37°C using 0.4 mM IPTG for 2 h with 250 rpm shaking	given by Asst. Prof. Kuakarun Krusong, Ph.D.
E231Y	pET17b	Induction at 16°C using 1 mM IPTG for 18 h with 250 rpm shaking	
P228Y	pET19b	Induction at 16°C using 1 mM IPTG for 18 h with 250 rpm shaking	Constructed by site-directed mutagenesis, subcloned and transformed to <i>E. coli</i> BL21(DE3)
A413F	pET19b	Addition of 1% glucose before induction period. Induction at 16 °C using 1 mM IPTG for 18 h with 250 rpm shaking	
G417F	pET19b	Addition of 1% glucose before induction period. Induction at 16 °C using 1 mM IPTG for 18 h with 250 rpm shaking	

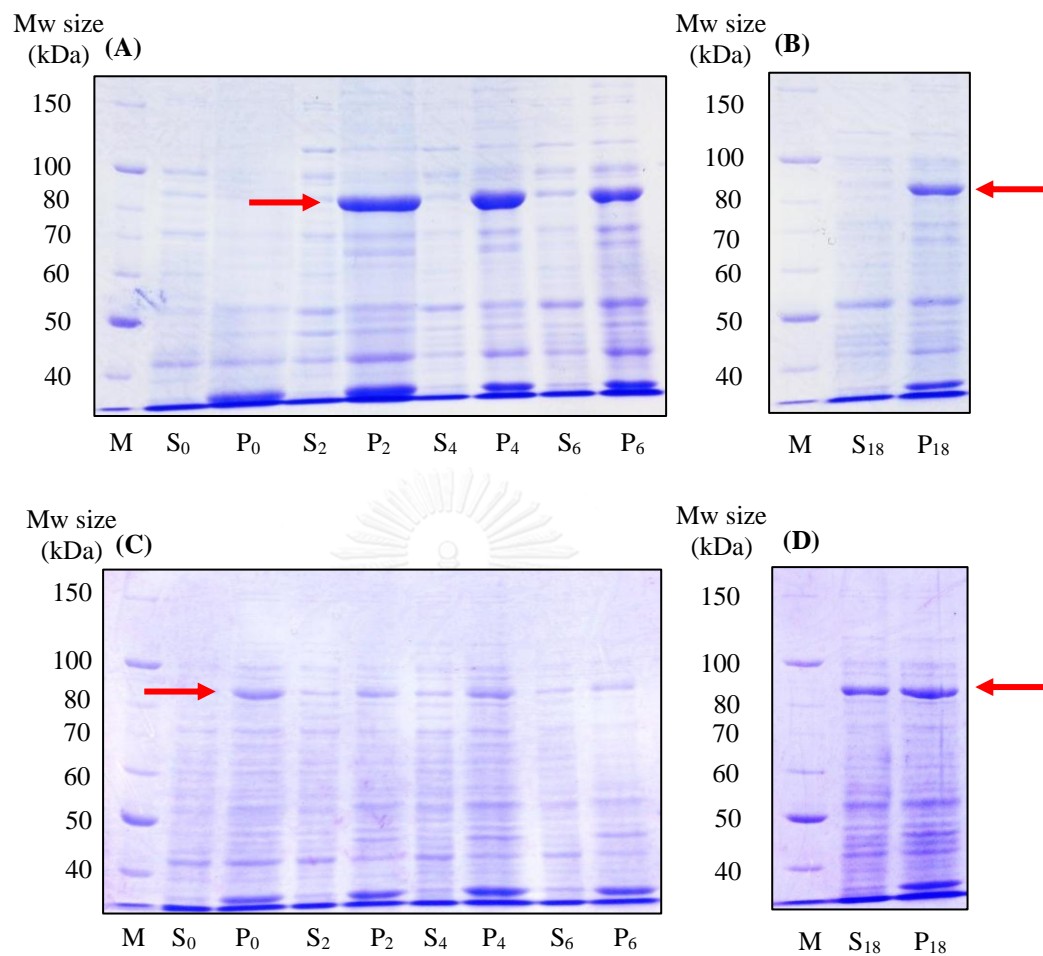


Figure 3.3 SDS-PAGE analysis of expression level of P228Y CgAM in BL21 (DE3) using 1mM IPTG for induction (A), (B) at 37°C, (C) and (D) at 16°C

Lane M = Protein marker, S = Soluble fraction, P = Pellet fraction and number = induction time (h)

The red arrow indicates the expected P228Y CgAM band of 78.6 kDa

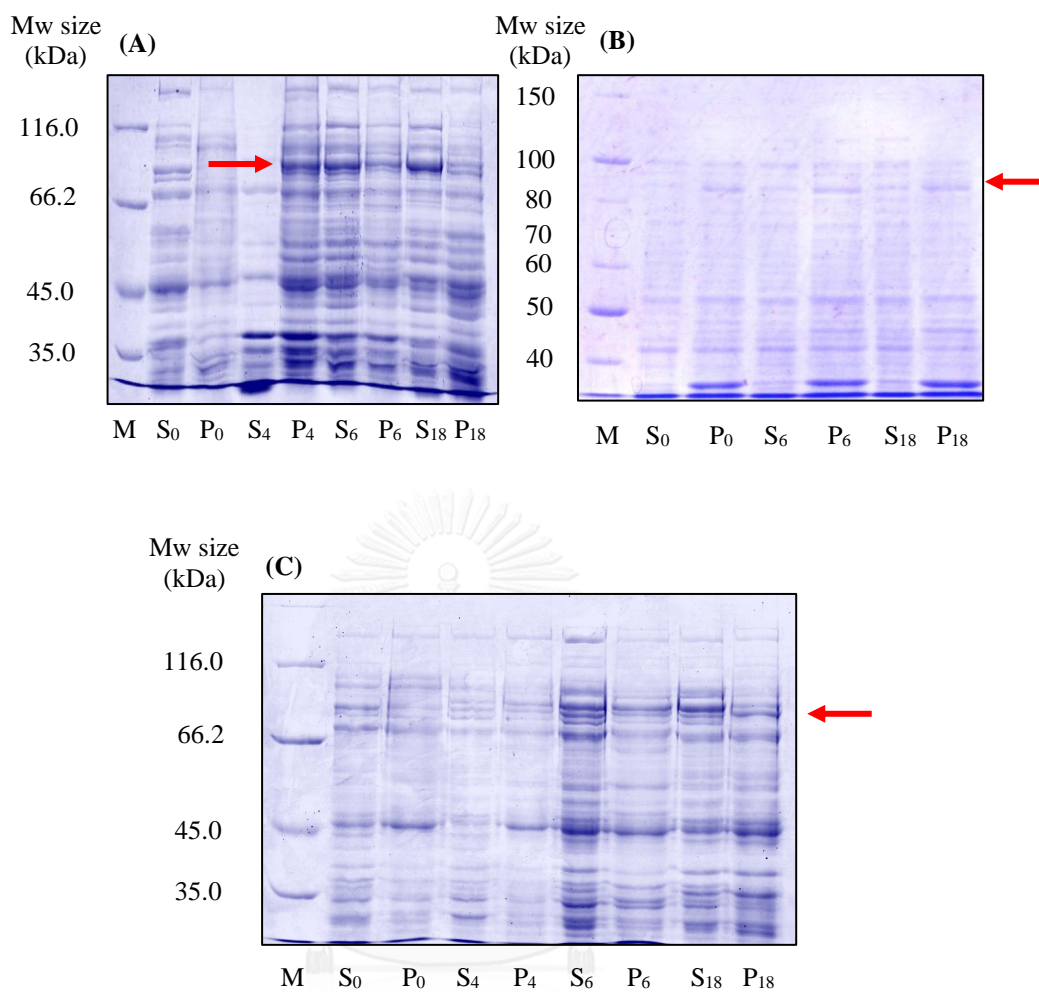


Figure 3.4 SDS-PAGE analysis of expression level of A413F CgAM in BL21 (DE3) using 1mM IPTG for induction at various temperatures (A) 20°C, (B) 16°C, (C) 16°C with 1% glucose

Lane M = Protein marker, S = Soluble fraction, P = Pellet fraction and number = induction time (h)

The red arrow indicates the expected A413F CgAM band of 78.6 kDa

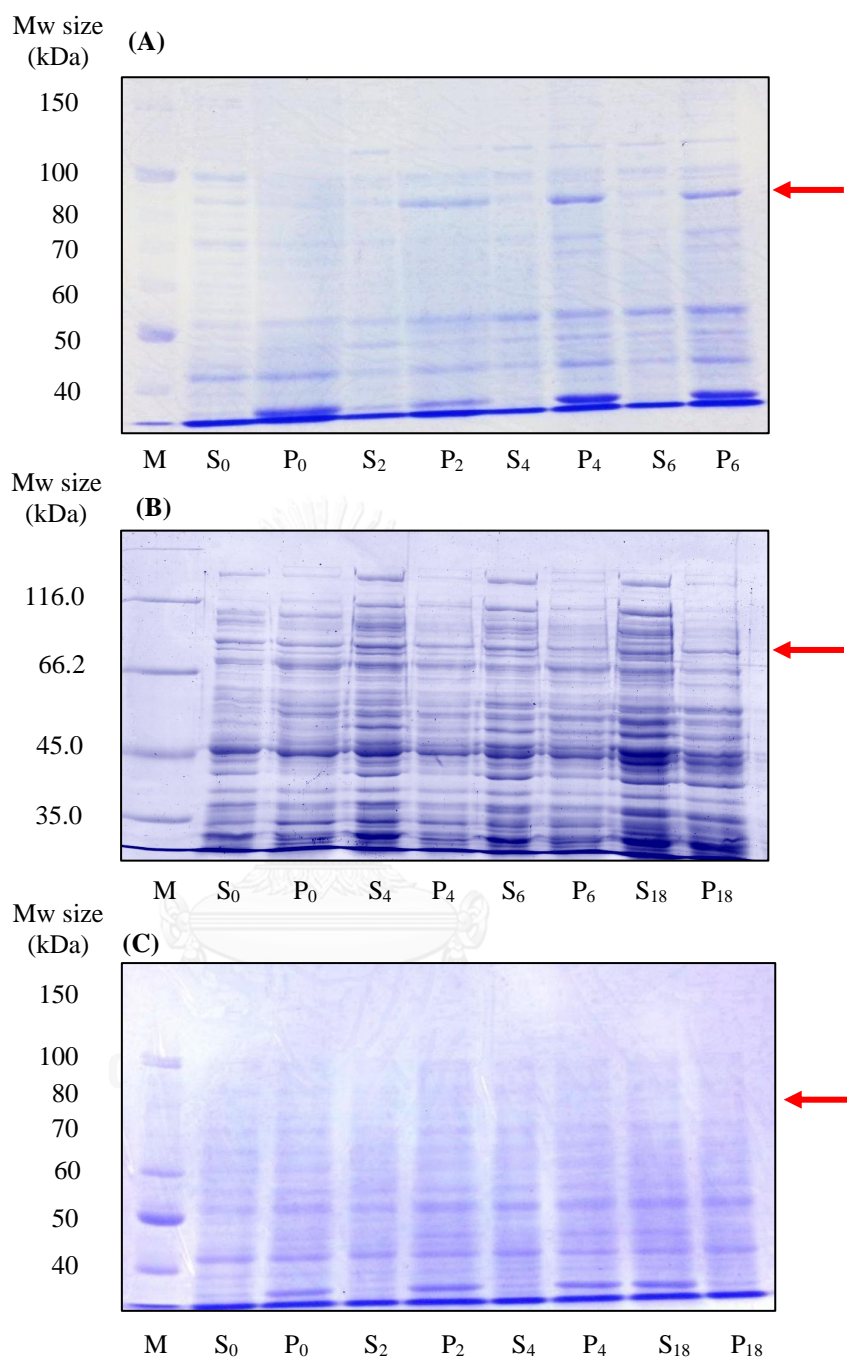


Figure 3.5 SDS-PAGE analysis of expression level of G417F CgAM in BL21 (DE3) using 1mM IPTG for induction at various temperatures (A) 37°C, (B) 20°C, (C) 16°C

Lane M = Protein marker, S = Soluble fraction, P = Pellet fraction and number = induction time (h)

The red arrow indicates the expected G417F CgAM band of 78.6 kDa

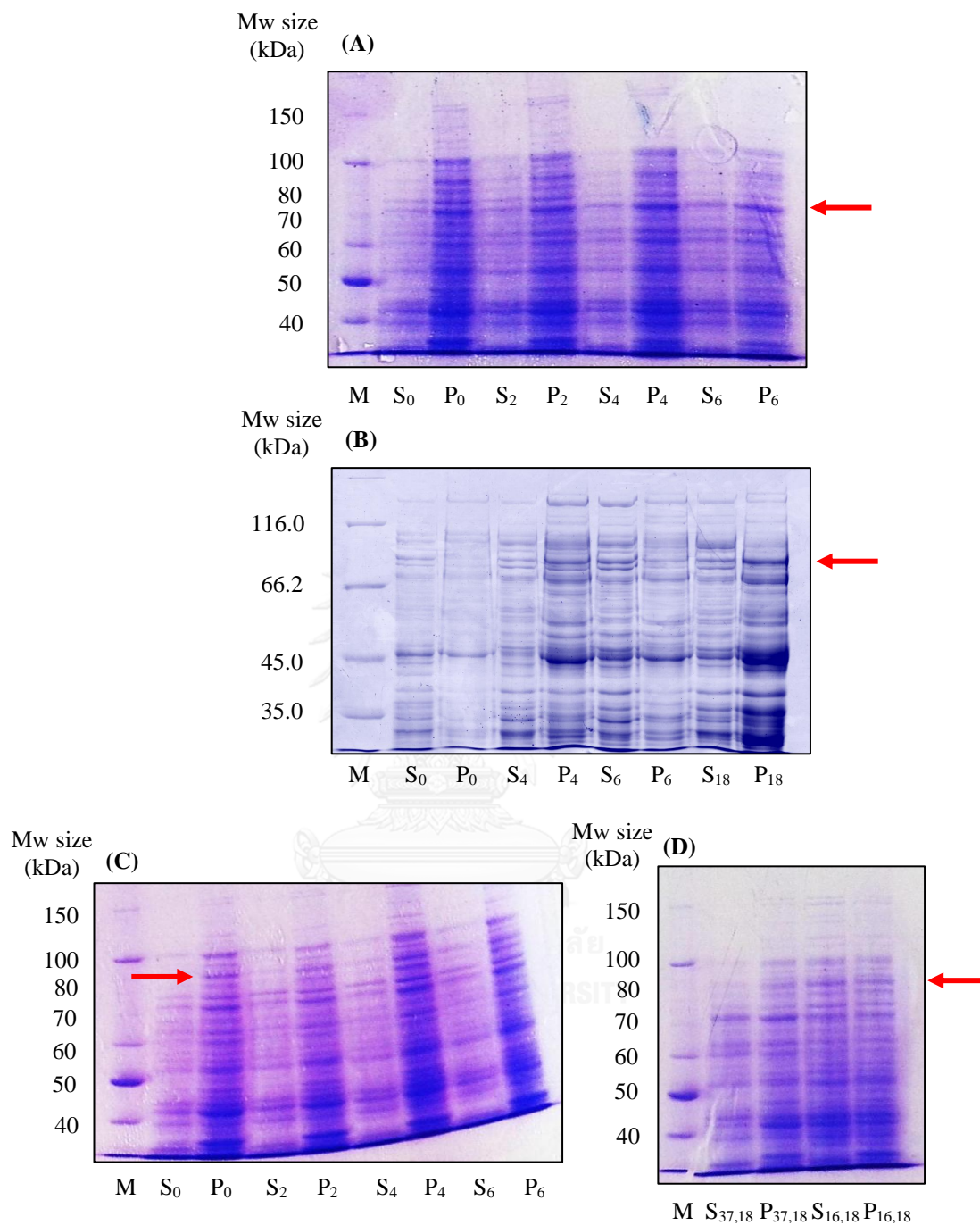


Figure 3.6 SDS-PAGE analysis of expression level of G417F CgAM in BL21 (DE3) with 1% glucose using 1mM IPTG for induction at various temperatures (A) 37°C, (B) 20°C, (C) 16°C, (D) 37 and 16°C

Lane M = Protein marker, S = Soluble fraction, P = Pellet fraction and number = induction time (h)

The red arrow indicates the expected G417F CgAM band of 78.6 kDa

3.3 Large scale production of CgAMs and preparation of CgAM crude extract

To obtain enough enzyme concentration, scale-up production of each mutant was performed at their optimum condition as described in Table 3.1 for at least 2 L. Purification table of all mutants were described in Table 3.2. Crude enzyme with specific activity of 2 and 2.3 U/mg were obtained from WT-pET17b and WT-pET19b, respectively. The specific activity of P228Y, E231Y, A413F and G417F CgAM were 2.7, 2.2, 2 and 1.9 U/mg, respectively (Table 3.2).

3.4 Purification of mutated CgAMs

3.4.1 Purification of E231Y by DEAE and phenyl column chromatography

E231Y was successfully purified by two-step purification; DEAE FF and phenyl FF columns. The specific activity of crude E231Y CgAM was 2.2 U/mg, while WT's was also about 2.0 U/mg. The purity of E231Y after purified through each purification step was determined by SDS-PAGE.

3.4.1.1 DEAE FFTM column chromatography

Initially, DEAE column was used to purify E231Y CgAM. Fractions eluted with 300 mM NaCl carried higher starch transglycosylation activity than those of eluted with 200 mM NaCl. Hence, fractions from 300 mM NaCl elution were pooled and dialyzed against 50 mM phosphate buffer pH 7.4 before subjecting to next purification step. E231Y CgAM was partially purified by 16.6-fold with a specific activity of 36.6 U/mg.

3.4.1.2 Phenyl FFTM column chromatography

Partially purified E231Y CgAM from section 3.4.1.1 was subjected to Phenyl column chromatography. Prior to use this column, (NH₄)₂SO₄ was added to

the partial purified enzyme to the final concentration of 1 M. The result showed that E231Y *CgAM* was eluted when the concentration of $(\text{NH}_4)_2\text{SO}_4$ reach 0 mM. The condition for purifying E231Y was reported in Table 3.3. A single band of purified E231Y enzyme with the size of 84 kDa was shown in Figure 3.7. The purified enzyme displayed a specific activity of 47.2 U/mg and the purity was increased by 21.5-fold.

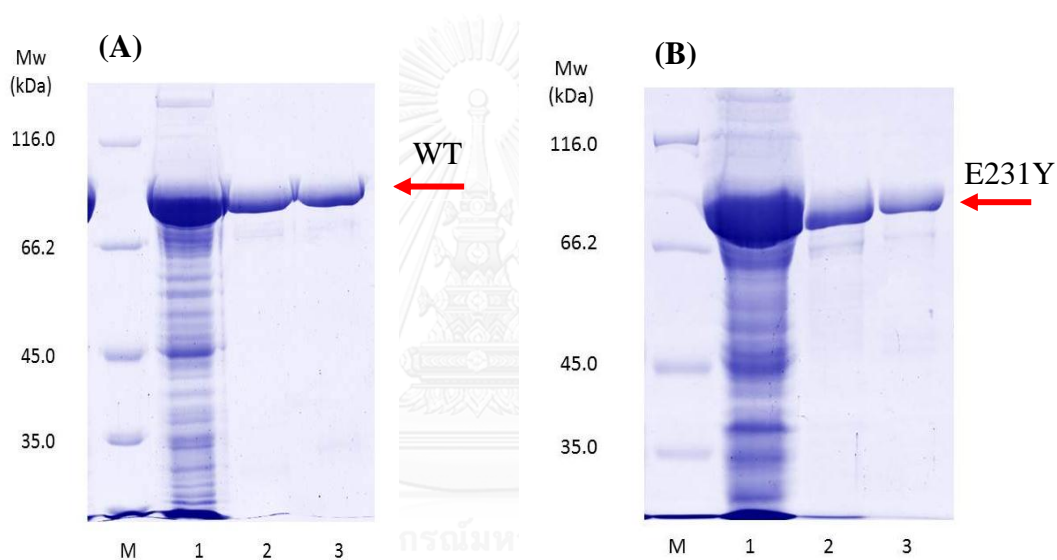


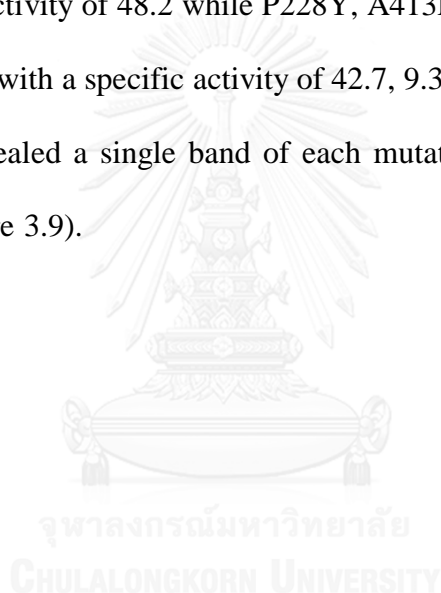
Figure 3.7 SDS-PAGE analysis of (A) WT *CgAM* (B) E231Y *CgAM*

Lane M = protein marker, lane 1 = crude extract (20 μg), lane 2 = partial purified enzyme from DEAE column (5 μg), lane 3 = purified enzyme from phenyl column chromatography (3 μg).

The red arrow indicates purified *CgAM*

3.4.2 Purification of P228Y, A413F and G417F by His trap column chromatography

HisTrap FF column, an affinity column that has a specificity towards Histidine tag (His-tag) protein, was used to purify P228Y, A413F and G417F CgAMs. The conditions for purifying these mutants were summarized in Table 3.3. P228Y, A413F and G417F CgAMs were eluted by 200 mM imidazole in 50 mM phosphate buffer pH 7.4 as indicated in Figure 3.8. WT enzyme was purified by 21.1-fold with a specific activity of 48.2 while P228Y, A413F and G417F were purified by 16, 4.7 and 19.2-fold with a specific activity of 42.7, 9.3 and 36.3, respectively (Table 3.2). SDS-PAGE revealed a single band of each mutated CgAM with an estimated MW of 84 kDa (Figure 3.9).



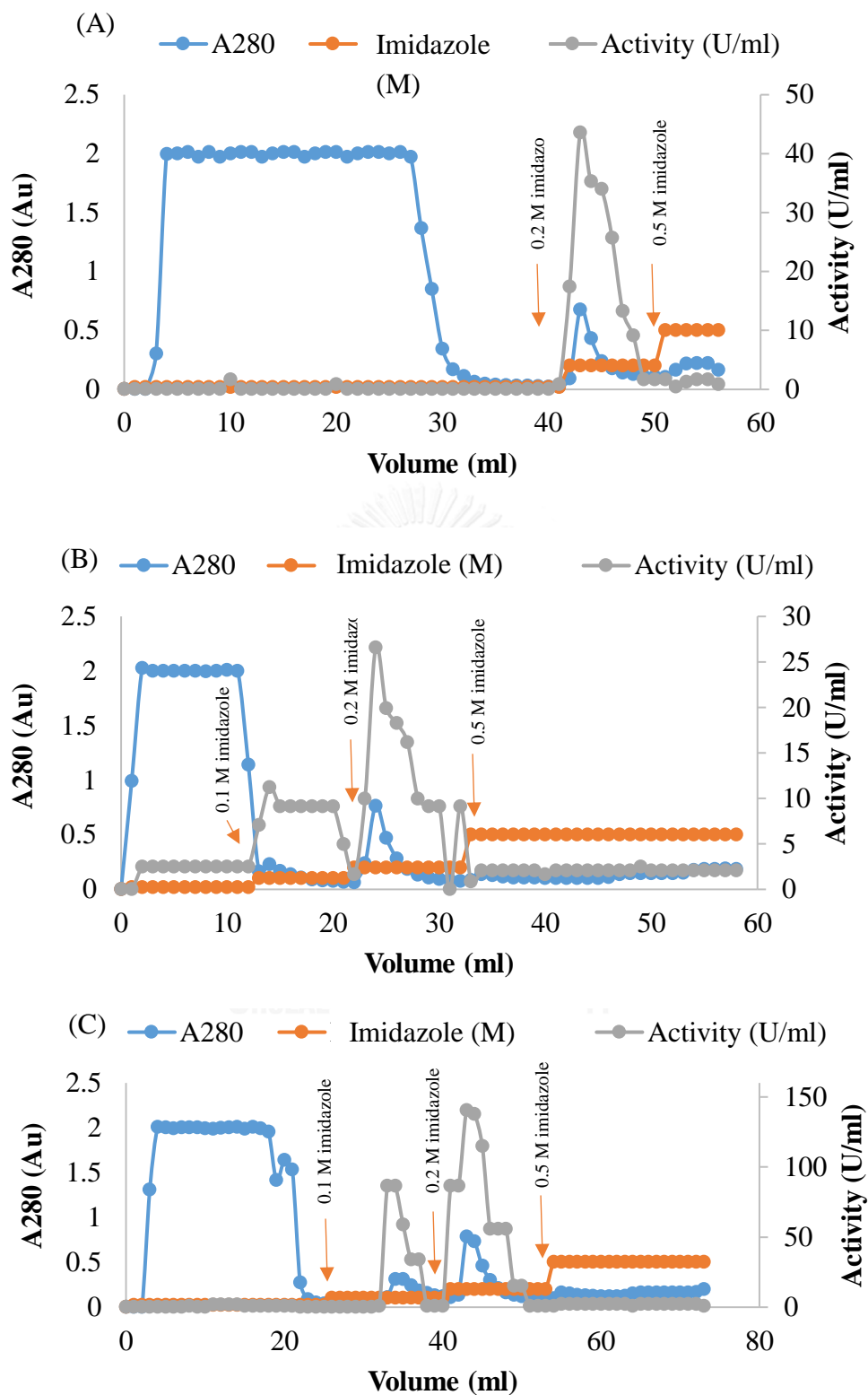


Figure 3.8 Purification profile of mutated CgAMs by HisTrap column chromatography (A) P228Y (B) A413F (C) G417F

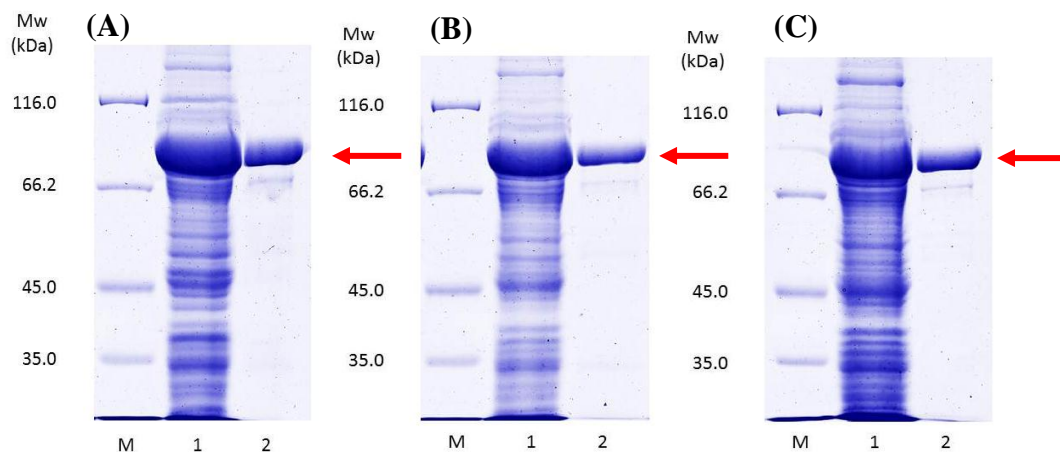


Figure 3.9 SDS-PAGE analysis of purified mutated CgAMs by HisTrap column (A) P228Y (B) A413F (C) G417F

Lane M = molecular weight marker, lane 1 crude extract (20 μg), lane 2 purified enzymes (3 μg)

The red arrow indicates purified CgAM

Table 3.2 Purification table of WT and mutated CgAMs

Enzyme	Purification step	Total protein (mg)	Total activity (U)	Specific activity ^a (U/mg)	Purification fold	Yield (%)
WT	Crude extract	217.1	441.5	2.0	1.0	100.0
	DEAE TM FF	12.4	438.1	35.3	17.6	99.3
	Phenyl TM FF	2.6	111.2	42.8	21.4	25.2
	Crude extract	184.7	421.6	2.3	1.0	100.0
	His Trap HP	2.1	103.7	48.2	21.1	24.6
E231Y	Crude extract	232.0	514.3	2.2	1.0	100.0
	DEAE TM FF	10.5	384.2	36.6	16.6	74.7
	Phenyl TM FF	3.1	146.4	47.2	21.5	28.5
P228Y	Crude extract	264.5	706.6	2.7	1.0	100.0
	His Trap HP	4.1	175.1	42.7	16.0	24.8
A413F	Crude extract	146.0	292.1	2.0	1.0	100.0
	His Trap HP	19.9	185.9	9.3	4.7	63.6
G417F	Crude extract	307.5	580.9	1.9	1.0	100.0
	His Trap HP	7.7	280.5	36.3	19.2	48.3

^aassayed by starch transglycosylation activity.

Table 3.3 Summary of purification conditions for *CgAM* mutants

Mutant	Purification Method	Purification condition
WT	DEAE/Phenyl (+)	DEAE FF™ : 50 mM Phosphate buffer pH 7.4 + 0.01% β – mercaptoethanol + 300 mM NaCl Phenyl FF™ : 50 mM Phosphate buffer pH 7.4 + 0.01% β – mercaptoethanol
	Ni-NTA (+)	50 mM Phosphate buffer pH 7.4 + 500 mM NaCl + 500 mM Imidazole
E231Y	DEAE/Phenyl (+)	DEAE FF™ : 50 mM Phosphate buffer pH 7.4 + 0.01% β – mercaptoethanol + 300 mM NaCl Phenyl FF™ : 50 mM Phosphate buffer pH 7.4 + 0.01% β – mercaptoethanol
P288Y	Ni-NTA (+)	50 mM Phosphate buffer pH 7.4 + 500 mM NaCl + 200 mM Imidazole
A413F	Ni-NTA (+)	50 mM Phosphate buffer pH 7.4 + 500 mM NaCl + 200 mM Imidazole
G417F	Ni-NTA (+)	50 mM Phosphate buffer pH 7.4 + 500 mM NaCl + 200 mM Imidazole

3.5 Characterization of WT and mutated CgAMs

3.5.1 Enzyme assay

All activities of starch transglycosylation, starch degradation, disproportionation, cyclization, coupling and hydrolysis were summarized in Table 3.4.

3.5.1.1 Starch Transglycosylation activity

From the Table 3.4, P228Y, E231Y and G417F CgAMs showed the similar specific activity of transglycosylation (52.2, 61.2 and 52.3 U/mg) to the WT enzyme (59.9 U/mg).

3.5.1.2 Starch degradation activity

The specific activities of starch degradation of WT, E231Y, P228Y and G417F were 0.37, 0.37, 0.32 and 0.31 U/mg, respectively. A413F displayed much lower specific activity of starch degradation (0.11 U/mg), in comparison to other CgAMs.

3.5.1.3 Disproportionation activity

E231Y and G417F showed higher specific activities of disproportionation than the WT enzyme (Table 3.4). However, P228Y and A413F displayed much lower specific activity of disproportionation than WT CgAM. The specific activities of disproportionation of WT, G417F, E231Y, P228Y and A413F were 43.5, 53.5, 50.2, 16.3 and 9.04, respectively.

3.5.1.4 Cyclization activity

The result indicated that E231Y had cyclization activity (0.013 U/mg) at the same level of the WT enzyme (0.012 U/mg). Meanwhile, P228Y and G417F

possessed lower cyclization activity than the WT by 2-fold. Among all mutants, A413F showed the lowest cyclization activity of about 0.0001 U/mg.

3.5.1.5 Coupling activity

E231Y displayed the similar coupling activity (0.0010 U/mg) to the WT enzyme (0.0012 U/mg). Meanwhile, P228Y, A413F and G417F showed lower coupling activity of 0.0002, 0.0001 and 0.0004 U/mg, respectively (Table 3.4).

3.5.1.6 Hydrolytic activity

Table 3.4 showed that specific activities of hydrolysis of all CgAMs were not significantly different. The specific activities of hydrolysis of WT, P228Y, E231Y, A413F and G417F CgAMs were 0.03, 0.02, 0.02, 0.01 and 0.03 U/mg, respectively.

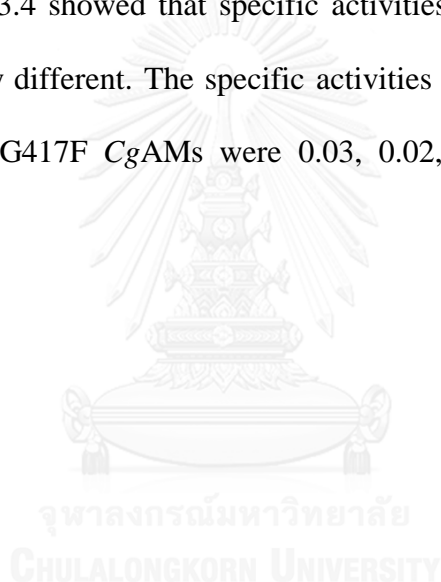


Table 3.4 Specific activity of WT and mutated CgAMs

CgAM activity	Specific activity (U/mg protein)				
	WT	P228Y	E231Y	A413F	G417F
Starch transglycosylation	59.9 ± 2.29	52.2 ± 0.54	61.2 ± 1.10	18.8 ± 1.99	52.3 ± 1.07
Starch degradation	0.37 ± 0.02	0.32 ± 0.01	0.37 ± 0.00	0.11 ± 0.02	0.31 ± 0.01
Disproportionation	43.5 ± 0.64	16.3 ± 1.05	50.2 ± 1.36	9.04 ± 1.05	53.5 ± 1.21
Cyclization	0.0012 ± 0.0005	0.0009 ± 0.0001	0.0013 ± 0.0001	0.0001 ± 0.0001	0.0007 ± 0.0003
Coupling	0.0012 ± 0.0007	0.0002 ± 0.0001	0.0010 ± 0.0005	0.0001 ± 0.0001	0.0004 ± 0.0001
Hydrolysis	0.03 ± 0.00	0.02 ± 0.00	0.02 ± 0.00	0.01 ± 0.00	0.03 ± 0.00

*Data was shown in term of mean ± S.D. from three independent repeats

3.5.2 Effect of temperature on starch transglycosylation activity

To determine the optimum temperature on *CgAM* activity, all purified *CgAMs* were tested for starch transglycosylation activity assay at various temperatures (20, 30, 35, 40, 50, 60 and 70°C). Transglycosylation activity was measured by iodine method. WT and G417F showed the same optimum temperature at 30°C whereas P228Y and A413F displayed optimum temperature at 25°C and 35°C, respectively (Figure 3.10). The optimum temperature of E231Y was 35°C which was reported in previous research (Pathomsoonthornchai, 2015).

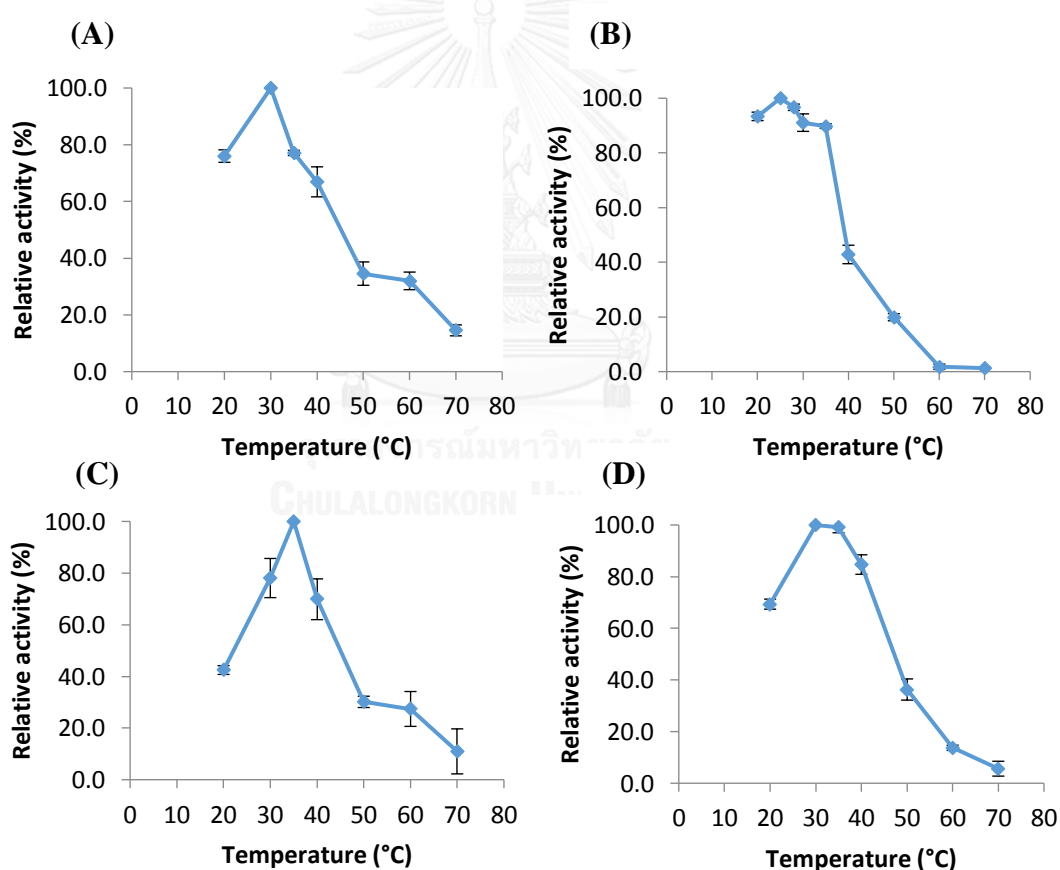


Figure 3.10 Effect of temperature on starch transglycosylation activity (A) wild-type (B) P228Y (C) A413F (D) G417F

3.5.3 Effect of temperature on starch transglycosylation stability

To determine the effect of temperature on *CgAM* stability, purified enzymes were pre-incubated at different temperature (20, 30, 35, 40, 50, 60 and 70°C) for 1 h before investigating residual starch transglycosylation activity by iodine method as described in section 2.8.1.1. The results showed that the enzyme maintained 80% of its activity in range of 20 to 30°C. At higher temperature than 30°C, the activity of all mutated *CgAM*s was dramatically dropped (Figure 3.11). The temperature stability of E231Y was reported in previous research (Pathomsoonthornchai, 2015).

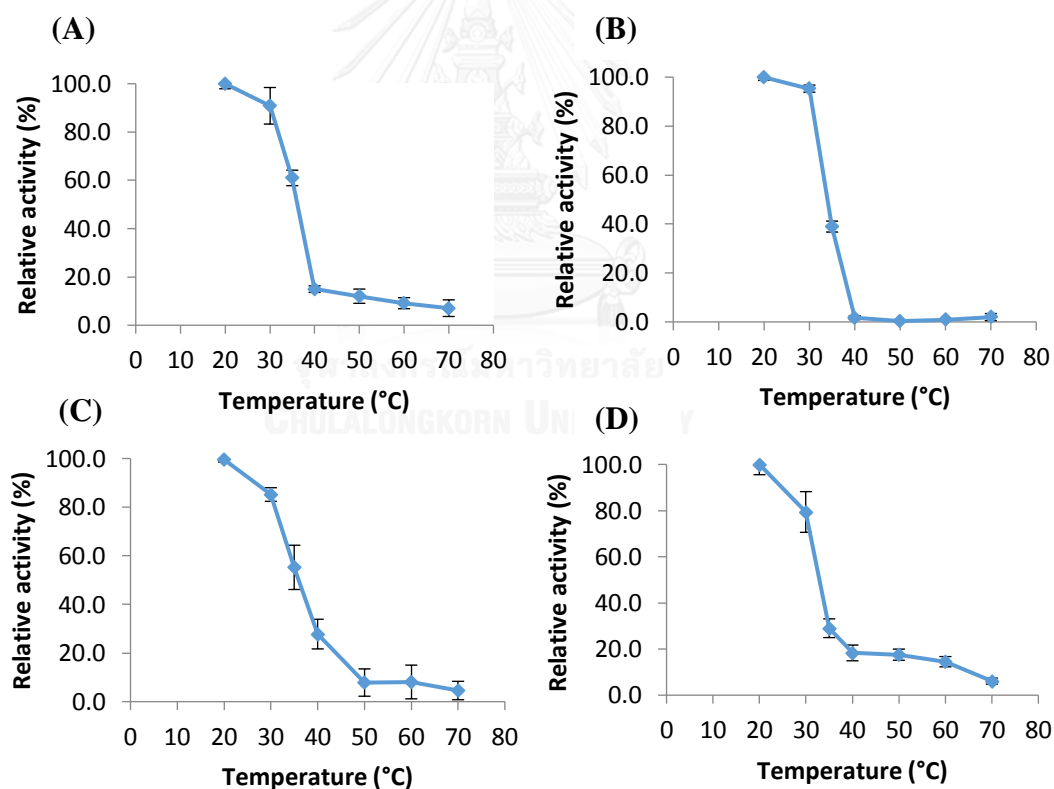


Figure 3.11 Effect of temperature on *CgAM* stability assayed by starch transglycosylation (A) wild-type (B) P228Y (C) A413F (D) G417F

3.5.4 Effect of pH on starch transglycosylation activity

The effect of pH on enzyme activity was examined at different pHs of three separately buffer systems as described in section 2.8.5. Starch transglycosylation activity was measured by iodine method as described in section 2.8.1.1. WT and P228Y displayed the optimum pH at pH 6.0. For G4117F *CgAMs*, the optimum pH was at pH 6.5. Meanwhile, the optimum pH of A413F *CgAM* was pH 7.5 (Figure 3.12). The optimum pH of E231Y was at pH 6.5, which was reported in previous research (Pathomsoonthornchai, 2015).

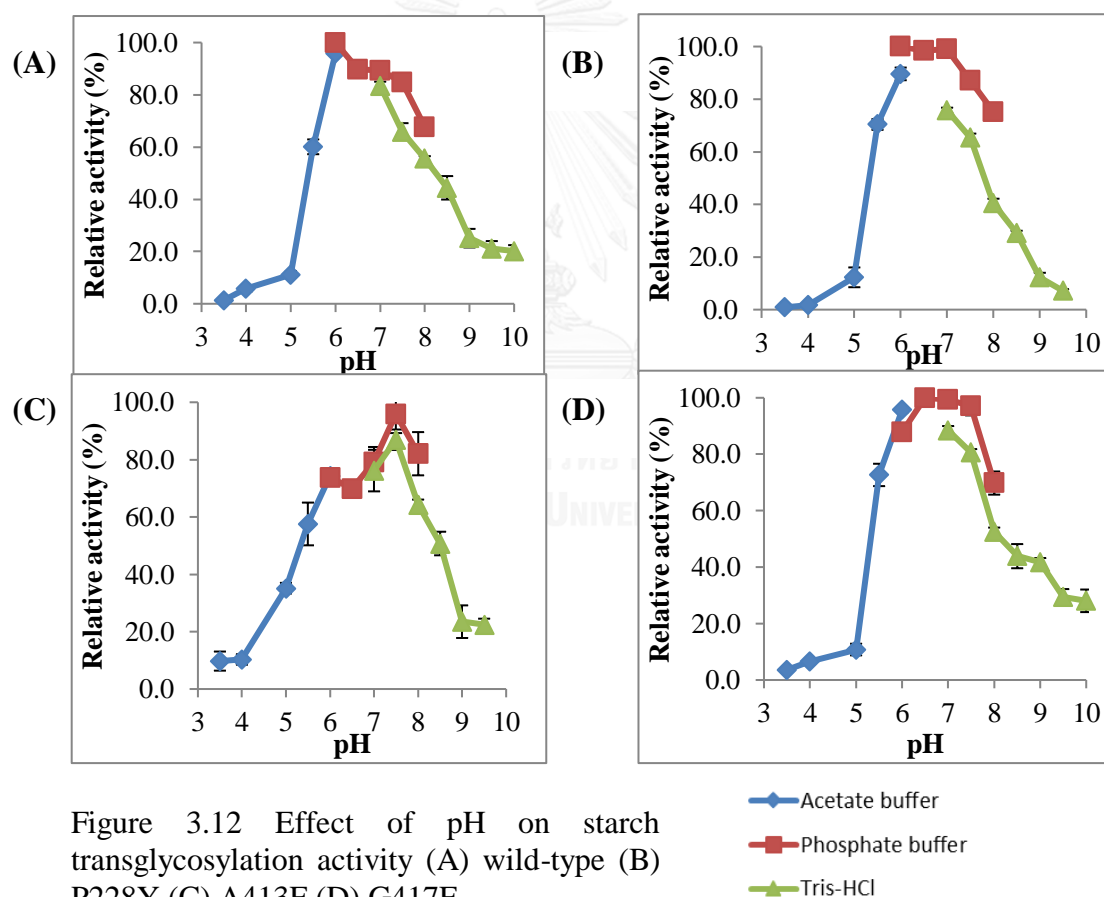


Figure 3.12 Effect of pH on starch transglycosylation activity (A) wild-type (B) P228Y (C) A413F (D) G417F

3.5.5 Effect of pH on starch transglycosylation stability

In order to determine the effect of pH on CgAM stability, purified enzymes were pre-incubated in different buffer, ranging from pH 3.5 to pH 10.0, for 1 h before determining residual starch transglycosylation activity by iodine method as described in section 2.8.1.1. The results revealed that WT and all mutated CgAMs, except A413F, were stable in pH range of 5.5 to 9.0 (Figure 3.13). In case of A413F CgAM, starch transglycosylation dropped by 40% under pH range of 7.0 to 10.0. The pH stability of E231Y was reported in previous research (Pathomsoonthornchai, 2015).

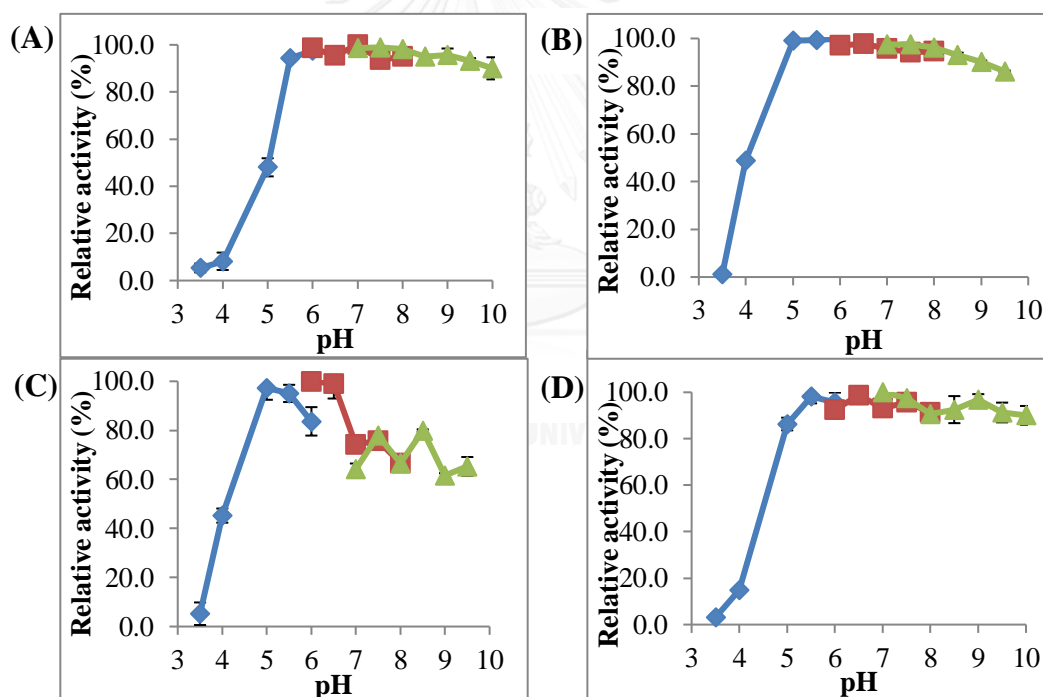


Figure 3.13 Effect of pH on CgAM stability assayed by starch transglycosylation (A) wild-type (B) P228Y (C) A413F (D) G417F

—◆— Acetate buffer
 —■— Phosphate buffer
 —▲— Tris-HCl

3.5.6 Substrate specificity of *CgAM*

Substrate specificity of *CgAM* towards different malto-oligosaccharides (G2 – G7) was observed by disproportionation activity assay. As shown in Figure 3.14, maltotriose (G3) was the best substrate for all *CgAM*s. E231Y *CgAM* displayed higher affinity towards G3 than the WT *CgAM*. The order of preferable substrate of P228Y, E231Y, A413F and G417F *CgAM* was $G3 > G4 > G5 \sim G6 \sim G7 > G2$.

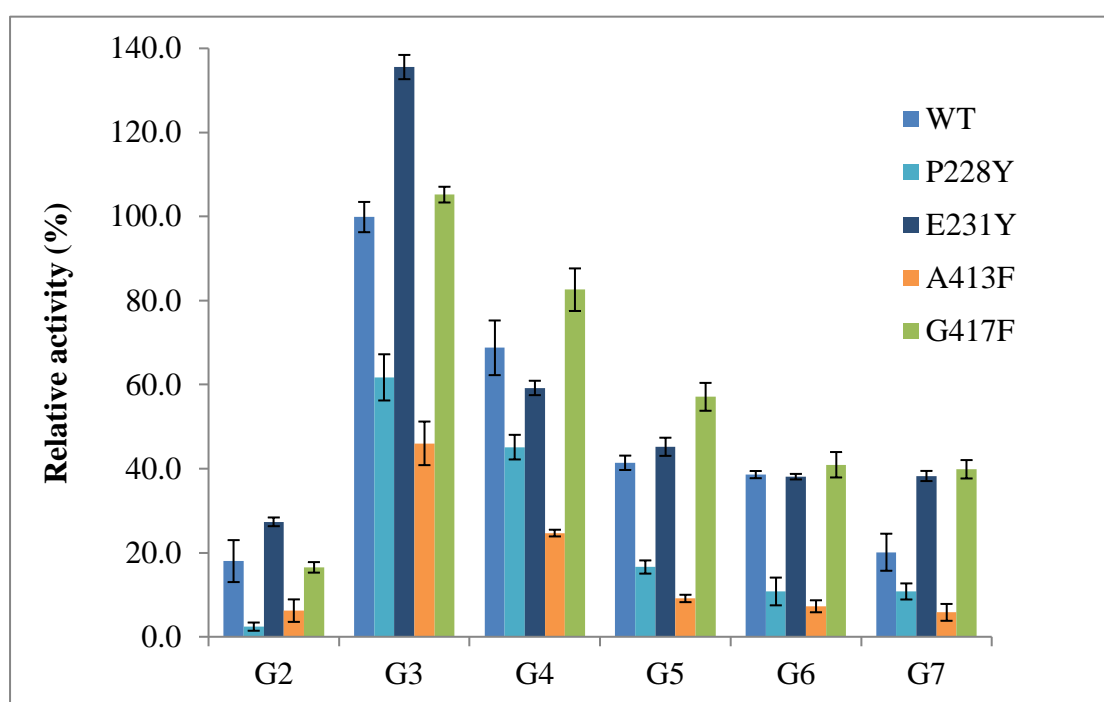


Figure 3.14 Substrate specificity WT and mutated *CgAM*s assayed by disproportionation activity

Table 3.5 Biochemical characteristics of WT and 4 mutant *CgAMs* (P228Y, E231Y, A413F and G417F)

Characteristic	WT	P228Y	E231Y***	A413F	G417F
Optimum temperature* (°C)	30	25	35	35	30
Temperature stability* (°C)	20-35	20-35	20-40	20-40	20-30
Optimum pH*	6.0	6.0	6.5	7.5	6.5
pH stability*	5.5-10.0	5.0-10.0	5.5-9.0	5.0-9.5	5.0-10.0
Substrate specificity**	G3	G3	G3	G3	G3

* by starch transglycosylation activity

** by disproportionation activity

*** obtained from previous research (Pathomsoonthornchai, 2015)

3.5.7 Enzyme conformation

Secondary structure of *CgAMs* was analyzed using circular dichroism spectrophotometry. The graph illustrated that the CD spectra of WT, A413F and G417F were almost the same, whereas a slight change was observed on P228Y spectrum (Figure 3.15). The percentage of secondary structure composition of all *CgAMs* was summarized in Table 3.6.

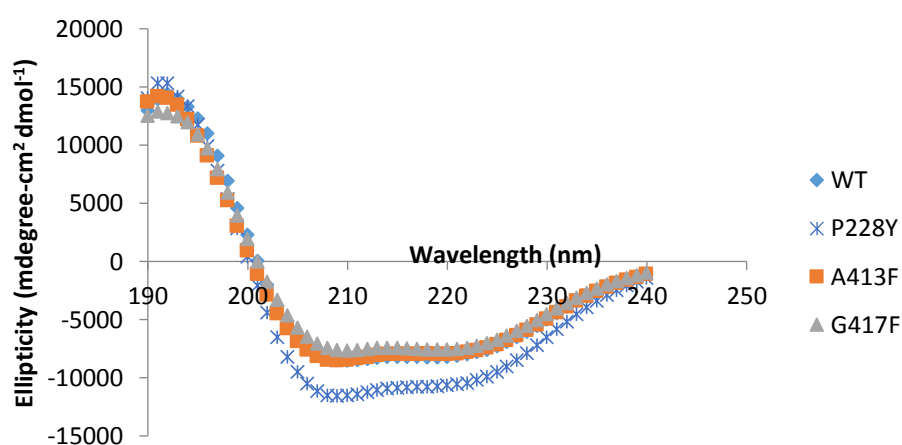


Figure 3.15 Circular dichroism spectra of *CgAMs*

Table 3.6 Percentage of secondary structure composition of *CgAMs* estimated by K2D3 program

<i>CgAM</i>	Percentage of secondary structure composition		
	α -helix	β -sheet	Others
Wild type	38%	16%	46%
P228Y	44%	14%	42%
A413F	38%	16%	46%
G417F	33%	18%	49%

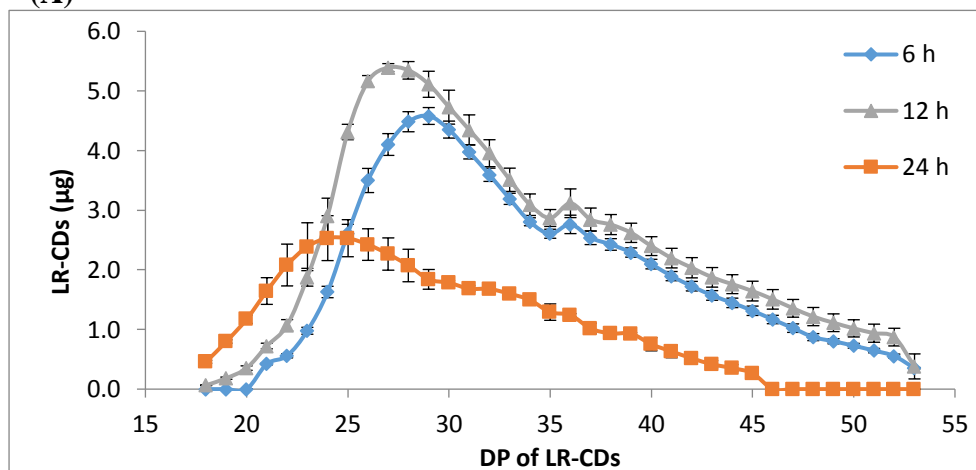
3.5.8 Synthesis of large-ring cyclodextrins

To observe the LR-CDs production profile, purified enzyme carrying of 0.05 U of starch degradation activity was used to synthesize LR-CDs from pea starch at incubation time of 6, 12 and 24 h. LR-CDs products profiles were analyzed by HPAEC-PAD. At 6 h incubation time, principal CDs of WT was CD28. Under the same incubation time of 6 h, E231Y gave smaller principal CD (CD26), while major LR-CDs were shifted upwards to CD36, CD40 and CD36 for P228Y, A413F and G417F, respectively. At 12 h incubation time, the major LR-CDs products were not significantly different from those of 6 h incubation time. For 24 h incubation time, the size of major products shifted to be smaller in comparison to these at 6 and 12 h incubation time. At 24 h, WT produced CD25 as the principal CD while E231Y, A413F and G417F produced CD25, CD33 and CD28 as the principal CD, respectively. It was noticed that P228Y maintained their major LR-CDs product although they were incubated under longer time (Table 3.7 and Figure 3.16).

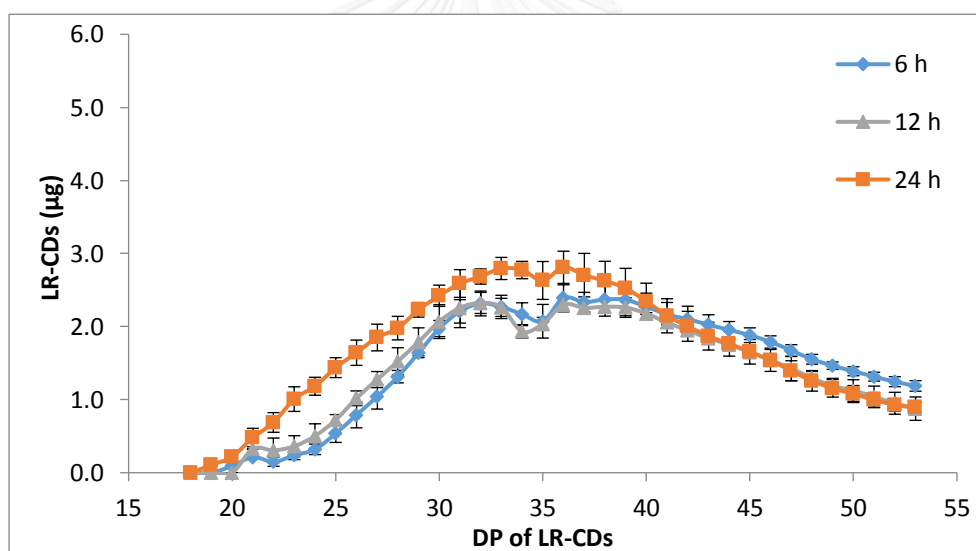
Table 3.7 The principal product of LR-CDs at 6, 12 and 24 h for WT and all mutants

Major LR-CDs product	6 h	12 h	24 h
Wild type	CD28	CD27	CD25
P228Y	CD36	CD36	CD36
E231Y	CD27	CD25	CD25
A413F	CD40	CD38	CD33
G417F	CD36	CD32	CD28

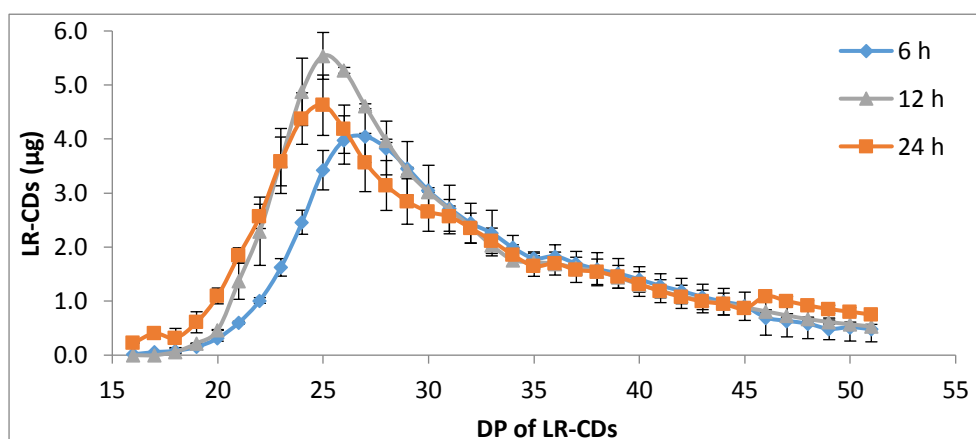
(A)



(B)



(C)



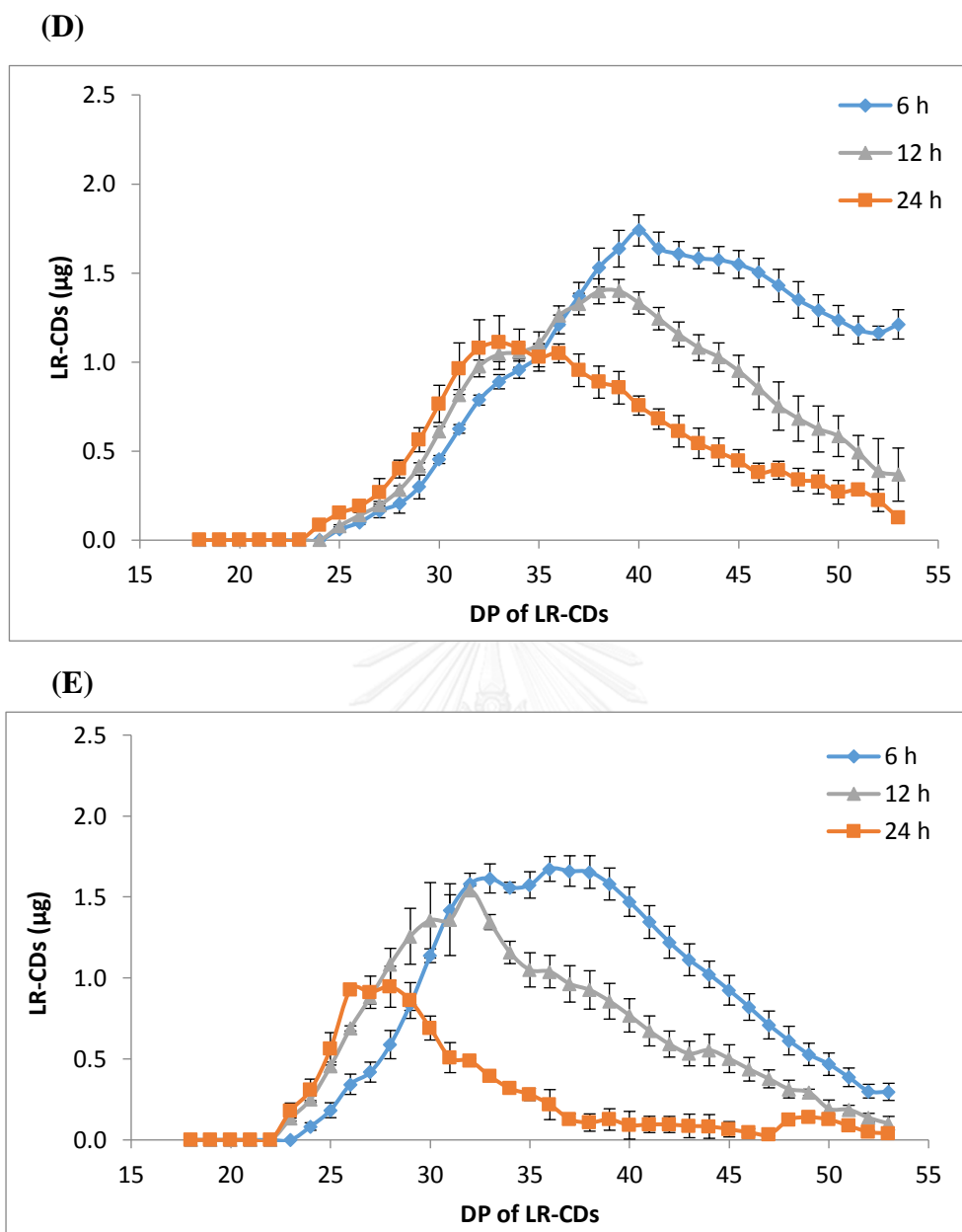


Figure 3.16 LR-CDs product patterns, analyzed by HPAEC-PAD, *CgAMs* of 0.05 U starch degradation activity were incubated with pea starch at various incubation times (A) wild-type (B) P228Y (C) E231Y (D) A413F (E) G417F

3.5.9 Determination of kinetic parameters

In this research, kinetic parameters of CgAMs were determined from three activities; starch transglycosylation, disproportionation and cyclization. Kinetic parameters including K_m and V_{max} were calculated from Lineweaver-Burk plot. Moreover, k_{cat} or turnover number and k_{cat}/K_m or catalytic efficiency were also determined.

3.5.9.1 starch transglycosylation activity

The reaction was performed as described in section 2.10.2 by varying concentrations of glucose acceptor. The result from Table 3.8 revealed that P228Y showed the highest k_{cat}/K_m value ($5.92 \text{ mM}^{-1} \text{ min}^{-1}$), followed by WT and E231Y ($5.74 \text{ mM}^{-1} \text{ min}^{-1}$) and G417F ($4.64 \text{ mM}^{-1} \text{ min}^{-1}$).

3.5.9.2 disproportionation activity

WT, E231Y and G417F showed similar disproportionation activity with k_{cat}/K_m of 3.42, 4.52 and $3.69 \times 10^2 \text{ mM}^{-1} \text{ min}^{-1}$, respectively. P228Y possessed much lower disproportionation activity ($1.39 \times 10^2 \text{ mM}^{-1} \text{ min}^{-1}$) than the WT enzyme. This was due to P228Y had much lower k_{cat} than the WT while K_m was similar.

3.5.9.3 cyclization activity

Pea starch in 3% DMSO was used as substrate for this assay and the LR-CDs product profiles were analyzed by HPAEC-PAD. WT, P228Y and E231Y showed similar efficiency on cyclization. However, G417F showed much lower cyclization activity than the WT enzyme. G417F mutation affected both k_{cat} and K_m .

Table 3.8 Kinetic parameters of WT and CgAM mutants

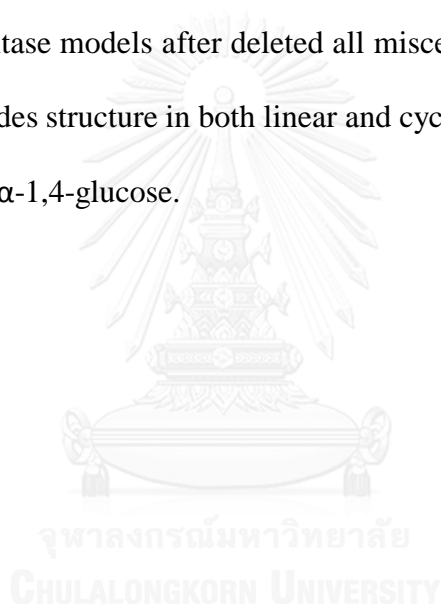
Starch transglycosylation activity				
CgAM	V_{max} ($\mu\text{g}/\text{min}$)	K_m (mM) [10^{-2}]	k_{cat} (min^{-1}) [10^{-1}]	k_{cat}/K_m (mM^{-1} min^{-1})
WT	9.08 ± 1.24	8.22 ± 2.63	4.37 ± 0.60	5.74 ± 0.78
P228Y	12.9 ± 1.75	7.41 ± 0.00	4.37 ± 0.60	5.92 ± 0.98
E231Y	17.6 ± 1.00	18.6 ± 2.33	10.76 ± 0.68	5.74 ± 0.64
G417F	10.5 ± 1.12	7.18 ± 1.31	3.27 ± 0.38	4.64 ± 0.76
Disproportionation activity				
CgAM	V_{max} ($\mu\text{mol}/\text{min}$)	K_m (mM)	k_{cat} (min^{-1}) [10^3]	k_{cat}/K_m (mM^{-1} min^{-1}) [10^2]
WT	0.006 ± 0.001	18.1 ± 2.28	6.18 ± 1.11	3.42 ± 0.53
P228Y	0.012 ± 0.001	19.7 ± 4.74	2.63 ± 0.22	1.39 ± 0.34
E231Y	0.013 ± 0.004	15.4 ± 6.03	6.68 ± 3.65	4.24 ± 0.36
G417F	0.008 ± 0.000	22.9 ± 3.04	8.37 ± 0.03	3.69 ± 0.48
Cyclization activity				
CgAM	V_{max} (mg/min)	K_m (mg/ml)	k_{cat} (min^{-1}) [10^{-2}]	k_{cat}/K_m ($\text{ml}/\text{mg}/\text{min}$) [10^{-2}]
WT	0.022 ± 0.004	6.14 ± 0.55	16.64 ± 4.24	2.73 ± 0.75
P228Y	0.046 ± 0.010	5.71 ± 1.45	13.68 ± 2.55	2.41 ± 0.22
E231Y	0.022 ± 0.006	5.33 ± 0.52	16.75 ± 3.62	2.97 ± 1.26
G417F	0.010 ± 0.001	2.38 ± 0.26	4.53 ± 0.45	1.92 ± 0.22

*Data was represented as mean \pm S.D. and derived from three independent repeats

3.6 Computational analysis

3.6.1 Preparation amyloamylase and oligosaccharides structure

According to published 3D structure of CgAM, amyloamylase model from crystal structure (Protein Data Bank (PDB) entry code 5B68) (Joo et al., 2016) was downloaded and deleted all miscellaneous atoms in PDB file by Discovery studio 2.5^{Accerys inc.}. Oligosaccharide and cyclodextrins (CD1 – CD28) was built and minimized the structure by HyperChem (TM) Professional 7.51. Figure 3.17A showed the amyloamylase models after deleted all miscellaneous atoms. Figure 3.17B showed oligosaccharides structure in both linear and cyclic conformations which were constructed based on α -1,4-glucose.



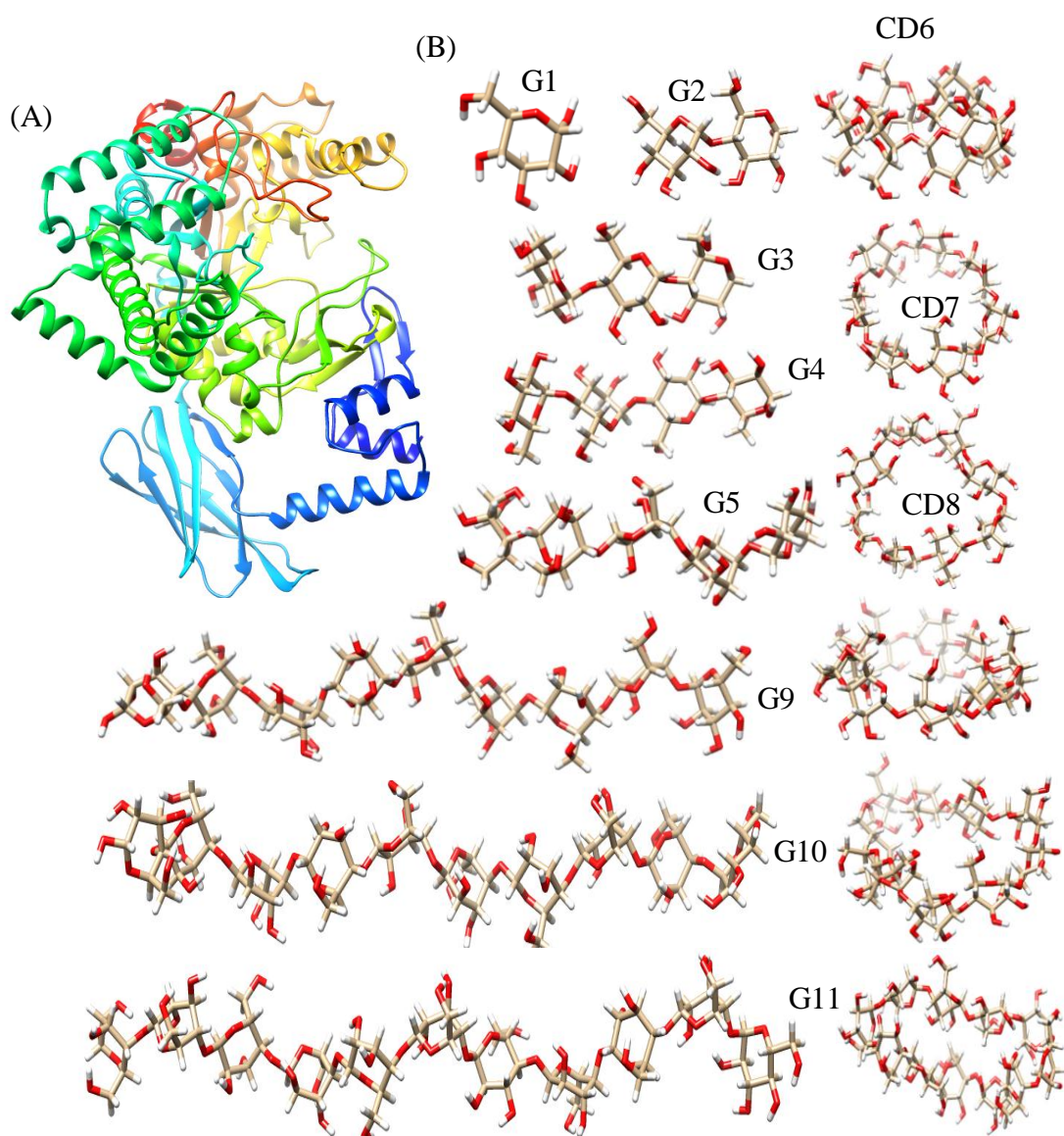


Figure 3.17 (A) CgAM crystal structure and (B) oligosaccharides (G1 - G11) both linear and cyclic conformation

3.6.2 Prediction 3-dimensional structure by molecular docking

Among docking web server such as SwissDock webserver (Grosdidier et al., 2011b, Grosdidier et al., 2011a), PatchDock Server (Schneidman et al., 2005), ZDOCK Server (Pierce et al., 2014), Molecular Docking Server (Bikadi and Hazai, 2009), and Haddock (Van Zundert et al., 2016, Dominguez et al., 2003), SwissDock webserver was used for this research. SwissDock web server used for prediction the molecular interactions between a target protein and a small molecule (Grosdidier et al., 2011b, Grosdidier et al., 2011a). Amylomaltase (Joo et al., 2016), oligosaccharide and cyclodextrins model, prepared from section 3.6.1, were uploaded to SwissDock web server. CgAM and each oligosaccharide was docked via SwissDock web server. The results displayed that only linear oligosaccharide was successfully docked into the active site. However, the maximum size of oligosaccharide which could dock into the active site is linear G11. This is due to the limited size of ligand in SwissDock which was not more than 250 atoms (Grosdidier et al., 2011b) (Figure 3.18). According to the limited size of ligand in SwissDock, G11 is the largest molecule for ligand that can dock via SwissDock. An α -1,4 D glucan was added into ligand molecule until the size increased up to 25 and 28 molecules in cyclic conformation using amyломaltase-G11 complex as a template. Discovery studio 2.5^{Accerys inc.} was used for this step.

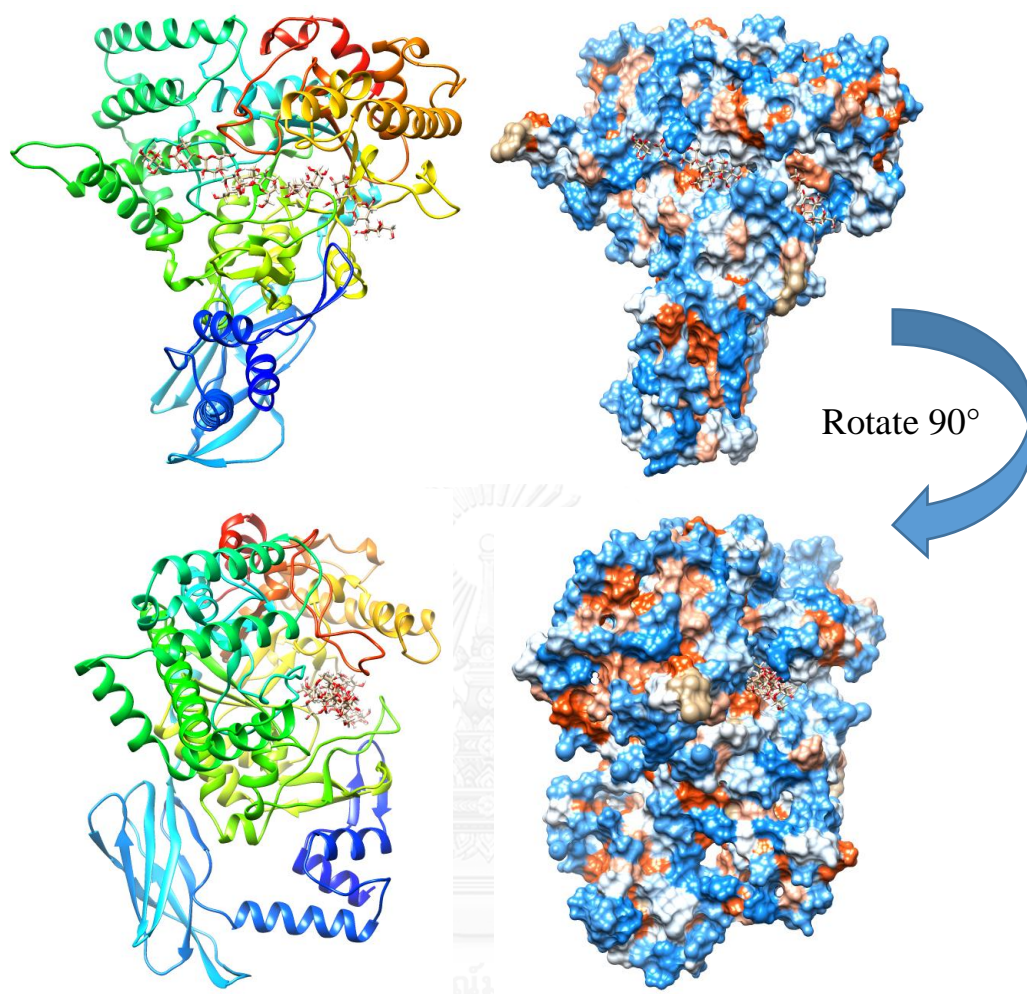


Figure 3.18 Docking complex between CgAM and G11 via SwissDock web server

3.6.3 Interaction analysis using molecular dynamic (MD) simulation

3.6.3.1 Starting models and system preparation

According to the docking complex that obtained from section 3.6.2, α -1,4 D glucan was added into initial conformation structure to increase ligand size up to 25 and 28 molecules in cyclic conformation using Discovery studio 2.5^{Accerys inc.}. Both of two complexes were prepared and minimized by AMBER14 package program (Case et al., 2014). The starting models for MD simulation was shown in Figure 3.19.

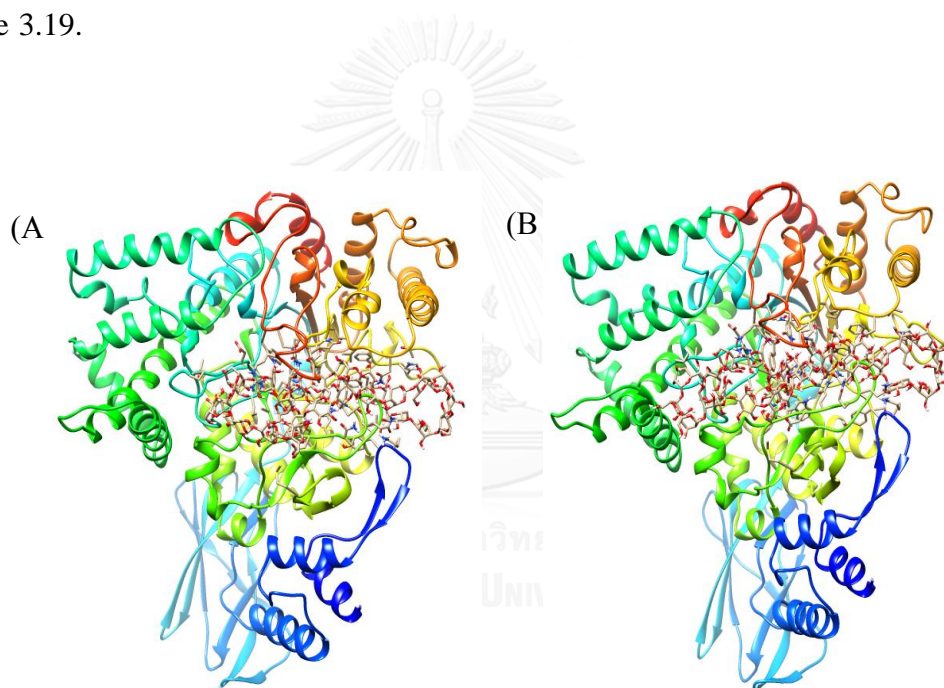


Figure 3.19 CgAM in complex with (A) CD25 (B) CD28 for MD simulation

3.6.3.2 Molecular dynamics (MD) simulations

MD simulation, which is a computer simulation method, was used for studying the physical movements of atoms and molecules. Docking complex was used as starting structure to study the possible binding between amylomaltase and LR-CDs. MD simulation of CgAM-CD25 and CgAM-CD28 complexes was performed at 298 K using 100-ns. According to the distance between C₁-O₄ bonding (3 Å), cyclodextrins (CD25 and CD28) cleaved at glucose residue between subsite -7 and -8 while MD simulation was performed. Although the movie from MD simulation showed that both cyclic oligosaccharides (CD25 and CD28) in two systems were broken after 10 ns, the binding interaction between CgAM and ligand at active site was the same position. To determine the results from MD simulation, five analysis methods were used to investigate the interaction between CgAM and ligand (CD25 or CD28). The parameters of each method were as follows; root-mean square displacement (RMSD), root-mean square fluctuation (RMSF), B-factor, hydrogen bond (H-bond) interaction and total energy (total binding free energy and per-residue decomposition free energy).

3.6.3.3 Stability of global structures

To determine the stability of both complex systems in MD simulation, the RMSDs of all atoms relative to these of initial structure *versus* the simulation time were plotted in Figure 3.20. The binding site of LR-CD displayed in Figure 3.21. The RMSD values of complex atoms increased in the first 10 ns and fluctuated around 2 to 3 Å till 100 ns. Both complexes tend to stabilize after passed 50 ns. Ligand showed the higher RMSD value in comparison with complexes. At 80 – 100 ns, ligand in CgAM-CD25 model showed the higher RMSD values than CgAM-CD28 system.

This meant that ligand in *CgAM*-CD25 model was more flexible than *CgAM*-CD28 system. This is therefore the MD trajectories from 80 – 100 ns of the two systems were extracted for further determination.

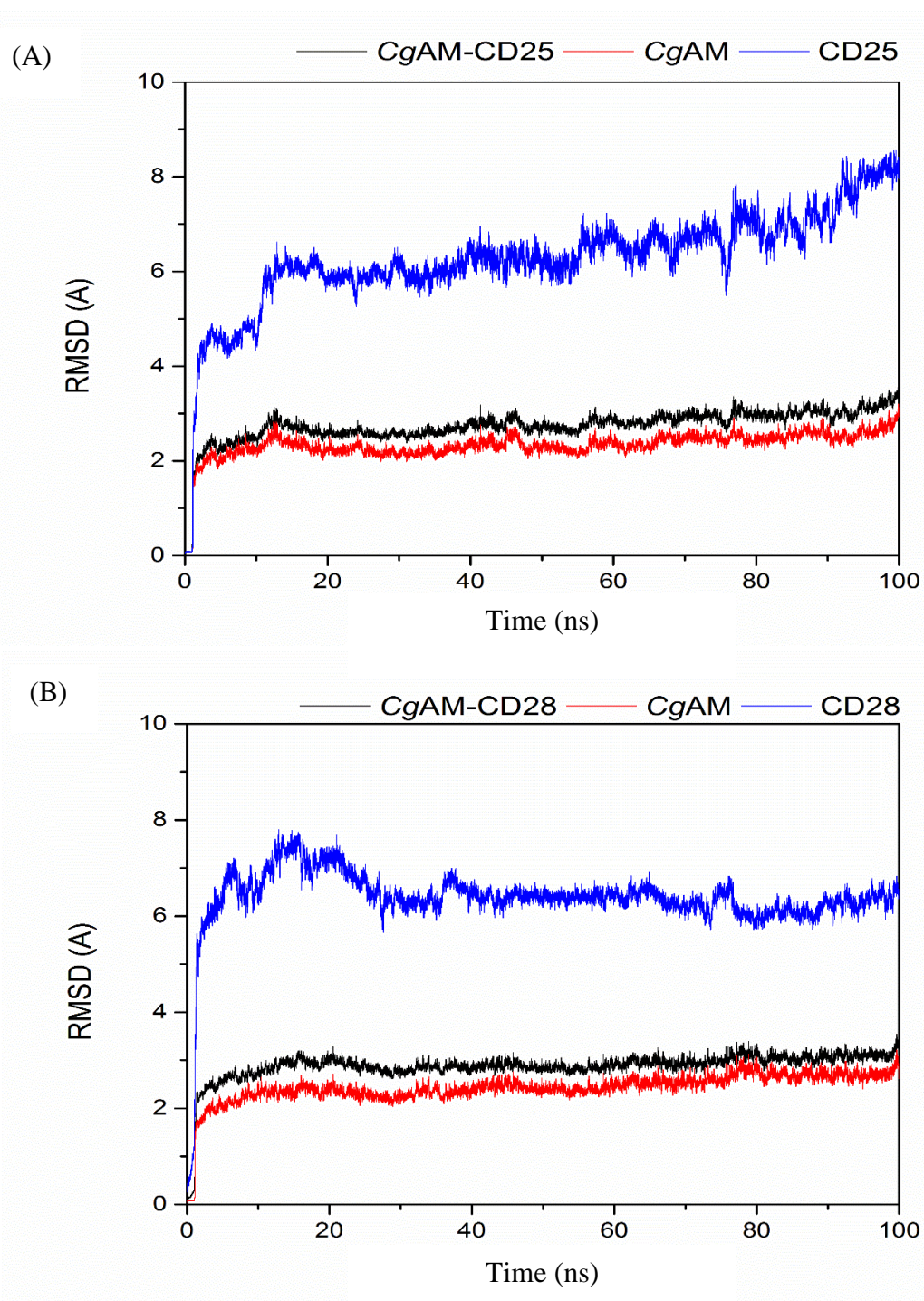


Figure 3.20 RMSD plots for all atoms of *CgAM* in complex with (A) CD25 and (B) CD28 (black) as well as the *CgAM* (red) and LR-CD (blue) alone.

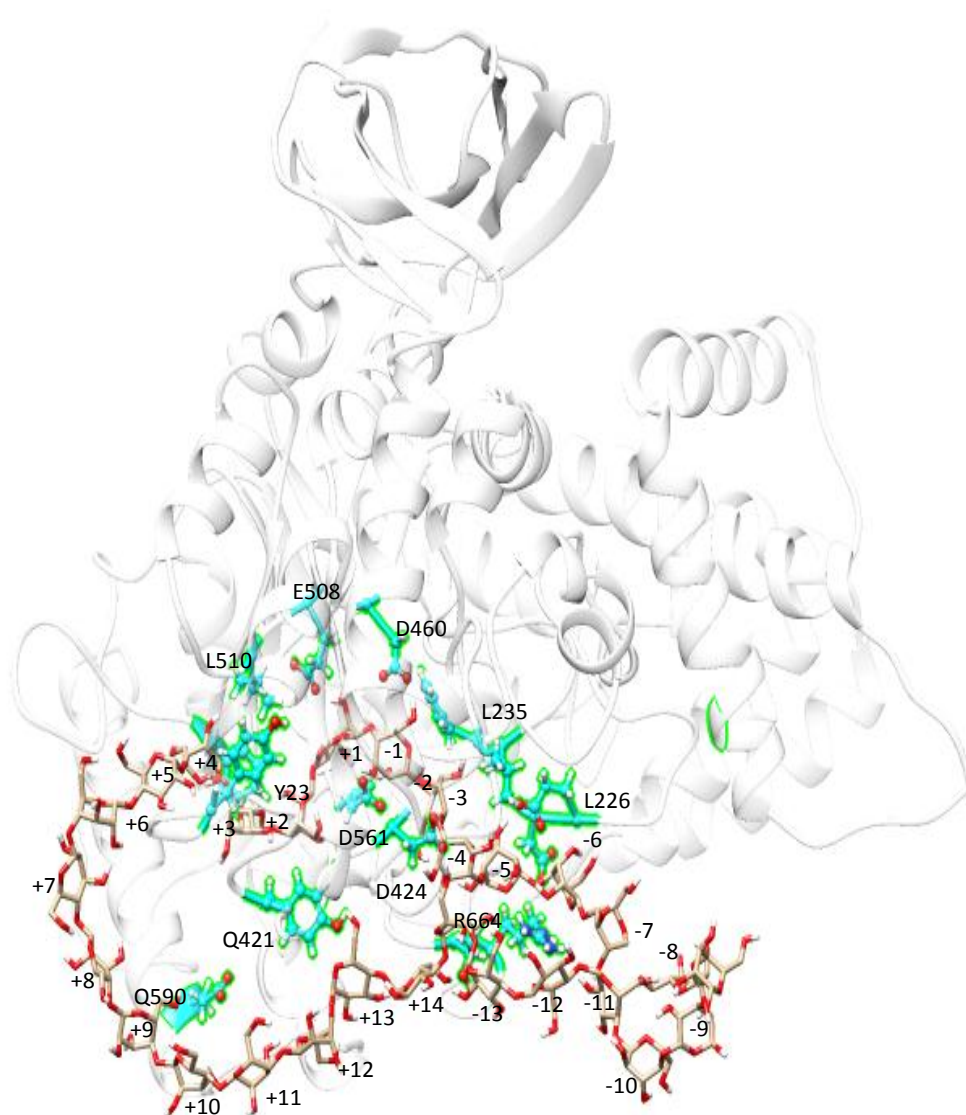


Figure 3.21 Binding site of CgAM in complex with CD28. Three catalytic residues (D460, E508 and D561) interacted with glucose residue in the subsite -1 and -2. CgAM was indicated in white ribbon. Amino acid residues displayed in light blue. Glucose units were labeled as -14 to +14 followed by subsite position.

3.6.3.4 Flexibility of protein structure

To evaluate the flexibility of the structure dynamics and fluctuation of each amino acid of *CgAM* along MD simulation, the RMSF and B-factor were investigated over the last 20 ns of the MD trajectories. Both protein models in complex with different CDs showed the same pattern of RMSF values. According to Figure 3.22, the amino acids in the position of 400 - 500 (binding site) were less fluctuated than the other regions which was in a same trend with B-factor (dark blue). Interestingly, the residues in a range of 250 to 300 in *CgAM*-CD28 complex had a higher RMSF value than those of another system. These residues located on surface area of *CgAM*. B-factor usually showed the rigid and flexible area in the protein structure. In Figure 3.23, the result showed that the binding site between *CgAM* and cyclodextrin (CD25 or CD28) had a rigid structure, shown as a dark blue. In contrast, the protein in surface area showed in a lighter color, was more flexible.

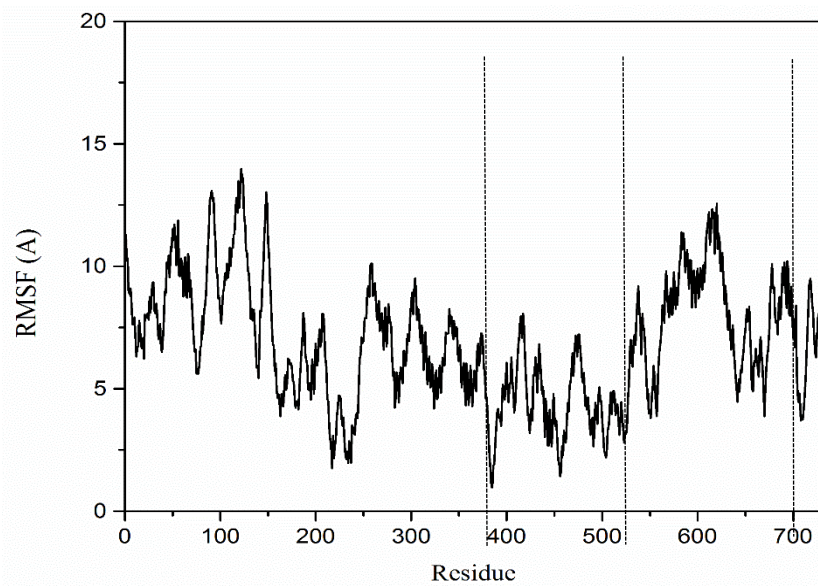
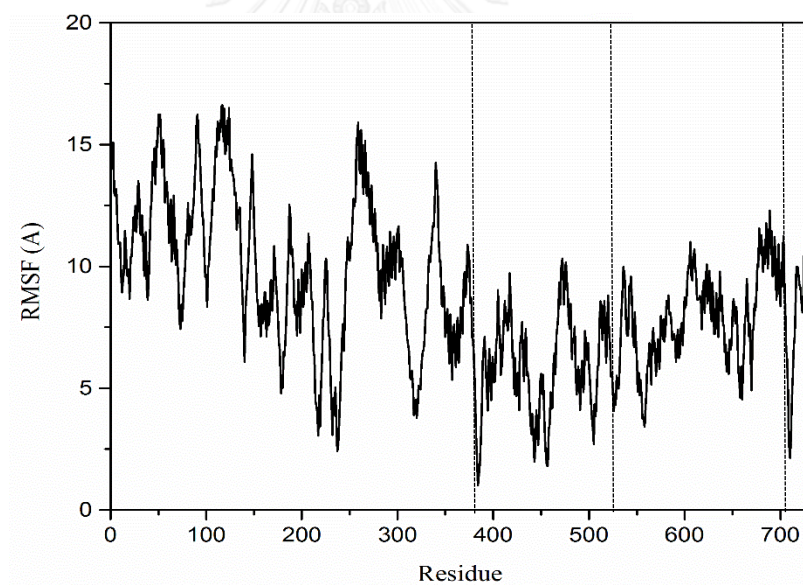
(A) *CgAM-CD25*(B) *CgAM-CD28*

Figure 3.22 Root-mean square fluctuations (RMSFs) for all amino acids in *CgAM* from MD simulation (A) *CgAM-CD25* (B) *CgAM-CD28*

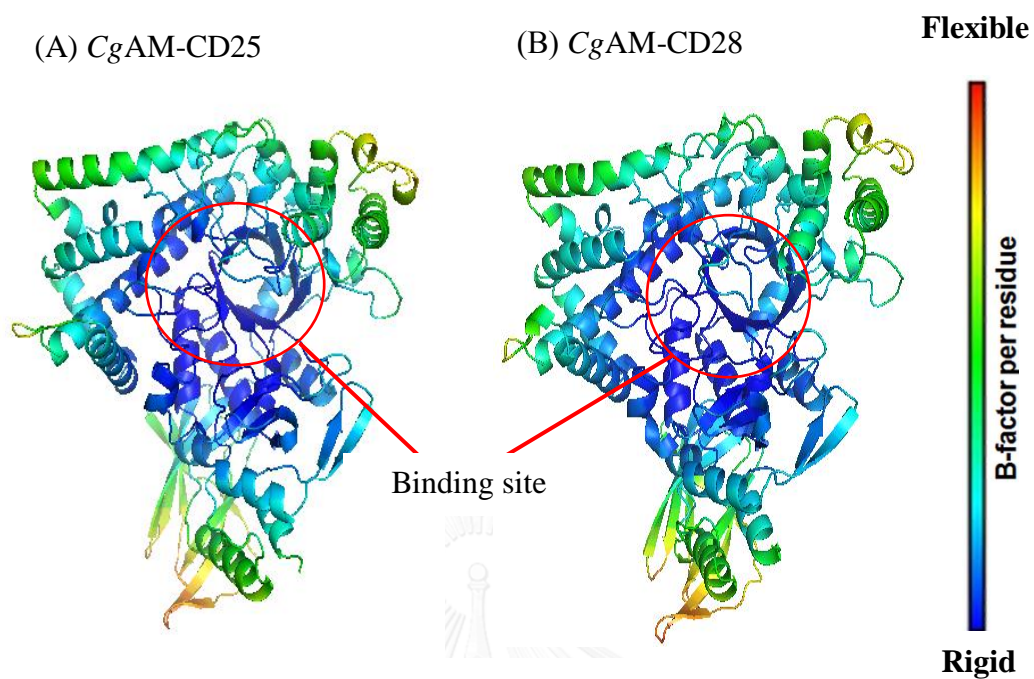
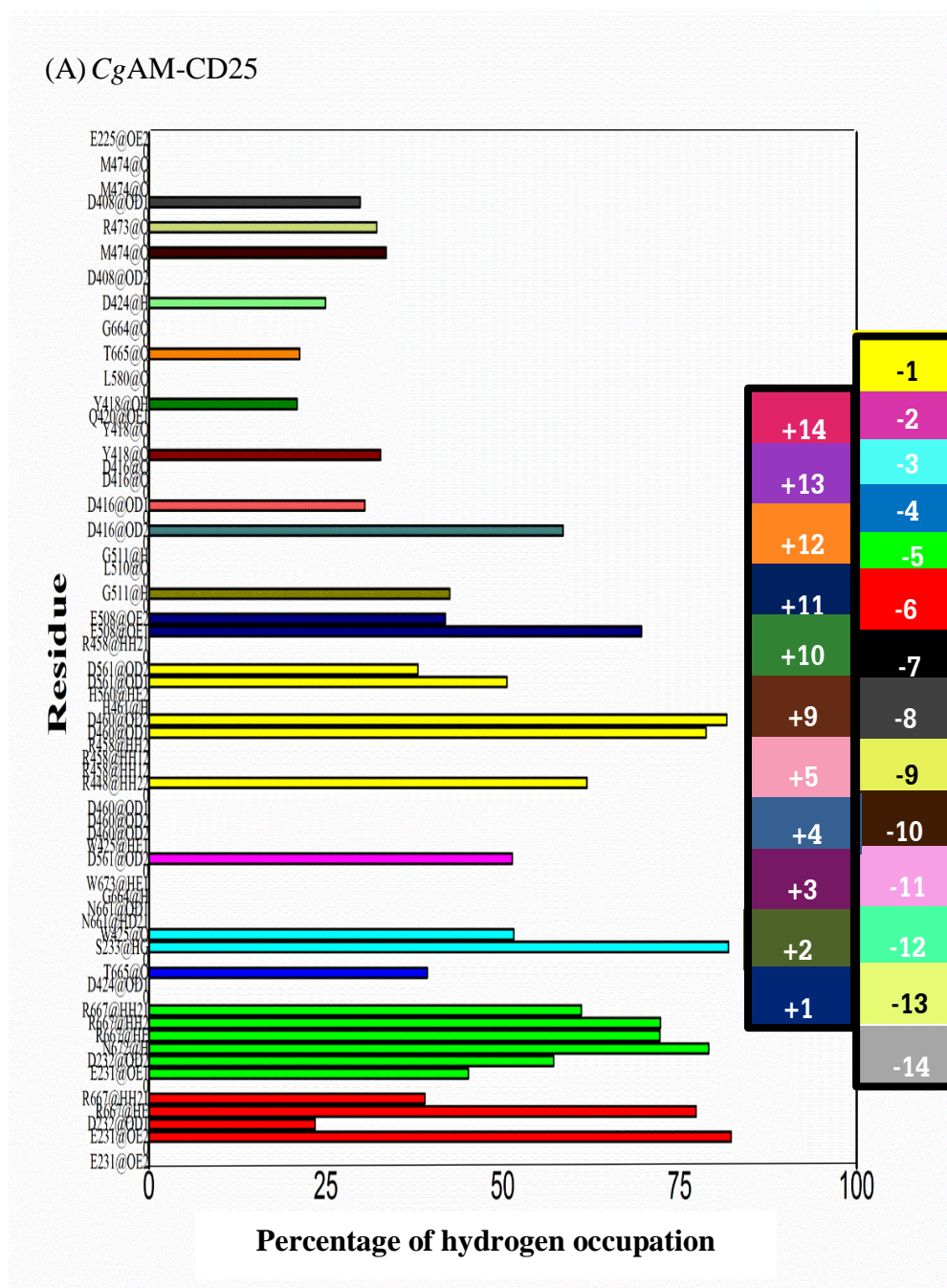


Figure 3.23 B-factor analysis for *CgAM* in complex with (A) CD25 and (B) CD28

3.6.3.5 Hydrogen bond interactions

The intramolecular hydrogen bonding interactions (H-bond) between CgAM and ligand (CD25 and CD28) were also essential for the binding strength of complexes. Therefore, it was important to consider the hydrogen interactions throughout the production phase of simulation. CgAM in complex with CD25 and CD28 had an H-bond interaction at the binding area. The criteria of H-bond was as follows; (i) the distance between H-bond donor and acceptor atoms had to be less than or equal to 3.5 Angstrom (ii) the angle of H-bond must be more than 120 degree. The H-bond occupations between CgAM and LR-CD were summarized in Figure 3.24. The result showed that the maximum % hydrogen bond occupation for CgAM-CD25 complex was 82.3% which was the bonding between E231 and the glucose residue in subsite -6. For CgAM-CD28 complex, the maximum percentage of hydrogen bond formed between D561 and glucose residue in subsite -1 was 79.6%. Although the maximum % hydrogen bond in CgAM-CD25 was higher than CgAM-CD28, but CgAM-CD28 had more residues that showed high % H-bond occupation (more than 70% occupation). The three catalytic residues (D460, E508 and D561) also had H-bond interaction with CD25 and CD28. E508 in both complex had an interaction with glucose residue in subsite +1 whereas D460 and D561 were different. D460 in CgAM-CD25 complex formed H-bond with glucose residue in subsite -1 and D561 formed with glucose residue in subsite -2 and -1. For CgAM-CD28 complex, it was conversed. D460 had H-bond interaction with glucose residue in subsite -2 and -1 while D561 formed only with glucose residue in subsite -1. Moreover, E231 showed the different interaction position with glucose residues. In CgAM-CD25, E231 formed H-bond with glucose residue in subsite -5 and -6 whereas in CgAM-CD28 shifted to

-6 and -7. W425 that was reported as an essential residue for substrate binding and supporting catalytic molecule (Rachadech et al., 2015) also showed H-bond interaction between CgAM-CD25 and glucose residue in subsite -3.



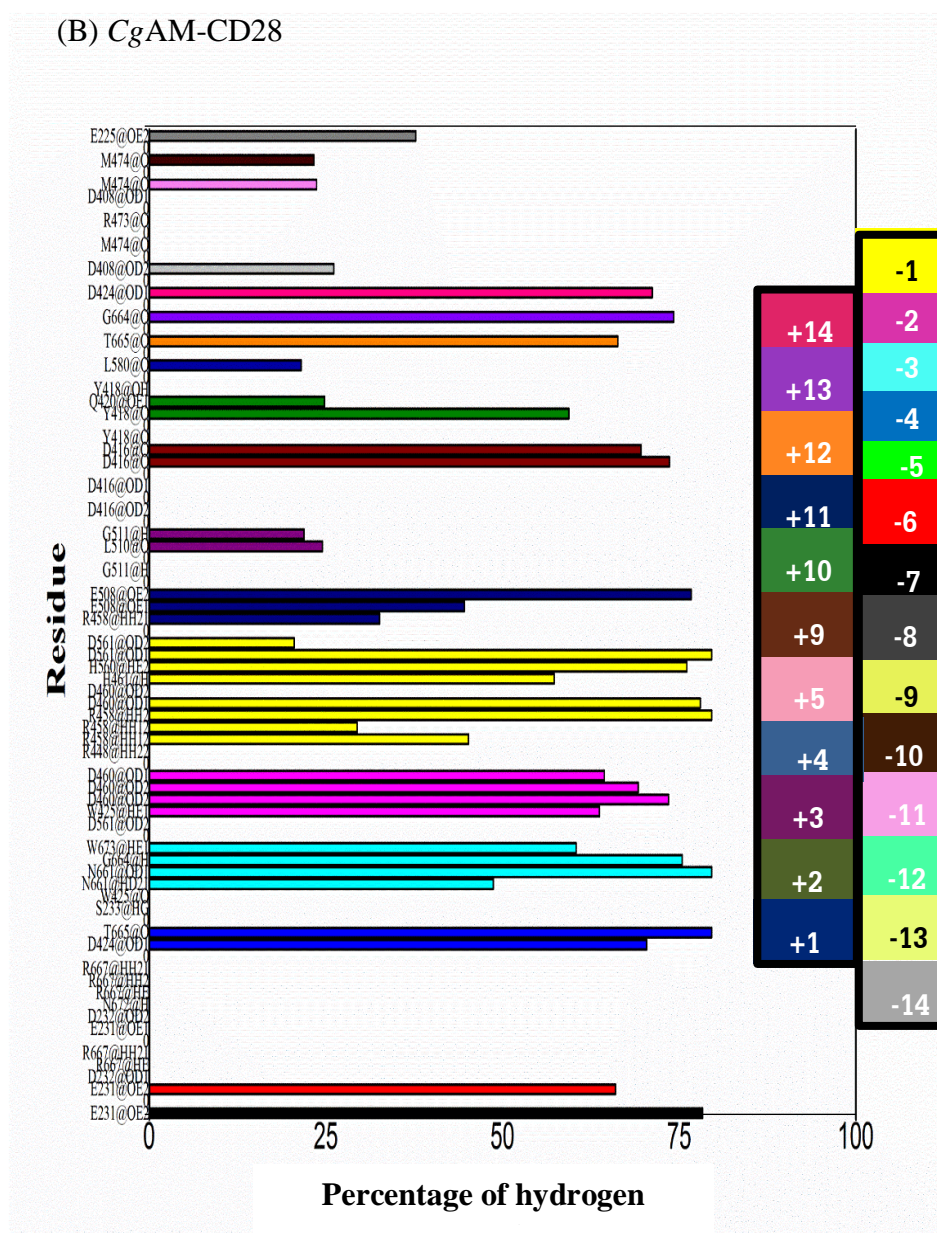


Figure 3.24 Hydrogen bond occupation between the (A) twenty-five glucose units (glucose residue in subsite of -12 to +13), (B) twenty-eight glucose units (glucose residue in subsite of -14 to +14) and the binding residues in *CgAM*. Each color showed glucose residue in each subsite. Starting bar graph in black color was glucose residue in subsite -7. The order of the bar graph was -6, -5, -4, -3, -2, -1, +1, +2, +3, ..., +13, -12, -11, ..., -8 for *CgAM-CD25* complex whereas another order (-6, -5, -4, -3, -2, -1, +1, +2, +3, ..., +14, -14, -13, ..., -8) was for *CgAM-CD28* complex.

3.6.3.6 Key residues of ligand binding

Total binding energy was calculated from two methods; MM/PBSA and MM/GBSA. From Table 3.9, total energy of CgAM-CD25 complex was -85.3 and -82.9 kcal/mol for MM/PBSA and MM/GBSA, respectively; whereas CgAM-CD28 complex was -73.5 kcal/mol for MM/PBSA and -102.1 kcal/mol, for MM/GBSA. Total energy of CgAM-CD25 complex was lower than CgAM-CD28 complex for MM/PBSA. In contrast, MM/GBSA calculation showed that CgAM-CD28 complex provided lower energy than MM/PBSA. The huge different values between MM/PBSA and MM/GBSA were from $\Delta G_{\text{ele,sol}}$ and ΔG_{sol} . Moreover, amino acids that had an interaction with ligand (CD25 and CD28) was reported in Figure 3.25. The per-residue decomposition energy of both complexes was examined using the MM/GBSA. The positive and negative values of per-residue decomposition energy specify the ligand destabilized and stabilized, respectively. According to per-residue decomposition free energy, R667 in CgAM-CD25 complex had a lowest energy which was -7.52 kcal/mol while in CgAM-CD28 system, H458 showed a lowest energy which was -7.61 kcal/mol. With per-residue decomposition free energy less than -1 kcal/mol, Y418, M474, L510, F534, Y23, R458, Q423, T666, Q475, L236, Q421, E231, Q420, N419 and Y235 in CgAM-CD25, ordered from the lower to higher (around -4 to -1 kcal/mol), had also shown favorable energy for binding to CD28. In CgAM-CD28 complex, there were several residues that provided low energy, but some residues were also shared key binding residues with CgAM-CD25 including Y23, Y235, Y418, L510, F534, and T666. Surprisingly, E231 in CgAM-CD25 showed a low energy which helped to stabilize in complex whereas in CgAM-CD28, E231 preferred to non-stabilize the complex and provided high energy. For

catalytic residues (D460, E508 and D561), total energy of each residues in both complexes was high ($\Delta E = +$) except D460 in CgAM-CD25 complex. These results demonstrated that those residues in both complexes were considered as important residues for binding between CgAM and CD.



Table 3.9 The results from MM/PBSA approach giving the energy components and average binding free energies for both complexes

	CgAM-CD25		CgAM-CD28	
	MM/PBSA	MM/GBSA	MM/PBSA	MM/GBSA
ΔE_{ele}	-341.0 ± 34.7		-339.0 ± 31.1	
ΔE_{vdw}	-171.8 ± 13.4		-213.2 ± 9.7	
ΔE_{MM}	-512.8 ± 40.5		-552.2 ± 33.7	
$\Delta G_{\text{nonpolar,sol}}$	-27.8 ± 1.2	-24.9 ± 1.4	-31.4 ± 1.1	-29.8 ± 1.2
$\Delta G_{\text{ele,sol}}$	455.3 ± 30.7	454.8 ± 28.2	510.1 ± 35.1	479.9 ± 29.5
ΔG_{sol}	427.5 ± 30.0	429.9 ± 27.4	478.7 ± 34.5	450.2 ± 28.8
ΔG_{total}	-85.3 ± 16.8	-82.9 ± 18.1	-73.5 ± 15.1	-102.1 ± 9.8

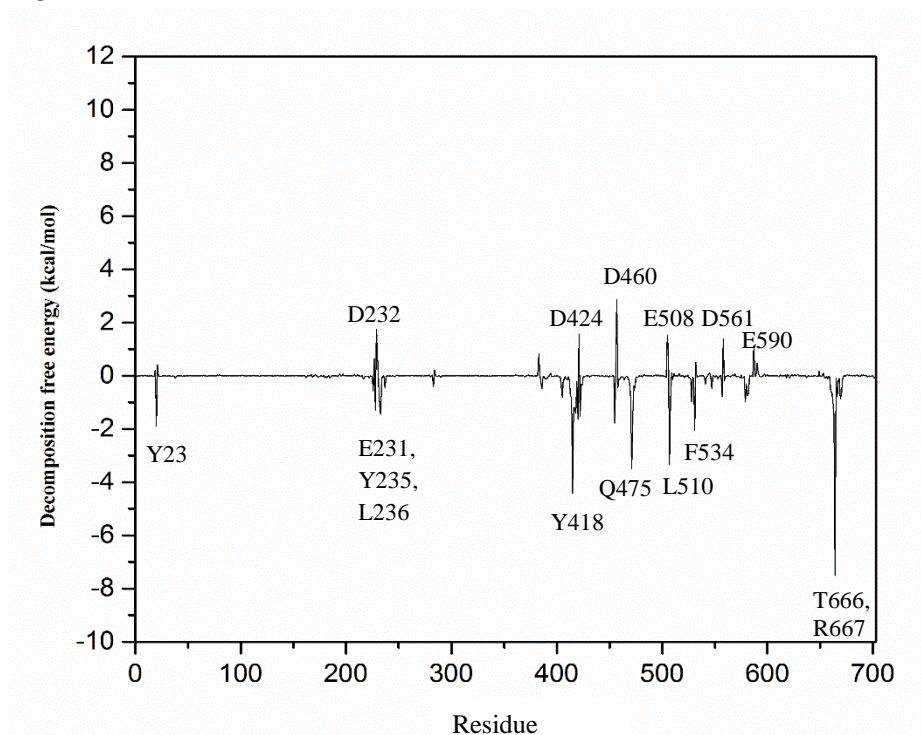
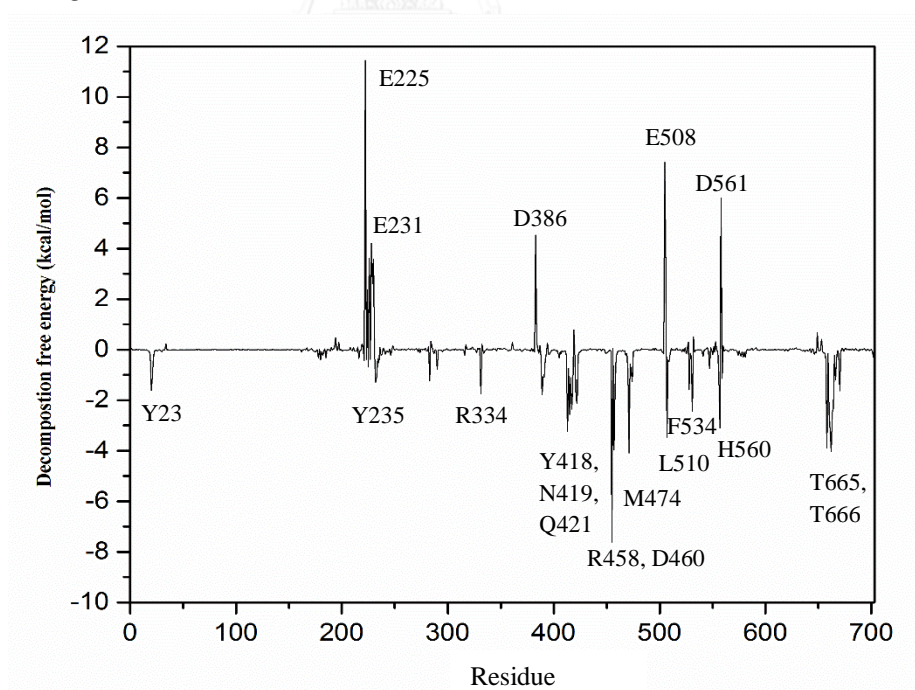
(A) *CgAM*-CD25(B) *CgAM*-CD28

Figure 3.25 Per-residue decomposition free energy obtained from MM/PBSA calculation for *CgAM* in complex with (A) CD25 and (B) CD28

CHAPTER IV

DISCUSSIONS

4.1 Site-directed mutagenesis of amyloamylase gene (P228Y, E231Y, A413F and G417F)

Corynebacterium glutamicum ATCC 13032 was obtained from Thailand institute of Scientific and Technological Research (TISTR) (Srisimarath et al., 2010). The open reading frame (ORF) of *Corynebacterium glutamicum* amyloamylase gene (CgAM) was 2,121 bp which was translated to 706 amino acids. From the amino acids sequence analysis, CgAM exhibited a low sequence identity when compared with other organisms (27.7% identity and 43.7% similarity of *Escherichia coli* (Krempel et al., 2014), 16.2% identity of *Thermus aquaticus* (Terada et al., 1999), 16.3% identity of *Thermus thermophilus* (Terada et al., 1999), 17.7% identity of *Thermus filiformis* (Kaewpathomsri et al., 2015), 16.2% identity of *Streptococcus pneumoniae* (Lacks et al., 1982)), % identity was calculated by EMBOSS Needle program (Rice et al., 2000) (Figure 4.1) (Srisimarath et al., 2010). *C. glutamicum* was mesophilic bacteria as same as *E. coli*, so the identity of amino acids sequence between CgAM and EcMalQ was closer than other organisms (Weiss et al., 2015, Srisimarath et al., 2010). This is possible that the mechanism of CgAM was similar to EcMalQ (Joo et al., 2016). The crystal structure from CgAM revealed that it consisted of two domains, N-terminal (Met1 - Arg165) and C-terminal domain (Leu166 - Asp706). N-terminal domain can be split into two subdomains, subdomain N1 (Met1 - Pro72) and subdomain N2 (Leu73 - Arg165), while C-terminal domain was divided into four subdomains, one core subdomain (CC-subdomain) and three auxiliary subdomains.

Catalytic site embedded in CC-subdomain. The catalytic residues located at Asp460, Glu508 and Asp561 (Joo et al., 2016). In this research, we mutated amino acids at the 250s and 410s loops which located on C-terminal domain of CgAM (P228Y, E231Y, A413F and G417F). P228Y and E231Y were for auxiliary subdomain I (CA1 subdomain), while A413F and G417F were for auxiliary subdomain II (CA2 subdomain) which was on 410s loop.



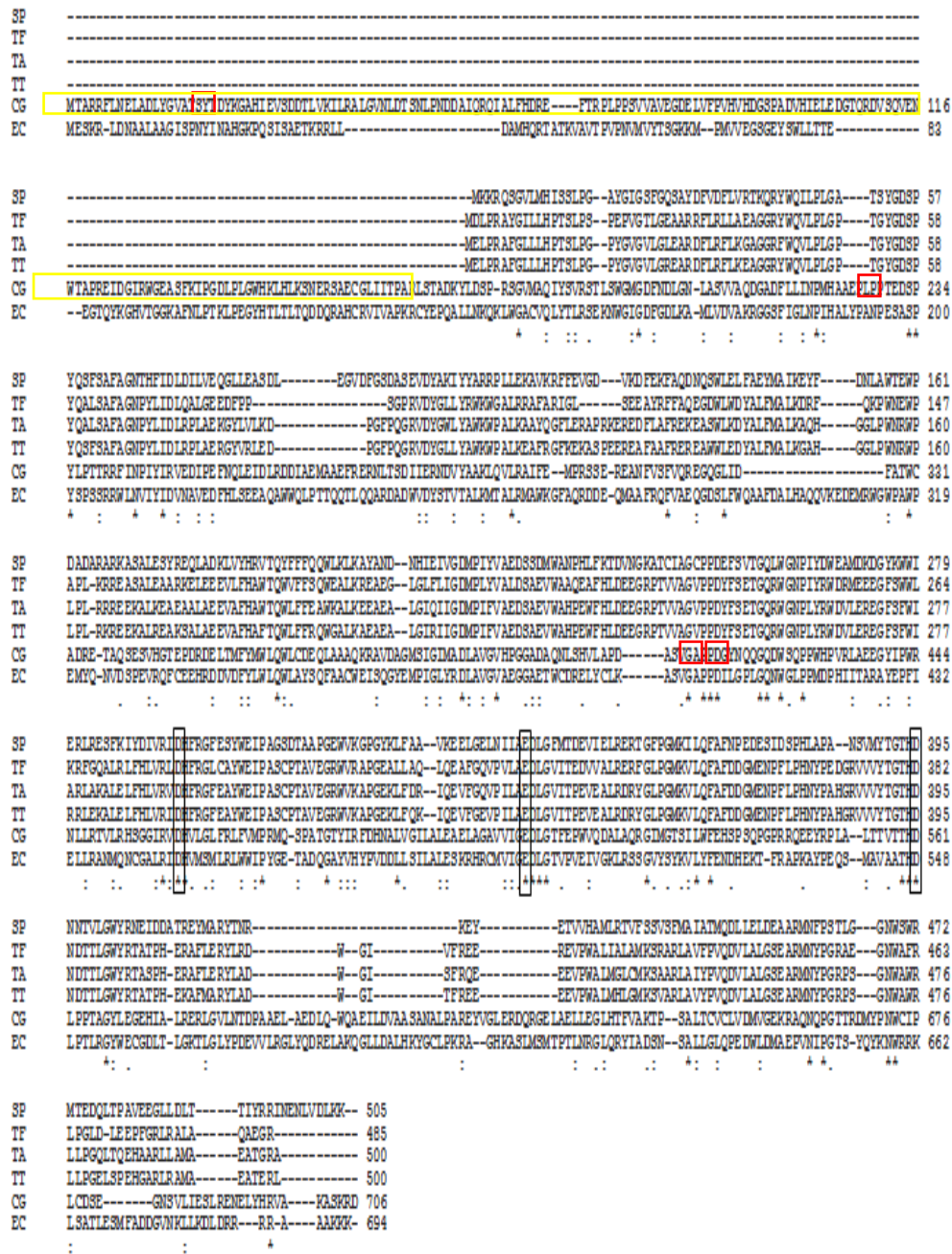


Figure 4.1 Amylomaltase amino acids sequence alignment of *SP Streptococcus pneumoniae* (AAA26923.1), *TF Thermus filiformis* (AKR04336.1), *TA Thermus aquaticus* (EED09753.1), *TT Thermus thermophiles* (BAA33728.1), *CG Corynebacterium glutamicum* (AKR04335.1) and *EC Escherichia coli* (CDZ22191.1). Catalytic residues were shown in black boxes. Positions of mutated residues were shown in red boxes. Deletion mutated in yellow box. Asterisk, colon and dot across the aligned sequences were represented identical, conserved substitutions and semi-conserved substitutions, respectively. (Srisimarat et al., 2010)

4.2 Condition for mutated amyloamylase gene expression

In this research, IPTG was used for induction. The mutants *E. coli* that contained corrected mutated gene was grown in LB medium containing ampicillin 100 µg/ml. For A413F and G417F, 1% glucose was added into LB broth for reduction and maintaining a low basal expression levels of T7 RNA polymerase in the λDE3 lysogenic expression hosts (Novy and Morris, 2001). In this research, we used *E. coli* BL21(DE3) as a host cell. Although WT CgAM was induced by 0.4 mM IPTG for 2 h (Srisimarath et al., 2010), the mutants preferred to be expressed at low temperature (16°C) with 1 mM IPTG. In this research, crude enzyme of WT-pET17b and pET19b contained 2 and 2.3 U/mg of specific activity, similar to previous reports (Srisimarath et al., 2010, Srisimarath et al., 2012). The specificity activities of WT enzymes produced in pET17b and pET19b expression vector were not different. The specific activity of P228Y, E231Y, A413F and G417F crude CgAM were 2.7, 2.0, 2.0 and 1.9 U/mg, respectively.

4.3 Purification of mutated amyloamylase

4.3.1 E231Y

HiTrap DEAE FF column and Phenyl column were used to purified WT and E231Y. The result from SDS-PAGE showed the single band of enzyme after it was purified with DEAE and Phenyl column, respectively. While WT and E231Y had a higher purity, the percentage yield of WT and E231Y were 25.2% and 24.6%, respectively. The purification fold of WT and E231Y was 17.6 and 5.8, respectively for DEAE column and was 21.4 and 14.7, respectively for Phenyl column. According

to the result, DEAE column can be applied to purify enzyme but the purity was not enough. So, it was necessary to further purify enzyme using Phenyl column.

4.3.2 P228Y, A413F and G417F

SDS-PAGE displayed a single band after mutants (P228Y, A413F and G417F) were purified by HisTrap column. The purification fold was 21.1, 16.0, 4.7 and 19.2 while %yield was 24.6, 24.8, 63.3 and 48.3% for WT, P228Y, A413F and G417F, respectively. Previous report of WT CgAM purification fold showed 10.8 fold which was 30.2% yield (Srisimararat et al., 2010) which was closely to our mutated enzyme except A413F. Moreover, amylomaltase from *Synechocystis* sp. PCC6803 was 2.9 purification fold with 84.5% yield (Lee et al., 2009) and from *Thermus brockinus* was 35 purification fold with 67% yield (Bang et al., 2006). SDS-PAGE showed a single band of purified enzyme after purification by HisTrap column.

4.4 Characterization of WT and mutated CgAM enzymes

4.4.1 Enzyme assay

The activities of amylomaltase was observed via 6 reactions; starch transglycosylation, starch degradation, disproportionation, cyclization, coupling and hydrolysis activity. WT, P228Y, E231Y and G417F had similar specific activities of starch transglycosylation and starch degradation (Table 3.4), suggesting that P228Y, E231Y and G417F mutation had no strong effects on starch transglycosylation and starch degradation. However, P228Y mutation seemed to affect disproportionation activity. E231Y possessed similar cyclization activity as the wild-type enzyme, while P228Y and G417F had lower cyclization activity, in comparison to the wild-type enzyme. It should be mentioned that A413F exhibited significantly lower activity of

starch transglycosylation, starch degradation, disproportionation and cyclization than the WT enzyme. This suggested that A413 might play a role in starch transglycosylation, starch degradation, disproportionation and cyclization.

In general, amylomaltase enzymes showed lower coupling activity, in comparison to CGTase enzyme (Van Der Veen et al., 2000). From Table 3.4, WT and E231Y had similar coupling activity, while P228Y, A413F and G417F showed less coupling activity than the WT enzyme. It is possible that P228, A413 and G417 play a role in coupling reaction.

4.4.2 Effect of temperature and pH on starch transglycosylation activity

According to the result, the optimum temperature of WT and mutants were around 25 - 35°C. When temperature increased up to 40°C, all enzymes had lost their activity. Optimum temperature for starch transglycosylation of CgAM was closely to other mesophilic bacteria such as *E. coli* (35°C and pH 6.5) (Kitahata et al., 1989), *Synechocystis* sp. (45°C and pH 7) (Lee et al., 2009), *Pseudomonas stutzari* (37°C and pH 7.7) (Schmidt and John, 1979) while amylomaltase from *Thermus* sp. like TaAM (75°C and pH 5.5) (Fujii et al., 2005, Terada et al., 1999) and TfAM (60°C and pH 6.5) (Kaewpathomsri et al., 2015) had high activity at high temperature. The proper pHs for starch transglycosylation activity of WT and mutants were around pH 6.0 - 7.5 in phosphate buffer. This optimum pH range was similar to previous report of CgAM (Srisimararat et al., 2010, Srisimararat et al., 2012, Nimpiboon et al., 2016a, Nimpiboon et al., 2016b) and other amylomaltase enzymes from *Thermus* species eg. TaAM (Fujii et al., 2005) and TfAM (Kaewpathomsri et al., 2015).

4.4.3 Effect of temperature and pH on starch transglycosylation stability

All enzymes were stable and maintained their activity at 20°C for 1 h. When temperature increased from 30°C to 70°C, the activity of all mutants decreased and finally lost all activity. This was the same pattern in previous research of WT-CgAM (Srisimararat et al., 2010). Previous research showed that A406V had improve thermostability (Nimpiboon et al., 2016a), In contrast, *Thermus* sp. was thermophilic bacteria and amyloamylase enzymes from *Thermus* sp. have a high activity in extreme temperature (Fujii et al., 2005, Kaewpathomsri et al., 2015). All CgAM mutants had a stability in range of pH 5.5 to pH 9.0.

4.4.4 Substrate specificity of amyloamylase

Substrate specificity of amyloamylase in disproportionation reaction was investigated by various oligosaccharides (G2 – G7) as a substrate. In the previous research showed that G3 is the best substrate for WT CgAM including other CgAM mutants such as Y172A, A406V, A406L and N287Y (Srisimararat et al., 2012, Srisimararat et al., 2013, Nimpiboon et al., 2016a, Nimpiboon et al., 2016b). The descending order of preferred substrate of WT CgAM was $G3 > G4 > G5 > G6 > G7 \sim G2$. Moreover, amyloamylase from other organisms such as *Thermus thermophilus* HB8 (Kaper et al., 2007) and *Pyrobaculum aerophilum* IM2 (Kaper et al., 2005) also had a same order of substrate preference. However, the pattern of substrate specificity of amyloamylase from *Thermus filiformis* was different ($G3 > G4 \sim G5 > G7 > G6 \gg G2$) (Kaewpathomsri et al., 2015). In this research, the substrate specificity of P228Y, E231Y, A413F and G417F were $G3 > G4 > G5 \sim G6 \sim G7 > G2$.

4.4.5 Enzyme conformation

Circular dichroism was one of methods for determination the secondary structure composition of the enzyme based on different array alignments of polypeptide backbone. The optical transition of the secondary structure was observed and reported in CD spectrum for each structure comparing with the reference spectrum (Louis-Jeune et al., 2011, Greenfield and Fasman, 1969, Greenfield, 2006). From the result, CD spectra of WT *CgAM* and mutant enzymes (P228Y, A413F and G417F) were closely to the previous report (Rachadech et al., 2015, Nimpiboon et al., 2016a, Nimpiboon et al., 2016b). In addition, K2D3 program (Louis-Jeune et al., 2011) was used to predict the secondary structure. The results showed that the secondary structure of mutated was not changed. So, the different specific activity of mutated enzyme was not from conformation change.

4.5 Synthesis of large-ring cyclodextrins

The amount of enzyme, incubation time, temperature and pH affected to size and amount of LR-CDs production (Srisimarath et al., 2012, Nimpiboon et al., 2016a, Terada et al., 1999, Vongpichayapaiboon et al., 2016). In this research, at 6 h, the principle LR-CDs product from WT, E231Y, A413F and G417F *CgAM* was CD29, CD27, CD40 and CD36, respectively. P228Y gave a CD36 as principle products. This was similar with LR-CDs product from *TfAM* which gave CD25 – CD29 as a principal product at 4 h (Kaewpathomsri et al., 2015). At 12 h, size of major LR-CDs product had a bit shift in WT, E231Y, A413F and G417F which became CD27, CD25, CD38 and CD32, respectively. Surprisingly, major LR-CDs product of P228Y remained at CD36. And at 24 h (long incubation time), CD24, CD36, CD25, CD33 and CD32 were principal products from WT, P228Y, E231Y, A413F and G417F,

respectively. In WT and all mutants, except P228Y, the product pattern seemed to be changed from larger to smaller size LR-CDs for long time incubation. This was similar to results from previous reported WT *CgAM* (Srisimararat et al., 2010), *CgAM* mutants (Srisimararat et al., 2012, Nimpiboon et al., 2016a, Nimpiboon et al., 2016b), *TaAM* (Terada et al., 1999), *TfAM* (Kaewpathomsri et al., 2015) and potato D enzyme (Takaha et al., 1996). Principal LR-CDs product from all mutants were different from WT *CgAM*. E231Y gave smaller LR-CDs while other mutants (P228Y, A413F and G417F) gave larger products. So, this showed that changing the sidechain amino acid to more hydrophobic side chain (Y and F) at position 228, 413 and 417 of *CgAM* had an affected to increase size of LR-CDs product. The order of hydrophobicity amino acid sidechain, was calculated from pH 7 system, was $F > I > W > L > V > M > Y > C > A > T > H > G > S > Q > R > K > N > E > P > D$ (Monera et al., 1995). The %yield of LR-CDs production from all mutants was lower than WT whereas in previous mutant *CgAM* research, A406V, A406L and N287Y gave higher yield than WT (Nimpiboon et al., 2016a). The amount of LR-CD products from P228Y at 6 h, 12 h and 24 h incubation time did not significantly change.

4.6 Determination of kinetic parameters

According to low specific activity of A413F, only three mutants (P228Y, E231Y and G417F) was used for determination of kinetic parameters.

4.6.1 Starch transglycosylation activity

Concentration of glucose was varied to determine the kinetic parameters. WT, P228Y, E231Y and G417F had similar k_{cat}/K_m . However, E231Y

mutation significantly increased k_{cat} and K_m . It is likely that E231 was important for both catalysis and binding.

4.6.2 Disproportionation activity

In previous research, disproportionation activity was usually used to determine kinetic parameter from WT-CgAM and some mutant-CgAM (Srisimarath et al., 2012, Nimpiboon et al., 2016a, Nimpiboon et al., 2016b). Kinetic parameter of WT was close to those in previous report. k_{cat}/K_m of E231Y was $425 \text{ mM}^{-1}\text{min}^{-1}$ which was slightly higher than WT. E231Y mutation significantly increased both k_{cat} and K_m . A406V and A406L in previous report was also give a high value of k_{cat}/K_m comparing with WT (Nimpiboon et al., 2016a). The k_{cat}/K_m of P228Y was significantly lower than that of WT. This was due to the fact that P228Y had the effect on catalysis. N287Y also showed the low value of k_{cat}/K_m (Nimpiboon et al., 2016b). This may occur from increasing hydrophobic interaction in CAI subdomain (both of P228Y and N287Y were located on CAI) (Joo et al., 2016).

4.6.3 Cyclization activity

The k_{cat}/K_m values of cyclization of WT, P228Y and E231Y was similar values, while G417F showed much lower k_{cat}/K_m of cyclization than those of WT and mutants (Table 3.7).

In this research, we divided our mutated enzyme into 2 group depending on their subdomains of CgAM; CAI subdomain and CAII subdomain.

The overall structure of C domain of CgAM quite well matched with other organisms such as *EcMalQ*, *TaAM*, *TtAM* and *AtDPE1* (Weiss et al., 2015, Joo et al., 2016, Barends et al., 2007, Terada et al., 1999, O'Neill et al., 2015). We interested in

CAI and CAII subdomain which contained loop nearly the catalytic site in *CgAM* structure (Joo et al., 2016).

P228Y and E231Y located on CA I subdomain. To create more hydrophobicity interaction, both of P228 and E231 were mutated to be tyrosine (Y), a polar and neutral side chain. As tyrosine contained the aromatic ring in the structure so sometime it also represented hydrophobic interaction (Monera et al., 1995). P228Y gave a lower activity in disproportionation while starch transglycosylation and starch degradation were similar to WT. This result showed that P228Y was prefer to use long chain substrate like starch more than maltotriose (G3). This led to a lower level of k_{cat}/K_m from disproportionation reaction in P228Y. Since P228Y showed similar k_{cat}/K_m of cyclization to the WT enzyme. It is possible that P228Y functions in inter-transglycosylation Although P228Y prefer to use starch, judging from the k_{cat}/K_m of starch transglycosylation the size of principal LR-CDs remained the same at long incubation time. This indicated that P228 may also play a role in coupling activity.

A413F and G417F located on CA II subdomain which was a 400s or 250s loop comparing in *EcMalQ* (Weiss et al., 2015) and *TaAM* (Przylas et al., 2000a). Previous research reported that the conformation of 400s (250s) loop was flexible and it involved in substrate binding at reducing end of scissile bond (Przylas et al., 2000b, Weiss et al., 2015, Jung et al., 2011). Both of mutants were mutated from aliphatic side chain to aromatic side chain. A413F and G417F significantly decreased their activities, especially A413F, by 3.19, 4.81 and 3.36 times in starch transglycosylation, disproportionation and starch degradation reaction. Although most of G417F activities were decreased, disproportionation activity was slightly increased in comparison to the WT. Synthesis of LR-CDs by A413F and G417F resulted in larger principal

products than the WT (CD36-CD40). In longer incubation time, LR-CDs from A413F was slightly decreased degree of polymerization (CD38 for 12 h and CD33 for 24 h), but for G417F, the dominant product was shifted to CD 32 at 12 h and become CD28 at 24 h. According to a low activity in A413F, we focused the kinetic parameter only in G417F. From starch transglycosylation and cyclization showed that k_{cat}/K_m of G417F was lower than WT, while k_{cat}/K_m of disproportionation was not different from WT. So, mutation at G417 to F417 affected the activity that used starch as a substrate. Changing position in CAII subdomain of CgAM to aromatic ring side chain may affect to the activity to bind with substrate including pattern of LR-CDs production.

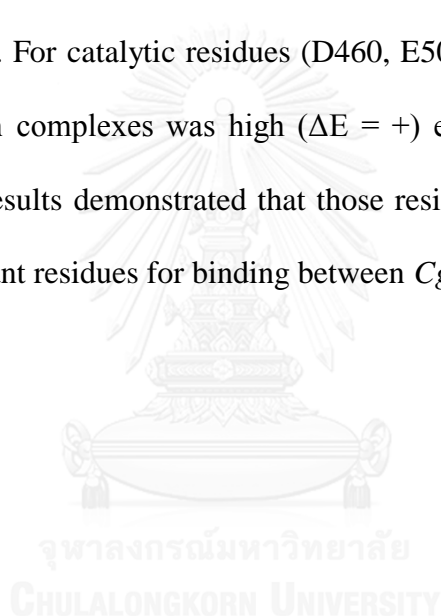
4.7 Computational analysis

Docking complex was used to study the interaction between amyloamylase and cyclodextrin via AMBER14 program (Case et al., 2014). Root-mean square displacement (RMSD), root-mean square fluctuation (RMSF), B-factor, hydrogen bond (H-bond) interaction and total energy (total binding free energy and per-residue decomposition free energy) were analyzed. From the movie showed that cyclic of ligand (CD25 and CD28) was broken after pass 10 ns of MD simulation. This may cause from the long distance (3 Å) between C₁-O₄ bonding at glucose residue in subsite -7 and -8. The interaction between CgAM and ligand (CD25 and CD28) at binding site pocket was the same while the changing interaction came from the end of oligosaccharide that could attach to several amino acids. According to no changing interaction in binding site, the complex was determined for MD simulation. The RMSD values of both complexes showed that both complexes tend to stabilize after passed 50 ns. In addition, after 80 ns, ligand in CgAM-CD25 model showed the higher RMSD values than CgAM-CD28 system. This meant CgAM-CD25 model was

more flexible than *CgAM-CD28* model. Using range 80 -100 ns, RMSF, H-bond, B-factor and total energy of both complexes were determined. Both RMSF and B-factor were used to investigate the flexibility of amino acids in complex. From RMSF result, amino acid in range 400 - 500 (Binding site) were fluctuated in low range of RMSF values which was a same trend with B-factor. The result showed that the binding site between *CgAM* and cyclodextrin (both CD25 and CD28) had a rigid structure while surface area was more flexible. *CgAM* in complex with CD25 and CD28 had an H-bond interaction at the binding area. The result showed that three catalytic residues (D460, E508 and D561) had H-bond interaction with CD25 and CD28. E508 in both complex had an interaction with glucose residue in subsite +1 whereas D460 and D561 were different. D460 in *CgAM-CD25* complex formed H-bond with glucose residue in subsite -1 and D561 formed with glucose residue in subsite -2 and -1. For *CgAM-CD28* complex, it was conversed. D460 had H-bond interaction with glucose residue in subsite -2 and -1 while D561 formed only with glucose residue in subsite -1. Moreover, E231 showed the different interaction position with glucose residues. In *CgAM-CD25*, E231 form H-bond with glucose residue in subsite -5 and -6 whereas in *CgAM-CD28* shifted to -6 and -7. W425 that was reported as an essential residue for substrate binding and supporting catalytic molecule (Rachadech et al., 2015, Nimpiboon et al., 2016a, Nimpiboon et al., 2016b) also showed H-bond interaction between *CgAM-CD25* and glucose residue in subsite -3.

The total binding energy was calculated from two methods; MM/PBSA and MM/GBSA. From the result in Table 3.8, total energy of *CgAM-CD25* complex was lower than *CgAM-CD28* complex for MM/PBSA. In contrast, MM/GBSA calculation showed that *CgAM-CD28* complex provided lower energy than MM/PBSA. The huge

different values between MM/PBSA and MM/GBSA were from $\Delta G_{ele,solv}$ and ΔG_{solv} . The per-residue decomposition free energy showed that R667 in CgAM-CD25 complex and H458 in CgAM-CD28 complex had a lowest energy in their systems. According to the Figure 3.25, the key shared binding residues in both complexes that provided low energy which was follows; Y23, Y235, Y418, L510, F534, and T666. Surprisingly, E231 in CgAM-CD25 showed a low energy which helped to stabilized in complex whereas in CgAM-CD28, E231 preferred to non-stabilize the complex and provided high energy. For catalytic residues (D460, E508 and D561), total energy of each residues in both complexes was high ($\Delta E = +$) except D460 in CgAM-CD25 complex. These all results demonstrated that those residues in both complexes were considered as important residues for binding between CgAM and CD.



CHAPTER V

CONCLUSIONS

1. P228Y, A413F and G417F CgAM mutants were successfully generated by site-directed mutagenesis.
2. Expression condition for P228Y was induction with 1 mM IPTG at 16°C for 6 h. A413F and G417F were grown in LB media containing 1% glucose prior to induction by 1 mM IPTG at 16 °C for 18 h.
3. E231Y was successfully purified by DEAE and Phenyl sepharose columns, while P228Y, A413F and G417F were purified by Nickle column.
4. For starch transglycosylation, P228Y had an optimum temperature at 25°C and optimum pH at 6.0. G417F showed an optimum temperature and pH at 30°C and pH 6.5. A413F exhibited an optimum temperature of 35°C and optimum pH of 7.5.
5. All mutant enzymes (P228Y, A413F and G417F) were stable in pH range 5.5 – 9 but unstable at temperature above 40°C.
6. In comparison to WT, P228Y, E231Y and G417F, A413F gave the lowest specific activity of all reactions (starch transglycosylation, starch degradation, disproportionation, cyclization, coupling and hydrolysis).
7. Although P228Y showed similar specific activities of starch transglycosylation and starch degradation to the WT enzyme, P228Y exhibited much lower disproportionation, cyclization and coupling than the WT enzyme.
8. All mutated enzymes can catalyze intermolecular transglycosylation reaction (disproportionation reaction) from malto-oligosaccharides G2 - G7.

Maltotriose (G3) is the best substrate for all enzymes. In addition, Glucose (G1) cannot use to be a substrate.

9. A preference order of substrate specificity for most of mutants (P228Y, E231Y, A413F and G417F) was $G3 > G4 > G5 \sim G6 \sim G7 > G2$.
10. For LR-CDs synthesis, principal product of WT at 6 h was CD29 while E231Y gave a smaller CD (CD27). In contrast, the other mutants (P228Y, A413F and G417F) gave larger size of principal LR-CDs (CD36, CD40 and CD36, respectively).
11. P228Y gave the same size of major LR-CD products although reaction was incubated for longer time. This may due to the fact that P228Y exhibited low coupling activity.
12. P228Y mutation affected disproportionation activity by lowering k_{cat} but not K_m .
13. G417F mutation affected both k_{cat} and K_m of cyclization activity.
14. From MD simulation, Y418, M474, L510, F534, Y23, R458, Q423, T666, Q475, L236, Q421, E231, Q420, N419 and Y235 might have an interaction with LR-CDs.

REFERENCES

- ALTING, A., VAN DE VELDE, F., KANNING, M., BURGERING, M., MULLENNERS, L., SEIN, A. & BUWALDA, P. 2009. Improved creaminess of low-fat yoghurt: The impact of amylomaltase-treated starch domains. *Food Hydrocolloids*, 23, 980-987.
- BANG, B., KIM, H., KIM, H., BAIK, M., AHN, S., KIM, C. & PARK, C. 2006. Cloning and overexpression of 4- α -glucanotransferase from *Thermus brockianus* (TBGT) in *E.coli*. *Journal of Microbiology and Biotechnology*, 16, 1809-1813.
- BARENDTS, T., BULTEMA, J., KAPER, T., VAN DER MAAREL, M., DIJKHUIZEN, L. & DIJKSTRA, B. 2007. Three-way stabilization of the covalent intermediate in amylomaltase, an α -amylase-like transglycosylase. *Journal of Biological Chemistry*, 282, 17242-17249.
- BIKADI, Z. & HAZAI, E. 2009. Application of the PM6 semi-empirical method to modeling proteins enhances docking accuracy of AutoDock *Journal of Cheminformatics*, 1, 15.
- BRADFORD, M. 1976. A rapid and sensitive method for the quantitation of microgram quantities of protein utilizing the principle of protein-dye binding. *Analytical Biochemistry*, 72, 248-254.
- CASE, D., BABIN, V., BERRYMAN, J., BETZ, R., CAI, Q., CERUTTI, D., CHEATHAM III, T., DARDEN, T., DUKE, R., GOHLKE, H., GOETZ, A., SERGEY GUSAROV, S., HOMEYER, N., JANOWSKI, P., KAUS, J., KOLOSSVÁRY, I., KOVALENKO, A., LEE, T., GRAND, S., LUCHKO, T., LUO, R., MADEJ, B., MERZ, K., PAESANI, F., ROE, D., ROITBERG, A.,

- SAGUI, C., SALOMON-FERRER, R., SEABRA, G., SIMMERLING, C., SMITH, W., SWAILS, J., WALKER, R., WANG, J., WOLF, R., WU, X. & KOLLMAN, P. 2014. *Amber 14*, San Francisco, University of California.
- CASE, D., CHEATHAM, T., DARDEN, T., GOHLKE, H., LUO, R., MERZ, K., ONUFRIEV, A., SIMMERLING, C., WANG, B. & WOODS, R. 2005. The amber biomolecular simulation programs. *Journal of chemical theory and computation*, 26, 1668–1688.
- CHAPLIN, M. F. & KENNEDY, J. F. 1994. *Carbohydrate analysis: A practical approach*, New York, Oxford University Press Inc.
- DOMINGUEZ, C., BOELEN, R. & BONVIN, A. 2003. HADDOCK: A protein-protein docking approach based on biochemical and/or biophysical information. *Journal of the American Chemical Society* 125, 1731-1737.
- FUJII, H., SHIN-YA, M., TAKEDA, S., HASHIMOTO, Y., MUKAI, S., SAWADA, S., ADACHI, T., AKIYOSHI, K., MIKI, T. & MAZDA, O. 2014. Cycloamylose-nanogel drug delivery system-mediated intratumor silencing of the vascular endothelial growth factor regulates neovascularization in tumor microenvironment. *Cancer Science*, 105, 1616-1625.
- FUJII, K., MINAGAWA, H., TERADA, Y., TAKAHA, T., KURIKI, T., SHIMADA, J. & KANEKO, H. 2005. Use of random and saturation mutageneses to improve the properties of *Thermus aquaticus* amyloamylase for efficient production of cycloamyloses. *Applied and Environmental Microbiology*, 71, 5823-5827.
- FUJIWARA, T., TANAKA, N. & KOBAYASHI, S. 1990. Structure of δ -cyclodextrin 13.75 H₂O. *Chemistry Letters*, 739-742.

- FUWA, H. 1954. A new method for microdetermination of amylase activity by the use of amylose as the substrate. *The Journal of Biochemistry*, 41, 583-603.
- GESSLER, K., USÓN, I., TAKAHA, T., KRAUSS, N., SMITH, S., OKADA, S., SHELDRIK, G. & SAENGER, W. 1999. V-Amylose at atomic resolution: X-ray structure of a cycloamylose with 26 glucose residues (cyclomaltohexacosose). *Proceedings of the National Academy of Sciences of the United States of America*, 96, 4246-4251.
- GOHLKE, H. & CASE, D. 2004. Converging free energy estimates: MM-PB(GB)SA studies on the protein-protein complex Ras-Raf. *Journal of Computational Chemistry*, 25, 238-250.
- GREEN, M. & SAMBROOK, J. 2001. *Molecular cloning: A laboratory manual* Cold Spring Harbor, NY, Cold Spring Harbor Laboratory Press.
- GREENFIELD, N. 2006. Using circular dichroism spectra to estimate protein secondary structure. *Nature Protocols*, 1, 2876-2890.
- GREENFIELD, N. & FASMAN, G. 1969. Computed circular dichroism spectra for the evaluation of protein conformation. *Biochemistry*, 8, 4108-4116.
- GROSDIDIER, A., ZOETE, V. & MICHIELIN, O. 2011a. Fast docking using the CHARMM force field with EADock DSS. *Journal of Computational Chemistry*, 32, 2149-2159.
- GROSDIDIER, A., ZOETE, V. & MICHIELIN, O. 2011b. SwissDock, a protein-small molecule docking web service based on EADock DSS. *Nucleic Acids Research*, 39, W270-W277.

- HANSEN, M., BLENNOW, A., PEDERSEN, S., NØRGAARD, L. & ENGELSEN, S. 2008. Gel texture and chain structure of amyloamylase-modified starches compared to gelatin. *Food Hydrocolloids*, 22, 1551-1566.
- HOU, T., WANG, J., LI, Y. & WANG, W. 2011. Assessing the performance of the MM/PBSA and MM/GBSA methods. 1. The accuracy of binding free energy calculations based on molecular dynamics simulations. *Journal of Chemical Information and Modeling* 51, 69-82.
- JOO, S., KIM, S., SEO, H. & KIM, K. 2016. Crystal structure of amyloamylase from *Corynebacterium glutamicum*. *Journal of Agricultural and Food Chemistry*, 64, 5662-5670.
- JORGENSEN, W., CHANDRASEKHAR, J., MADURA, J., IMPEY, R. & KLEIN, M. 1983. Comparison of simple potential functions for simulating liquid water. *The Journal of Chemical Physics* 79, 926-935.
- JUNG, J., JUNG, T., SEO, D., YOON, S., CHOI, C., PARK, B., PARK, C. & WOO, E. 2011. Structural and functional analysis of substrate recognition by the 250s loop in amyloamylase from *Thermus brockianus*. *Proteins: Structure, Function, and Bioinformatics*, 79, 633-644.
- KAEWPATHOMSRI, P., TAKAHASHI, Y., NAKAMURA, S., KAULPIBOON, J., KIDOKORO, S., MURAKAMI, S., KRUSONG, K. & PONGSAWASDI, P. 2015. Characterization of amyloamylase from *Thermus filiformis* and the increase in alkaline and thermo-stability by E27R substitution. *Process Biochemistry*, 50, 1814-1824.
- KAPER, T., LEEMHUIS, H., UITDEHAAG, J., VAN DER VEEN, B., DIJKSTRA, B., VAN DER MAAREL, M. & DIJKHUIZEN, L. 2007. Identification of

- acceptor substrate binding subsites +2 and +3 in the amylomaltase from *Thermus thermophilus* HB8. *Biochemistry*, 46, 5261-5269.
- KAPER, T., TALIK, B., ETTEMA, T., BOS, H., VAN DER MAAREL, M. & DIJKHUIZEN, L. 2005. Amylomaltase of *Pyrobaculum aerophilum* IM2 produces thermoreversible starch gels. *Applied and Environmental Microbiology*, 71, 5098-5106.
- KAPER, T., VAN DER MAAREL, M., EUVERINK, G. & DIJKHUIZEN, L. 2004. Exploring and exploiting starch-modifying amylomaltases from thermophiles. *Biochemical Society Transactions*, 32, 279-282.
- KINOSHITA, S., UDAKA, S. & SHIMONO, M. 2004. Studies on the amino acid fermentation. Part 1. Production of L-glutamic acid by various microorganisms. *The Journal of General and Applied Microbiology*, 50, 331-343.
- KITAHATA, S., MURAKAMI, H. & OKADA, S. 1989. Purification and some properties of amylomaltase from *Escherichia coli* IFO 3806. *Agriculture and Biological Chemistry*, 53, 2653-2659.
- KITAMURA, S., NAKATANI, K., TAKAHA, T. & OKADA, S. 1999. Complex formation of large-ring cyclodextrins with iodine in aqueous solution as revealed by isothermal titration calorimetry. *Macromolecular Rapid Communications*, 20, 612-615.
- KNEGTEL, R., STROKOPYTOV, B., PENNINGA, D., FABER, O., ROZEBOOM, H., KALK, K., DIJKHUIZEN, L. & DIJKSTRA, B. W. 1995. Crystallographic studies of the interaction of cyclodextrin glycosyltransferase

from *Bacillus circulans* strain-251 with natural substrates and products. *The Journal of Biological Chemistry*, 270, 29256-29264.

KOIZUMI, K., SANBE, H., KUBOTA, Y., TERADA, Y. & TAKAHA, T. 1999. Isolation and characterization of cyclic α -(1 \rightarrow 4)-glucans having degrees of polymerization 9–31 and their quantitative analysis by high-performance anion-exchange chromatography with pulsed amperometric detection. *Journal of Chromatography A*, 852, 407-416.

KOLLMAN, P., MASSOVA, I., REYES, C., KUHN, B., HUO, S., CHONG, L., LEE, M., LEE, T., DUAN, Y., WANG, W., DONINI, O., CIEPLAK, P., SRINIVASAN, J., CASE, D. & CHEATHAM, T. 2000. Calculating structures and free energies of complex molecules: Combining molecular mechanics and continuum models. *Accounts of Chemical Research*, 33, 889-897.

KREMPL, P., MAIRHOFER, J., STRIEDNER, G. & THALLINGER, G. 2014. Finished genome sequence of the laboratory strain *Escherichia coli* K-12 RV308 (ATCC 31608). *Genome Announcements*, 2, e00971-e009714.

KUMAGAI, H. 2000. Microbial production of amino acids in Japan. *Advances in Biochemical Engineering/Biotechnology*, 69, 71-85.

KUTTIYAWONG, K., SAEHU, S., ITO, K. & PONGSAWASDI, P. 2015. Synthesis of large-ring cyclodextrin from tapioca starch by amylomaltase and complex formation with vitamin E acetate for solubility enhancement. *Process Biochemistry*, 50, 2168-2176.

LACKS, S., DUNN, J. & GREENBERG, B. 1982. Identification of base mismatches recognized by the heteroduplex-DNA-repair system of *Streptococcus pneumoniae*. *Cell*, 31, 327-336.

- LARSEN, K. 2002. Large Cyclodextrins. *Journal of Inclusion Phenomena and Macrocyclic Chemistry*, 43, 1-13.
- LEE, B., OH, D. & YOO, S. 2009. Characterization of 4- α -glucanotransferase from *Synechocystis* sp. PCC 6803 and its application to various corn starches. *New Biotechnology*, 26, 29-36.
- LEE, H., AUH, J., YOON, H., KIM, M., PARK, J., HONG, S., KANG, M., KIM, T., MOON, T., KIM, J. & PARK, K. 2002. Cooperative action of α -glucanotransferase and maltogenic amylase for an improved process of isomaltooligosaccharide (IMO) production. *Journal of Agricultural and Food Chemistry*, 50, 2812-2817.
- LEE, K., KIM, Y., PARK, K. & LEE, H. 2006. Effects of α -glucanotransferase treatment on the thermo-reversibility and freeze-thaw stability of a rice starch gel. *Carbohydrate Polymers*, 63, 347-354.
- LI, X., ZHANG, W., QIAO, X. & XIAOJIE XU, X. 2007. Prediction of binding for a kind of non-peptic HCV NS3 serine protease inhibitors from plants by molecular docking and MM/PBSA. *Bioorganic & Medicinal Chemistry*, 15, 220-226.
- LOUIS-JEUNE, C., ANDRADE-NAVARRO, M. & PEREZ-IRATXETA, C. 2011. Prediction of protein secondary structure from circular dichroism using theoretically derived spectra. *Proteins: Structure, Function, and Bioinformatics*, 80, 374-381.
- MACHIDA, S., OGAWA, S., SHI, X., TAKAHA, T., FUJII, K. & HAYASHI, K. 2000. Cycloamylose as an efficient artificial chaperone for protein refolding. *FEBS Letters*, 486, 131-135.

- MATEOS, L., ORDÓÑEZ, E., LETEK, M. & GIL, J. 2006. *Corynebacterium glutamicum* as a model bacterium for the bioremediation of arsenic. *International Microbiology*, 9, 207-215.
- MEEPRASERT, A., HANNONGBUA, S. & RUNGROTMONGKOL, T. 2014. Key Binding and Susceptibility of NS3/4A Serine Protease Inhibitors against Hepatitis C Virus. *Journal of Chemical Information and Modeling*, 54, 1208-1217.
- MIYAZAWA, I., UEDA, H., NAGASE, H., ENDO, T., KOBAYASHI, S. & NAGAI, T. 1995. Physicochemical properties and inclusion complex formation of δ -Cyclodextrin. *European Journal of Pharmaceutical Sciences*, 3, 153-162.
- MONERA, O., SEREDA, T., ZHOU, N., KAY, C. & HODGES, R. 1995. Relationship of sidechain hydrophobicity and alpha-helical propensity on the stability of the single-stranded amphipathic α -helix. *Journal of peptide science: an official publication of the European Peptide Society*, 1, 319-329.
- MUN, S., KIM, Y., KANG, C., PARK, K., SHIM, J. & KIM, Y. 2009. Development of reduced-fat mayonnaise using 4 α GTase-modified rice starch and xanthan gum. *International Journal of Biological Macromolecules*, 44, 400-407.
- NAUMTHONG, W., ITO, K. & PONGSAWASDI, P. 2015. Acceptor specificity of amyloamylase from *Corynebacterium glutamicum* and transglucosylation reaction to synthesize palatinose glucosides. *Process Biochemistry*, 50, 1825-1834.
- NIMPIBOON, P., KAULPIBOON, J., KRUSONG, K., NAKAMURA, S., KIDOKORO, S. & PONGSAWASDI, P. 2016a. Mutagenesis for improvement of activity and thermostability of amyloamylase from

Corynebacterium glutamicum. *International Journal of Biological Macromolecules*, 86, 820-828.

NIMPIBOON, P., KRUSONG, K., KAULPIBOON, J., KIDOKORO, S. & PONGSAWASDI, P. 2016b. Roles of N287 in catalysis and product formation of amyloamylase from *Corynebacterium glutamicum*. *Biochemical and Biophysical Research Communications*, 478, 759-764.

NOVY, R. & MORRIS, B. 2001. Use of glucose to control basal expression in the pET System. *inNovations*, 8-10.

O'NEILL, E., STEVENSON, C., TANTANARAT, K., LATOUSAKIS, D., DONALDSON, M., REJZEK, M., NEPOGODIEV, S., LIMPASENI, T., FIELD, R. & LAWSON, D. 2015. Structural dissection of the maltodextrin disproportionation cycle of the *Arabidopsis* plastidial disproportionating enzyme 1 (DPE1). *Journal of Biological Chemistry*, 290, 29834-29853.

OLSSON, M., SØNDERGAARD, C., ROSTKOWSKI, M. & JENSEN, J. 2011. PROPKA3: Consistent treatment of internal and surface residues in empirical pKa predictions. *Journal of chemical theory and computation*, 7, 525-537.

PALMER, T., RYMAN, B. & WHELAN, W. 1976. The action pattern of amyloamylase from *Escherichia coli*. *European Journal of Biochemistry*, 69, 105-115.

PARK, J., KIM, H., KIM, Y., CHA, H., KIM, Y., KIM, T., KIM, Y. & PARK, K. 2007. The action mode of *Thermus aquaticus* YT-1 4- α -glucanotransferase and its chimeric enzymes introduced with starch-binding domain on amylose and amylopectin. *Carbohydrate Polymers*, 67, 164-173.

- PATHOMSOONTHORNCHAI, T. 2015. *Screening of mutate Corynebacterium glutamicum amyloamylase to identify amino acids involved in large-ring cyclodextrin formation*. Master degree, chalongkorn University.
- PIERCE, B., WIEHE, K., HWANG, H., KIM, B., VREVEN, T. & WENG, Z. 2014. ZDOCK server: Interactive docking prediction of protein-protein complexes and symmetric multimers. *Bioinformatics* 30(12): 1771-3. , 30, 1771-1773.
- PRZYLAS, I., TERADA, Y., FUJII, K., TAKAHA, T., SAENGER, W. & STRÄTER, N. 2000a. X-ray structure of acarbose bound to amyloamylase from *Thermus aquaticus* implications for the synthesis of large cyclic glucans. *European Journal of Biochemistry*, 267, 6903-6913.
- PRZYLAS, I., TOMOO, K., TERADA, Y., TAKAHA, T., FUJII, K., SAENGER, W. & STRÄTER, N. 2000b. Crystal structure of amyloamylase from *Thermus Aquaticus*, a glycosyltransferase catalysing the production of large cyclic glucans *Journal of Molecular Biology*, 296, 873-886.
- PUGSLEY, A. P. & DUBREUIL, C. 1988. Molecular characterization of malQ, the structural gene for the *Escherichia coli* enzyme amyloamylase. *Molecular Microbiology* 2, 473-479.
- RACHADECH, W., NIMPIBOON, P., NAUMTHONG, W., NAKAPONG, S., KRUSONG, K. & PONGSAWASDI, P. 2015. Identification of essential tryptophan in amyloamylase from *Corynebacterium glutamicum*. *International Journal of Biological Macromolecules*, 76, 230-235.
- RICE, P., LONGDEN, I. & BLEASBY, A. 2000. EMBL: The european molecular biology open software suite. *Trends in Genetics* 16, 6, 276-277.

- RYCKAERT, J., CICCOTTI, G. & BERENDSEN, H. 1977. Numerical integration of the cartesian equations of motion of a system with constraints: molecular dynamics of n-alkanes. *Journal of Computational Physics*, 23, 327-341.
- SAENGER, W., JACOB, J., GESSLER, K., STEINER, T., HOFFMANN, D., SANBE, H., KOIZUMI, K., SMITH, S. & TAKAHA, T. 1998. Structures of the common cyclodextrins and their larger analogues - Beyond the doughnut. *Chemical Reviews*, 98, 1787-1802.
- SCHMIDT, A., COTTAZ, S., DRIGUEZ, H. & SCHULZ, G. 1998. Structure of cyclodextrin glycosyltransferase complexed with a derivative of its main product β -cyclodextrin. *Biochemistry*, 37, 5509-5915.
- SCHMIDT, J. & JOHN, M. 1979. Starch metabolism in *Pseudomonas stutzeri*. II. Purification and properties of a dextrin glycosyltransferase (D-enzyme) and amyloamylase *Biochimica et Biophysica Acta (BBA) - Enzymology*, 566, 100-114.
- SCHNEIDMAN, D., INBAR, Y., NUSSINOV, R. & WOLFSON, H. 2005. PatchDock and SymmDock: servers for rigid and symmetric docking. *Nucleic Acids Research*, 33, W363-W367.
- SINNER, M. & PULS, J. 1978. Non-corrosive dye reagent for detection of reducing sugars in borate complex ion-exchange chromatography. *Journal of Chromatography A*, 156, 197-204.
- SRISIMARAT, W., KAULPIBOON, J., KRUSONG, K., ZIMMERMANN, W. & PONGSAWASDI, P. 2012. Altered large-ring cyclodextrin product profile due to a mutation at Tyr-172 in the amyloamylase of *Corynebacterium glutamicum*. *Applied and Environmental Microbiology*, 78, 7223-7228.

- SRISIMARAT, W., MURAKAMI, S., PONGSAWASDI, P. & KRUSONG, K. 2013. Crystallization and preliminary X-ray crystallographic analysis of the amyloamylase from *Corynebacterium glutamicum*. *Acta Crystallographica Section F Structural Biology and Crystallization Communications*, 69, 1004-1006.
- SRISIMARAT, W., POWVIRIYAKUL, A., KAULPIBOON, J., KRUSONG, K., ZIMMERMANN, W. & PONGSAWASDI, P. 2010. A novel amyloamylase from *Corynebacterium glutamicum* and analysis of the large-ring cyclodextrin products. *Journal of Inclusion Phenomena and Macrocyclic Chemistry*, 70, 369-375.
- SURIYAKUL NA AYUDHAYA, P., PONGSAWASDI, P., LAOHASONGKRAM, K. & CHAIWANICHSIRI, S. 2016. Properties of cassava starch modified by amyloamylase from *Corynebacterium glutamicum*. *Journal of Food Science*, 81, C1363-C1369.
- TAKAHA, T. & SMITH, S. 1999. The functions of 4- α -glucanotransferase and their use for the production of cyclic glucans. *Biotechnology & genetic engineering reviews*, 16, 257-280.
- TAKAHA, T., YANASE, M., TAKATA, H., OKADA, S. & SMITH, S. 1996. Potato D-enzyme catalyzes the cyclization of amylose to produce cycloamylose, a novel cyclic glucan. *The Journal of Biological Chemistry*, 271, 2902-2908.
- TERADA, Y., FUJII, K., TAKAHA, T. & OKADA, S. 1999. *Thermus aquaticus* AtCC 33923 amyloamylase gene cloning and expression and enzyme characterization: production of cycloamylose. *Applied and Environmental Microbiology* 65, 910-915.

- TOITA, S., MORIMOTO, N. & AKIYOSHI, K. 2010. Functional cycloamylose as a polysaccharide-based biomaterial: Application in a gene delivery system. *Biomacromolecules*, 2010.
- TOMONO, K., MUGISHIMA, A., SUZUKI, T., GOTO, H., UEDA, H., NAGAI, T. & WATANABE, J. 2002. Interaction between cycloamylose and various drugs. *Journal of Inclusion Phenomena and Macrocyclic Chemistry*, 44, 267-270.
- UDAKA, S. 1959. Screening method for microorganisma accumulating metabolites and its use in the isolation of *Micrococcus glutamicus*. *Journal of Bacteriology*, 79, 754-755.
- UEDA, H. 2002. Physicochemical properties and complex formation abilities of large-ring cyclodextrins. *Journal of Inclusion Phenomena and Macrocyclic Chemistry*, 44, 53-56.
- VAN DER MAAREL, M., CAPRON, I., EUVERINK, G., BOS, H., KAPER, T., BINNEMA, D. & STEENEKEN, P. 2005. A novel thermoreversible gelling product made by enzymatic modification of starch. *Starch - Stärke*, 57, 465-472.
- VAN DER MAARL, M., VAN DER VEEN, B., UITDEHAAG, J., LEEMHUIS, H. & DIJKHUIZEN, L. 2002. Properties and applications of starch-converting enzymes of the α -amylase family. *Journal of Biotechnology*, 94, 137-155.
- VAN DER VEEN, B., UITDEHAAG, J., DIJKSTRA, B. & DIJKHUIZEN, L. 2000. Engineering reaction and product specificity of cyclodextrin glycosyltransferase from *Bacillus circulans* strain 251. *Biochimica et Biophysica Acta: Protein and proteomic*, 1543, 336-360.

- VAN ZUNDERT, G., RODRIGUES, J., TRELLET, M., SCHMITZ, C., KASTRITIS, P., KARACA, E., MELQUIOND, A., VAN DIJK, M., DE VRIES, S. & BONVIN, A. 2016. The HADDOCK2.2 webserver: User-friendly integrative modeling of biomolecular complexes. *Journal of Molecular Biology*, 428, 720-725.
- VERTÈS, A., INUI, M. & YUKAWA, H. 2005. Manipulating Corynebacteria, from individual genes to chromosomes. *Applied and Environmental Microbiology*, 71, 7633-7642.
- VONGPICHAYAPAIBOON, T., PONGSAWASDI, P. & KRUSONG, K. 2016. Optimization of large-ring cyclodextrin production from starch by amyloamylase from *Corynebacterium glutamicum* and effect of organic solvent on product size. *Journal of Applied Microbiology*, 120, 912-920.
- WATANASATITARPA, S., RUDEEKULTHAMRONG, P., KRUSONG, K., SRISIMARAT, W., ZIMMERMANN, W., PONGSAWASDI, P. & KAULPIBOON, J. 2014. Molecular mutagenesis at Tyr-101 of the amyloamylase transcribed from a gene isolated from soil DNA. *Applied Biochemistry and Microbiology*, 50, 243-252.
- WEISS, S., SKERRA, A. & SCHIEFNER, A. 2015. Structural basis for the interconversion of maltodextrins by MalQ, the amyloamylase of *Escherichia coli*. *Journal of Biological Chemistry*, 290, 21352-21364.
- YORK, D., DARDEN, T. & PEDERSEN, L. 1993. The effect of long-range electrostatic interactions in simulations of macromolecular crystals: A comparison of the Ewald and truncated list methods. *the Journal of Chemical Physics*, 99, 8345-8348.

ZHENG, M., ENDO, T. & ZIMMERMANN, W. 2002. Enzymatic synthesis and analysis of large-ring cyclodextrins. *Australian Journal of Chemistry* 55, 39-48.



APPENDICES



จุฬาลงกรณ์มหาวิทยาลัย
CHULALONGKORN UNIVERSITY

Appendix 1

Preparation for Sodium Dodecyl Sulfate-Polyacrylamide Gel Electrophoresis (SDS-PAGE)

Stock reagent

1. 1 M Tris-HCl (pH 6.8)

Tris(hydroxymethyl)-aminomethane	12.1	g
----------------------------------	------	---

Adjusted pH to 6.8 with 1 N HCl and volume to 100 ml with distilled water

2. 1.5 M Tris-HCl (pH 8.8)

Tris(hydroxymethyl)-aminomethane	18.15	g
----------------------------------	-------	---

Adjusted pH to 8.8 with 1 N HCl and volume to 100 ml with distilled water

3. 10% APS

Ammonium persulfate	0.1	g
---------------------	-----	---

Distilled water	1	ml
-----------------	---	----

4. 10% (w/v) SDS

Sodium dodecyl sulfate	10	g
------------------------	----	---

Adjusted volume to 100 ml with distilled water

5. 50% (v/v) Glycerol

100% Glycerol	50	ml
---------------	----	----

Distilled water	50	ml
-----------------	----	----

6. 1% (w/v) Bromophenol blue

Bromophenol blue	100	mg
------------------	-----	----

Distilled water	10	ml
-----------------	----	----

The solution was stirred until it dissolved. To remove aggregated dye, use filter (Whatman No 2).

Working solution

1. 5x SDS loading dye	(Total volume 10 ml)
1% (w/v) Bromophenol blue	1 ml
2-Mercaptoethanol	0.5 ml
50% (v/v) Glycerol	5 ml
10% SDS	2 ml
1 M Tris-HCl pH 6.8	0.6 ml
Distilled water	0.9 ml
2. Coomassie destaining solution	(Total volume 1 l)
Glacial acetic acid	100 ml
Methanol	100 ml
Distilled water	800 ml
3. Coomassie staining solution	(Total volume 1 l)
Coomassie Brilliant Blue R-250	1 g
Glacial acetic acid	100 ml
Methanol	450 ml
Distilled water	450 ml

4. Electrophoresis buffer (Total volume 1 l)

Tris(hydroxymethyl)-aminomethane	3	g
Glycine	14.4	g
Sodium dodecyl sulfate	1	g

Adjust volume to 1 litre with distilled water

5. Separating Gel 8% (Total volume 10 ml)

Distilled water	4.60	ml
1.5 M Tris-HCl (pH 8.8)	2.53	ml
30% Acrylamide mix	2.67	ml
10% SDS	100	μ l
10% APS	100	μ l
TEMED	4	μ l

6. Stacking Gel 5% (Total volume 4 ml)

Distilled water	2.75	ml
1 M Tris-HCl (pH 6.8)	0.5	ml
30% Acrylamide mix	0.67	ml
10% SDS	40	μ l
10% APS	40	μ l
TEMED	4	μ l

Appendix 2

Preparation of Iodine solution

Iodine solution (0.2% I₂ / 2% KI)

Potassium iodide	2	g
Iodine	0.2	g

Adjusted to 100 ml with distilled water and stir the solution overnight prior to use



Appendix 3

Preparation of DNS reagent

DNS Reagent

2-hydroxy-3,5-dinitrobenzoic acid	5	g
2 N NaOH	100	ml
Potassium sodium tartrate	150	g

Adjusted to 500 ml with distilled water



Appendix 4

Preparation of bicinchoninic acid reagents

bicinchoninic acid reagent

1. Solution A

4,4'-dicarboxy-2,2'-biquinoline	0.1302 g
---------------------------------	----------

Dissolved in 85 ml of distilled water

NaCO ₃	6.2211 g
-------------------	----------

Adjusted to 100 ml with distilled water

2. Solution B

Component 1

L-aspartic acid	0.642 g
-----------------	---------

NaCO ₃	0.8681 g
-------------------	----------

Dissolved in 15 ml of distilled water

Component 2

CuSO ₄	0.1736 g
-------------------	----------

Dissolved in 5 ml of distilled water

Mix component 1 and 2 and then adjusted volume to 25 ml with distilled water

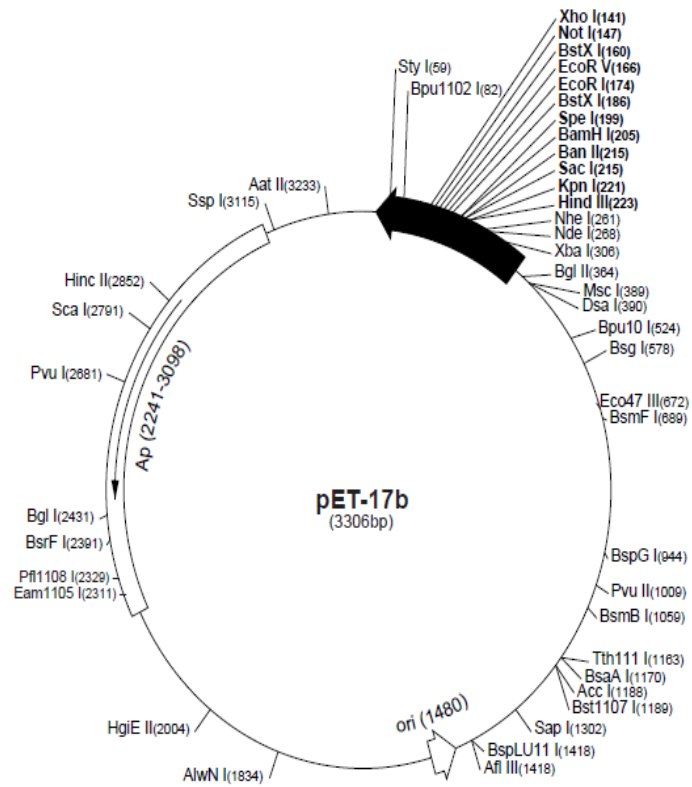
*** Mix solution A 24 ml with solution B 1 ml and used within 24 h.***

Appendix 5

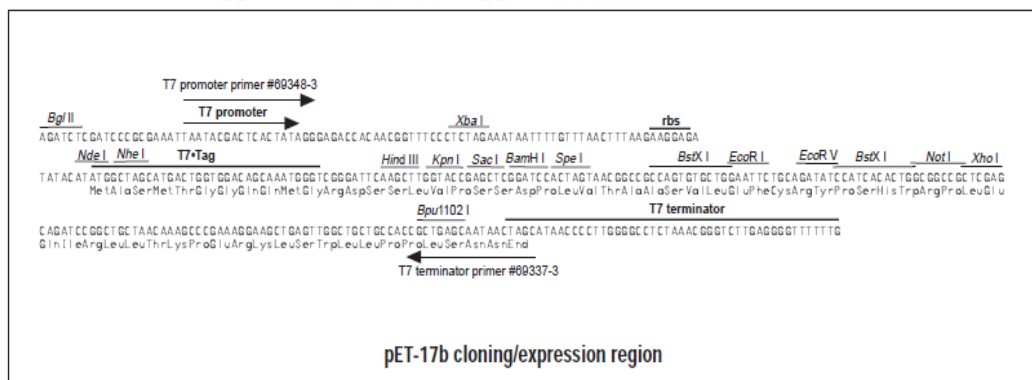
Restriction map of pET-17b (Novagen)

pET-17b sequence landmarks

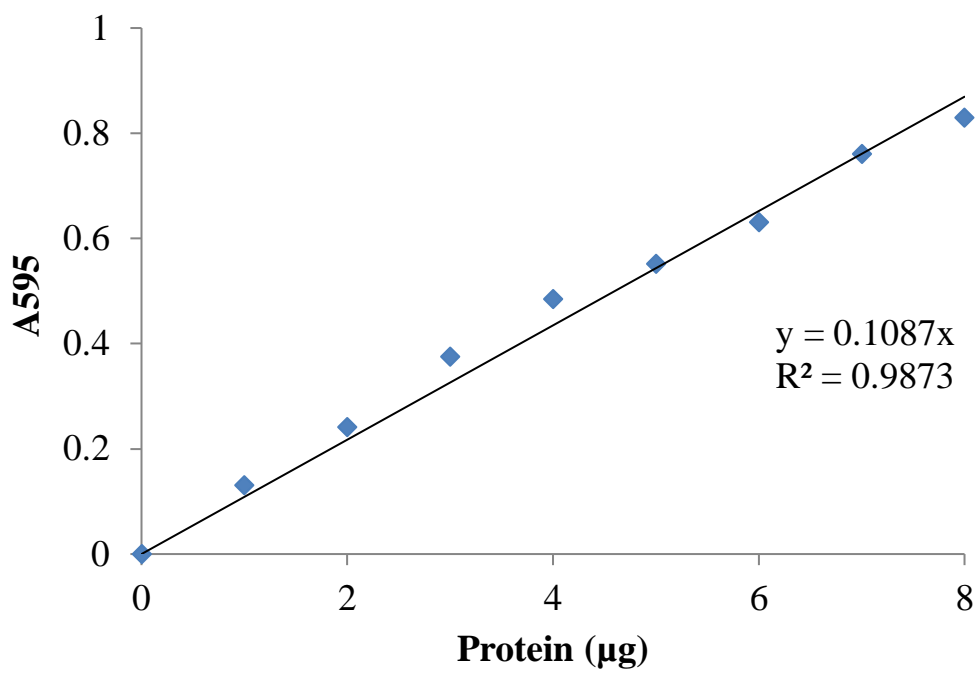
T7 promoter	333-349
T7 transcription start	332
T7•Tag coding sequence	237-269
Multiple cloning sites (<i>Hind</i> III - <i>Xho</i> I)	141-228
T7 terminator	28-74
pBR322 origin	1480
<i>bla</i> coding sequence	2241-3098

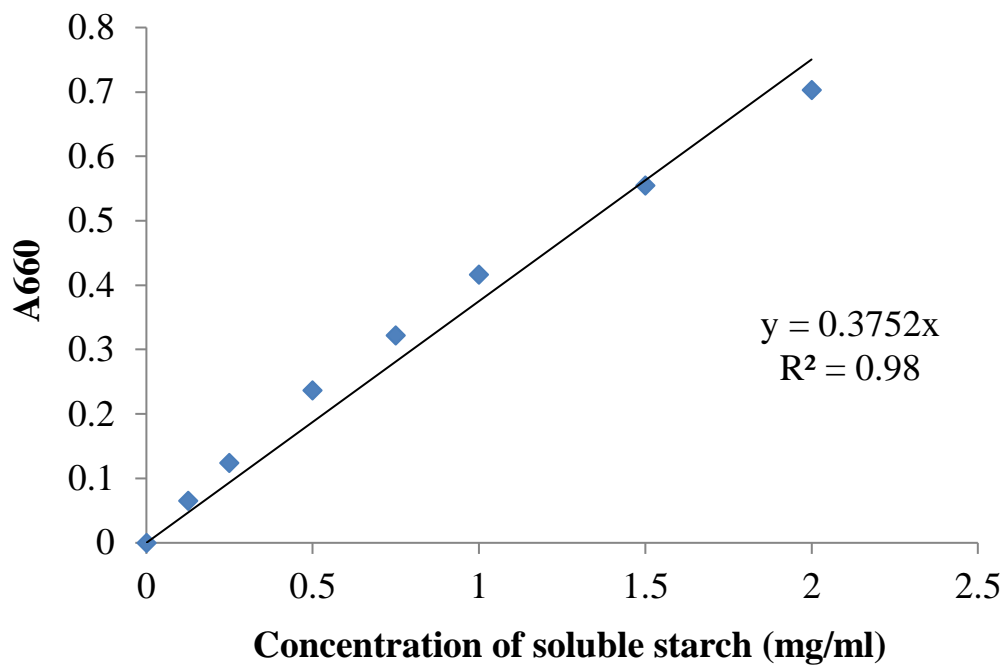


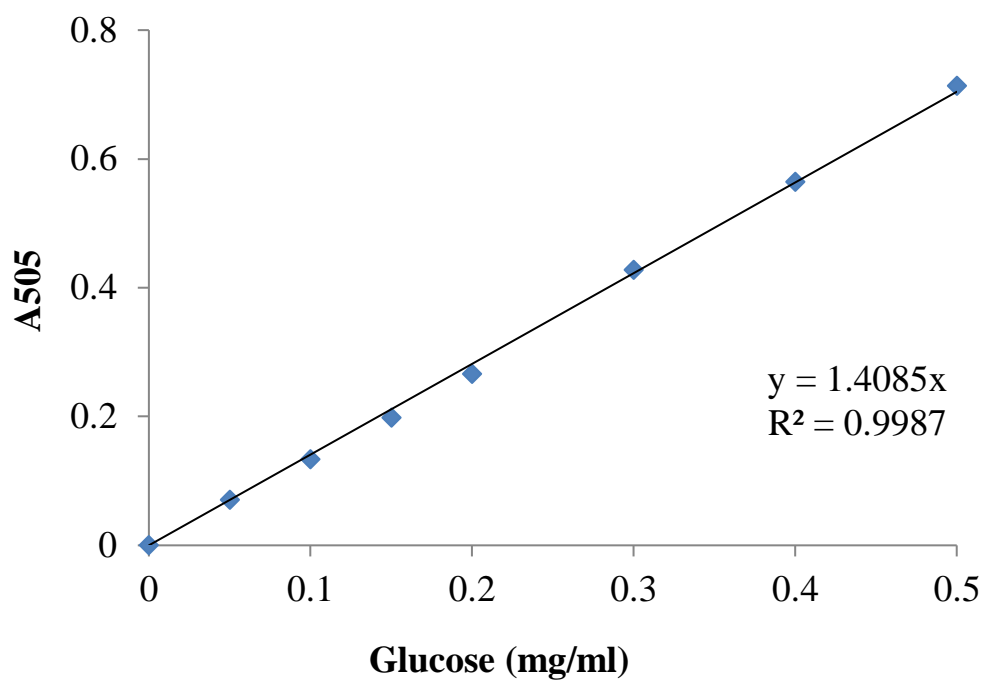
จุฬาลงกรณ์มหาวิทยาลัย



pET-17b cloning/expression region

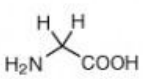
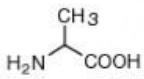
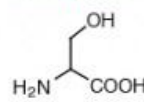
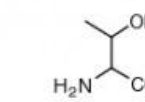
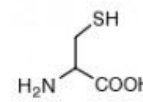
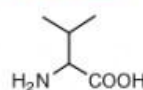
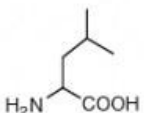
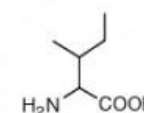
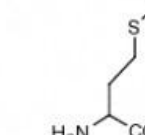
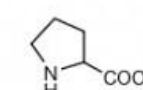
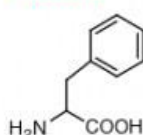
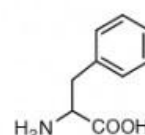
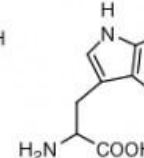
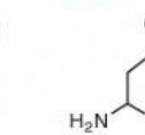
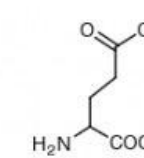
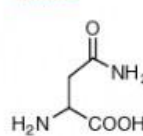
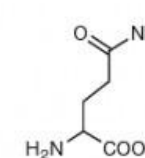
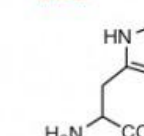
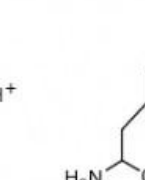
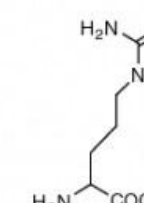
Appendix 7**Standard curve for protein determination by Bradford assay**

Appendix 8**Standard curve for starch determination by starch degradation assay**

Appendix 9**Standard curve for glucose determination by glucose oxidase assay**

Appendix 10

Amino acid reference chart

Small		Nucleophilic		
				
Glycine (Gly, G) MW: 57.05	Alanine (Ala, A) MW: 71.09	Serine (Ser, S) MW: 87.08, pK _a ~ 16	Threonine (Thr, T) MW: 101.11, pK _a ~ 16	Cysteine (Cys, C) MW: 103.15, pK _a = 8.35
Hydrophobic				
				
Valine (Val, V) MW: 99.14	Leucine (Leu, L) MW: 113.16	Isoleucine (Ile, I) MW: 113.16	Methionine (Met, M) MW: 131.19	Proline (Pro, P) MW: 97.12
Aromatic		Acidic		
				
Phenylalanine (Phe, F) MW: 147.18	Tyrosine (Tyr, Y) MW: 163.18	Tryptophan (Trp, W) MW: 186.21	Aspartic Acid (Asp, D) MW: 115.09, pK _a = 3.9	Glutamic Acid (Glu, E) MW: 129.12, pK _a = 4.07
Amide		Basic		
				
Asparagine (Asn, N) MW: 114.11	Glutamine (Gln, Q) MW: 128.14	Histidine (His, H) MW: 137.14, pK _a = 6.04	Lysine (Lys, K) MW: 128.17, pK _a = 10.79	Arginine (Arg, R) MW: 156.19, pK _a = 12.48

VITA

Miss Sirikul Ngawiset was born on October 19th, 1991. She has graduated the Bachelor's degree from Department of Biochemistry, Faculty of Science, Chulalongkorn University. Then, she has studied in Master's degree in the major field of Biochemistry and Molecular biology, Department of Biochemistry, Faculty of Science, Chulalongkorn University.

She was an exchange student to School of Agriculture, Ikuta campus, Meiji University, Japan for 3 months (Jan 2016 – March 2016). In addition, On November 2016, she has attended the 28th Annual Meeting of the Thai Society for Biotechnology and International Conference (TSB2016) at The Empress Hotel, Chaing Mai, Thailand for poster presentation. The title of presentation is "Role of A413 of *Corynebacterium glutamicum* amyloamylase in LR-CD production" is selected to publish in Chiang Mai University Journal of Natural Sciences (Scopus indexed).